

# <sub>1</sub> Chapter 1

## <sub>2</sub> The Pella-Tomlinson Model

## Abstract

4 Stock assessments often assume a two-parameter functional form (e.g., Beverton-Holt or  
5 Ricker) for the expected recruitment produced by a given level of spawning output. [Mangel](#)  
6 [et al. \(2013\)](#) and others have shown that biological reference points such as  $\frac{F^*}{M}$  and  $\frac{B^*}{B(0)}$   
7 are largely determined by a single parameter (steepness) when using two-parameter rela-  
8 tionships. These functions introduce strong correlations between reference points that are  
9 pre-determined by the functional form, rather than a biological characteristic of the stock.  
10 Mangel et al. note that use of a three-parameter stock-recruitment relationship allows for  
11 independent estimation of these reference points. This research seeks to understand the  
12 nature of biases in reference points resulting from fitting a two-parameter functional form  
13 when the true relationship follows a three-parameter stock-recruitment relationship. This  
14 work demonstrates the useful limits of misspecified two-parameter models, and suggests the  
15 mechanisms of model failure which arise from mapping a three-dimensional parameter space  
16 into two dimensions.

# 1 Introduction

The most fundamental model in modern fisheries management is the surplus-production model. These models focus on modeling population growth via nonlinear parametric ordinary differential equations (ODE). Key management quantities called reference points (RPs) are commonly derived from the ODE equilibrium equations and depend upon the parameterization of biomass production. Two-parameter forms of the production function have been shown to limit the theoretical domain of RPs (Mangel et al., 2013). The limited RP-space of two parameter models are a major source of model misspecification for RPs and thus induce bias in RP estimation. The behavior of RP estimation bias is not well understood and as a result often underappreciated. A metamodeling approach is developed here to describe RP biases and explore mechanisms of model failure under the most common two parameter models.

Data for a typical surplus-production model comes in the form of an index of abundance through time which is assumed to be proportional to the reproducing biomass for the population of interest. The index is often observed alongside a variety of other known quantities, but at a minimum, each observed index will be observed in the presence of some known catch for the period. Figure (3.14) shows the classic Namibian Hake dataset exemplifying the form.

Indices are assumed to have multiplicative log-normal errors, and thus the following observation model arises naturally,

$$I_t = qB_te^\epsilon \quad \epsilon \sim N(0, \sigma^2). \quad (1.1)$$

Above  $q$  is often referred to as the “catchability parameter”; it serves as the proportionality constant mapping between the observed index of abundance and biomass.  $\sigma^2$  models residual variation. Biologically speaking  $q$  and  $\sigma^2$  are often treated as nuisance parameters with the “biological parameters” entering the model through a process model on biomass.

Biomass is assumed to evolve as an ODE; in this case I focus on the following form

$$\frac{dB}{dt} = P(B(t); \boldsymbol{\theta}) - Z(t)B(t). \quad (1.2)$$

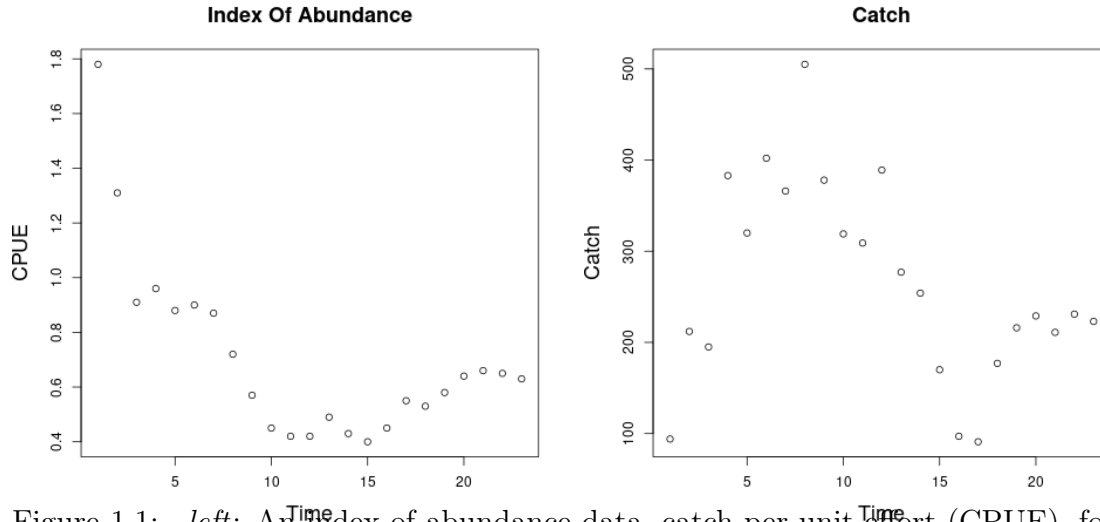


Figure 1.1: *left*: An index of abundance data, catch per unit effort (CPUE), for Namibian Hake from 1965 to 1987 (Hilborn & Mangel, 1997). *right*: The associated catch data for Namibian Hake over the same time period.

Here biomass is assumed to change in time by two processes, net production of biomass into the population,  $P(B)$ , and various sources of biomass removal,  $Z$ , from the population.

Firstly, the population grows through a production function,  $P(B)$ . Production in this setting is defined as the net biomass increase due to all reproduction and maturation processes. The production function is assumed to be a parametric (generally non-linear) function relating the current biomass of the population to an aggregate production of biomass.

Secondly, the population decreases as biomass is removed by various sources that are assumed to remove biomass linearly with biomass. Above,  $Z(t)$ , is an aggregate rate of removal. When the fishing rate,  $F(t)$ , is the only source of removal  $Z(t) = F(t)$ , however often models will also included other linear terms in  $Z(t)$ . Commonly the rate of “natural mortality”,  $M$ , is also included as an additional term so that  $Z(t) = M + F(t)$ .

From a management perspective a major goal of modeling is to accurately infer a quantity known as *maximum sustainable yield* (MSY). One could maximize simple yield at a particular moment in time (and only for that moment) by fishing all available biomass in that moment. This strategy is penny-wise but pound-foolish (not to mention ecologically devastating) since it doesn’t leave biomass in the population to reproduce in the future. We seek to fish in a way that allows (or even encourages) future productivity in the population. This is accomplished by maximizing the equilibrium level of catch over time. Equilibrium yield is considered by

replacing the steady state biomass ( $\bar{B}$ ) in the assumed form for catch, so that  $\bar{Y} = F\bar{B}(F)$ , where  $\bar{\cdot}$  indicates a value at steady state. MSY is found by maximizing  $\bar{Y}(F)$  with respect to  $F$ , and  $F^*$  is the fishing rate at MSY. Going forward let  $*$  decorate any value derived under the condition of MSY.

Fisheries are very often managed based upon reference points which serve as simplified heuristic measures of population behavior. The mathematical form of RPs depends upon the model assumptions through the production function. While a number of different RPs exist which describe the population in different (but related) ways, the most common RPs revolve around the concept of MSY (or robust ways of measuring MSY (Hilborn, 2010; Punt et al., 2016)). Here the focus is primarily on the RPs  $\frac{B^*}{B(0)}$  and  $F^*$  ( $\frac{F^*}{M}$  when appropriate) for their pervasive use in modern fisheries (Punt & Cope, 2019).

$F^*$  is the afore mentioned fishing rate which results in MSY.  $\frac{B^*}{B(0)}$  is the depletion of the stock at MSY. That is to say  $\frac{B^*}{B(0)}$  describes the fraction of the unfished population biomass that will remain in the equilibrium at MSY. In general  $F^* \in \mathbb{R}^+$  and  $\frac{B^*}{B(0)} \in (0, 1)$ , however under the under the assumption of a two parameter production function production models will be structurally unable to capture the full theoretical range of RPs.

Many of the most commonly used production functions depend only on two parameters. For example, the Schaefer model depends only on the biological parameters  $r$  and  $K$ , and limits RP inference so that under the Schaefer model  $\left(F^*, \frac{B^*}{B(0)}\right) \in \left(\mathbb{R}^+, \frac{1}{2}\right)$ . The two parameter Fox model (Fox Jr., 1970) limits  $\left(F^*, \frac{B^*}{B(0)}\right) \in \left(\mathbb{R}^+, \frac{1}{e}\right)$ . Similarly the two parameter Cushing (Cushing, 1971), Beverton-Holt (Beverton & Holt, 1957, BH) and Ricker (Ricker, 1954) production functions do not model the full theoretical space of RPs (Mangel et al., 2013; Yeakel & Mangel, 2015).

The bias-variance trade-off (Ramasubramanian & Singh, 2017) makes it clear that the addition of a third parameter in the production function will necessarily reduce estimation bias. However the utility of this bias reduction is still under debate because the particular mechanisms and behavior (direction and magnitude) of these biases for key management quantities are not fully understood or described. Lee et al. (2012) provides some evidence that estimation of productivity parameters are dependent on biomass contrast as well as model specification. Conn et al. (2010) comes to similar conclusions via calibration modeling

88 techniques. These studies indicate important factors that contribute to inferential failure.  
 89 However they do not offer mechanisms of model failure, nor do their experimental designs  
 90 allow for the control of different types of model misspecification.

91 In this study I consider the behavior of inference when index data are simulated from  
 92 three parameter PT and Schnute production models, but the simulated data are fit using  
 93 intentionally misspecified two parameter logistic or BH production models. The work begins  
 94 with a derivation of RPs under the three parameter models. A method is then presented  
 95 for generating simulation designs based on the parametric form of RPs which serves as a  
 96 control on the nature of simulated model misspecification. Finally a Gaussian Process (GP)  
 97 metamodel ([Gramacy, 2020](#)) is constructed for exploration and analysis of RP biases.

98 A key insight of this approach is that bias is considered broadly across RP-space to  
 99 uncover patterns and correlations between RPs. The GP metamodel is explicit about trade-  
 100 offs between RPs so as to inform the full utility of reducing bias, as well as to suggest  
 101 mechanisms for understanding what causes bias. Further, the effect of contrast on estimation  
 102 is considered together with model misspecification.

## 103 2 Methods

### 104 2.1 Pella-Tomlinson Model

The three parameter Pella-Tomlinson (PT) family has a convenient form that includes, among others ([Fox Jr., 1970](#); [Rankin & Lemos, 2015](#)), the logistic production function as a special case. PT production function is parameterized so that  $\boldsymbol{\theta} = [r, K, \gamma]$  and the family takes the following form,

$$P_p(B; [r, K, \gamma]) = \frac{rB}{\gamma - 1} \left( 1 - \left( \frac{B}{K} \right)^{(\gamma-1)} \right). \quad (1.3)$$

$\gamma$  is a parameter which breaks PT out of the restrictive symmetry of the logistic curve. In general  $\gamma \in (1, \infty)$ , with the logistic model appearing in the special case of  $\gamma = 2$ , and the Fox model appearing as a limiting case as  $\gamma \rightarrow 1$ . The parameter  $r$  controls the maximum reproductive rate of the population in the absence of competition for resources (i.e. the slope of production function at the origin).  $K$  is the so called "carrying capacity" of the population. In this context the carrying capacity can be formally stated as steady state biomass in the absence of fishing (i.e.  $\bar{B}(0) = K$ ). In Figure (3.15) PT recruitment is shown for a range of parameter values so as to demonstrate the various recruitment shapes that can be achieved by PT recruitment.

While the form of the PT curve produces some limitations (Fletcher, 1978), importantly the introduction of a third parameter allows enough flexibility to fully describe the space of reference points used in management. To see this, the reference points are analytically derived for the PT model below.

### PT Reference Points

With  $B(t)$  representing biomass at time  $t$ , under PT production, the dynamics of biomass are defined by the following ODE,

$$\frac{dB}{dt} = \frac{rB}{\gamma - 1} \left( 1 - \left( \frac{B}{K} \right)^{\gamma-1} \right) - FB. \quad (1.4)$$

An expression for the equilibrium biomass is attained by setting Eq (3.16) equal to zero, and rearranging the resulting equation to solve for  $B$ . Thinking of the result as a function

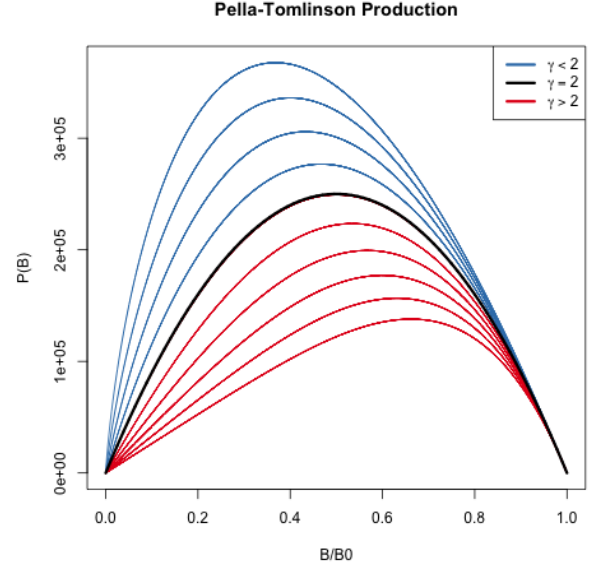


Figure 1.2: The Pella-Tomlinson production function plotted across a variety of parameter values. The special cases of Logistic production is shown in black, and the left-leaning and right-leaning regimes are shown in blue and red respectively.

of  $F$  gives,

$$\bar{B}(F) = K \left( 1 - \frac{F(\gamma - 1)}{r} \right)^{\frac{1}{\gamma-1}}. \quad (1.5)$$

At this point it is convenient to notice that  $\bar{B}(0) = K$ . The expression for  $B^*$  is given by evaluating Eq (3.17) at  $F^*$ . To get an expression for  $F^*$ , the equilibrium yield is maximized with respect to  $F$ ,

$$F^* = \operatorname{argmax}_F F \bar{B}(F). \quad (1.6)$$

In the case of PT production this maximization can be done analytically, by differentiating the equilibrium yield with respect to  $F$  as follows,

$$\frac{d\bar{Y}}{dF} = \bar{B}(F) + F \frac{d\bar{B}}{dF} \quad (1.7)$$

$$\frac{d\bar{B}}{dF} = -\frac{K}{r} \left( 1 - \frac{F(\gamma - 1)}{r} \right)^{\frac{1}{\gamma-1}-1}. \quad (1.8)$$

Setting Eq (3.19) equal to 0, substituting  $\bar{B}(F)$  and  $\frac{d\bar{B}}{dF}$  by Equations (3.17) and (3.20) respectively, and solving for  $F$  produces the following expression for the fishing rate required to produce MSY,

$$F^* = \frac{r}{\gamma} \quad (1.9)$$

Plugging the above expression for  $F^*$  back into Eq (3.17) gives the following expression for biomass at MSY,

$$B^* = K \left( \frac{1}{\gamma} \right)^{\frac{1}{\gamma-1}}. \quad (1.10)$$

The above derived expressions for  $\bar{B}(0)$ ,  $B^*$ , and  $F^*$  can then be used to build a specific analytical form for the biological reference points in terms of only productivity parameters.

$$F^* = \frac{r}{\gamma} \quad \quad \quad \frac{B^*}{\bar{B}(0)} = \left( \frac{1}{\gamma} \right)^{\frac{1}{\gamma-1}} \quad (1.11)$$



## 132 Simulation

Generating simulated indices of abundance from the PT model requires inverting the relationship between  $\left(F^*, \frac{B^*}{B(0)}\right)$ , and  $(r, \gamma)$ . It is not generally possible to analytically invert this relationship for many three parameter production functions (Punt & Cope, 2019; J. T. Schnute & Richards, 1998). Most three parameter production functions lead to RPs that require expensive numerical methods to invert; more over the numerical inversion procedure can often be unstable. That said, for the case of PT this relationship is analytically invertible, and leads to the following relationship

$$r = \gamma F^* \qquad \gamma = \frac{W\left(\frac{B^*}{B(0)} \log\left(\frac{B^*}{B(0)}\right)\right)}{\log\left(\frac{B^*}{B(0)}\right)}. \quad (1.12)$$

133 Above  $W$  is the Lambert product logarithm function. More details about this derivation,  
134 and the Lambert product logarithm, are given in Appendix (7 ).

135 Using Eq. (3.24) to obtain production parameters, a PT production model can be fully  
136 defined for any combination of the RPs  $F^*$  and  $\frac{B^*}{B(0)}$ . Since  $K$  does not enter the RP  
137 calculation its value is fixed arbitrarily at 10000.

138 Indices of abundance are simulated from the three parameter PT production model  
139 broadly over the space of  $F^*$  and  $\frac{B^*}{B(0)}$  via a space filling design as described in Section  
140 (5 .3). A small amount of residual variation,  $\sigma = 0.01$ , is added to the simulated index, and  
141 these data are then fit with a Schaefer model, at various degrees of misspecification, so as to  
142 observe the effect of productivity model misspecification upon RP inference.

## 143 PT Design

144 Letting  $\mathcal{F}$  and  $\mathcal{B}$  be regular grids, of size  $n = 100$ , on  $F^* \in (0.1, 0.7)$  and  $\frac{B^*}{B_0} \in (0.2, 0.6)$   
145 respectively, a LHS design of size 100 is collected among the cells produced by  $\mathcal{F} \times \mathcal{B}$ .

146 Each of the sampled LHS design locations represent a unique PT model with the sampled  
147 RP values. Since the relationship mapping RPs analytically to productivity parameters can  
148 be found for the PT model, LHS designs the the PT model are computed directly in RP  
149 space and Eq. (3.24) is used to map the sampled RP design locations to PT productivity  
150 parameters.

## 2.2 Gaussian Process Metamodel

At its core, a metamodel is simply a model of some mapping of inputs to outputs (the mapping itself is typically defined by a computer model). By modeling the mapping with a statistical model (that explicitly defines the relevant features of the mapping) a metamodel defines a specific ontology for the mapping. By simulating examples of the mapping, the inferential infrastructure of the statistical model is used to empirically learn an effective emulation of the mapping within the ontology defined by the statistical model. The predictive infrastructure of the statistical model is then useful as an approximate abstraction of the system itself to better understand the system through further data collection, cheap approximation of the mapping, and/or study of the mapping itself.

In this setting, the aim of metamodeling is to study how well RPs are inferred when typical two parameter models of productivity (Logistic and BH) are misspecified for populations that are actually driven by more complicated dynamics. The simulation design,  $\mathbf{X}$ , provides a sample of different population dynamics that are driven by three parameter production functions broadly in RP space. By simulating index of abundance data from the three parameter model, and fitting those data with the two parameter production model, we observe particular instances of how well RPs are inferred at the given misspecification of the two parameter model relative to the true three parameter production model. By gathering all of the simulated instances of how RPs are inferred (under the two parameter model), we form a set of example mappings to train a metamodel which represents the mapping of true RPs (under the three parameter model) to estimates of RPs under the misspecified two parameter production model. The metamodel is essentially a surrogate for inference under the misspecified two parameter production model that controls for the specific degree of model misspecification.

A flexible GP model is assumed for the structure of the metamodel to describe the mapping of RPs under misspecified two parameter models of productivity. A GP is a stochastic process generalizing the multivariate normal distribution to an infinite dimensional analog. GP models are often specified primarily through the choice of a covariance (or correlation) function which defines the relationship between locations in the input space. Typically corre-

180 lation functions are specified so that points closely related in space result in correlated effects  
 181 in the model. In this setting the inputs to the GP metamodel are the space of reference points  
 182 which define the simulated three parameter production models.

While index of abundance data are generated from three parameter models, at each design location of the simulation, fitting the restricted two parameter model results in a maximum likelihood estimate (MLE; and associated estimation uncertainty) of each of the productivity parameters (i.e. Schaefer:  $[\log(r), \log(K)]$ , BH:  $[\log(\alpha), \log(\beta)]$ ). To simplify the specification of the metamodel, let  $\mathbf{y}$  be a vector collecting the fitted MLEs for one of the productivity parameters, and let  $\boldsymbol{\omega}$  be a vector of estimates of the estimator variances (via the inverted Fisher information) at each  $\mathbf{y}$ . Each of the fitted productivity parameter estimates are then modeled using independent instances of the following GP metamodel.

$$\begin{aligned}\mathbf{y} &= \beta_0 + \mathbf{X}\boldsymbol{\beta} + \mathbf{v} + \boldsymbol{\epsilon} \\ \mathbf{v} &\sim N_n(\mathbf{0}, \tau^2 \mathbf{R}_\ell) \\ \boldsymbol{\epsilon} &\sim N_n(\mathbf{0}, \boldsymbol{\omega}' \mathbf{I})\end{aligned}\tag{1.13}$$

183  $\mathbf{X}$  is the  $n \times 2$  LHS design matrix of RPs for each simulated three parameter data  
 184 generating model as described in Section (5.3).  $\epsilon$  models independent normally distributed  
 185 error, which provides an ideal mechanism for propagating uncertainty from inference in the  
 186 simulation step into the metamodel. By matching each  $\mathbf{y}_i$  with an observed  $\omega_i$  variance term,  
 187  $\epsilon$  serves to down weight the influence of each  $\mathbf{y}_i$  in proportion to the inferred production model  
 188 sampling distribution uncertainty. This has the effect of smoothing the GP model in a way  
 189 similar to the nugget effect (Gramacy & Lee, 2012), although the application here models  
 190 this effect heterogeneously.

The term,  $\mathbf{v}$ , contains spatially correlated GP effects. The correlation matrix,  $\mathbf{R}_\ell$  describes how RPs close together in the simulation design are more correlated than those that are far away. This spatial effect is modeled with a squared exponential correlation function,

$$R(\mathbf{x}, \tilde{\mathbf{x}}) = \exp \left( \sum_{i=1}^2 \frac{-(x_i - \tilde{x}_i)^2}{2\ell_j^2} \right).\tag{1.14}$$

$R$  has an anisotropic separable form which allows for differing length scales,  $\ell_1$  and  $\ell_2$ , in the different RP axes. The flexibility to model correlations separately in the different RP axes is key due to the differences in the extent of the RP domains marginally. The metamodel parameters  $\beta_0$ ,  $\boldsymbol{\beta}$ ,  $\tau^2$ ,  $\ell_1$  and  $\ell_2$  are fit via MLE against the observations  $\mathbf{y}$ ,  $\mathbf{X}$ , and  $\boldsymbol{\omega}$  from simulation fits.

Fitting the metamodel allows for a full predictive description of inference under the misspecified restricted models. Predictive estimates are obtained via kriging (Cressie, 2015)

$$\hat{y}(\mathbf{x}) = \beta_0 + \mathbf{x}\boldsymbol{\beta} + \mathbf{r}(\mathbf{x})'\mathbf{R}_\ell^{-1}\left(\mathbf{y} - (\beta_0 + \mathbf{X}\boldsymbol{\beta})\right) \quad (1.15)$$

$\hat{y}(\mathbf{x})$  is the predicted value of the modeled productivity parameter MLE under the two parameter production model, when the index of abundance is generated from the three parameter production model at RP location  $\mathbf{x}$ .  $\mathbf{r}(\mathbf{x})$  is a vector-valued function of correlation function evaluations for the predictive location  $\mathbf{x}$  against all observations in  $\mathbf{X}$  (i.e.  $\mathbf{r}(\mathbf{x}) = \mathbf{R}(\mathbf{x}, \mathbf{x}_i) \forall \mathbf{x}_i \in \mathbf{X}$ ).

While metamodeling occurs on the inferred productivity parameters of the restricted production model, the metamodel can also be used to build estimates of major biological RPs. For the BH model the relevant transformations for relating productivity parameters with RPs are given in Eqs. (3.29, 3.32) with  $\gamma$  fixed to -1; for the Schaefer model  $\hat{B}^* = \frac{\hat{K}}{2}$  and  $\hat{F}^* = \frac{\hat{r}}{2}$ . Applying the metamodel predictive surfaces on the scale of RP estimates allows for the quantification of estimation bias that is induced by fitting a misspecified two parameter production model to indices of abundance generated under three parameter productivity.

## 2.3 Catch

It is known that contrast in the observed index and catch time series can effect inference on the productivity parameters (Hilborn & Walters, 1992). In this setting contrast refers to changes in the long term trends of index data. Figure (3.20, *right*) demonstrates an example of biomass that includes contrast induced by catch. It is not well understood how contrast may factor into inferential failure induced by model misspecification. Thus catch is parameterized so as to allow for a spectrum of possible contrast simulation settings.

217 Catch is parameterized so that  $F(t)$  can be controlled with respect to  $F^*$ . Recall that  
 218 catch is assumed to be proportional to biomass, so that  $C(t) = F(t)B(t)$ . To control  $F(t)$   
 219 with respect to  $F^*$ ,  $C(t)$  is specified by defining the quantity  $\frac{F(t)}{F^*}$  as the relative fishing rate.  
 220  $B(t)$  is defined by the solution of the ODE, and  $F^*$  is defined by the biological parameters  
 221 of the model. By defining  $\frac{F(t)}{F^*}$ , catch can then be written as  $C(t) = F^* \left( \frac{F(t)}{F^*} \right) B(t)$ .

222 Intuitively  $\frac{F(t)}{F^*}$  describes the fraction of  $F^*$  that  $F(t)$  is specified to for the current  $B(t)$ .  
 223 When  $\frac{F(t)}{F^*} = 1$ ,  $F(t)$  will be held at  $F^*$ , and the solution of the ODE brings  $B(t)$  into  
 224 equilibrium at  $B^*$ . When  $\frac{F(t)}{F^*}$  is held constant in time biomass comes to equilibrium as an  
 225 exponential decay from  $K$  approaching  $B^*$ . When  $\frac{F(t)}{F^*} < 1$ ,  $F(t)$  is lower than  $F^*$  and  $B(t)$  is  
 226 pushed toward  $\bar{B} > B^*$ . Contrarily, when  $\frac{F(t)}{F^*} > 1$ ,  $F(t)$  is higher than  $F^*$  and  $B(t)$  is pushed  
 227 toward  $\bar{B} < B^*$ ; the precise values of  $\bar{B}$  can be calculated from the steady state biomass  
 228 equations provided above and depend upon the specific form of the production function.

For the simulations presented here, a family of fishing behaviors are considered where the fishing rate accelerates as technology and fishing techniques improve rapidly until management practices are applied, which ultimately brings fishing into equilibrium at  $F^*$ . This is parameterized as three distinct phases, over a total of 45 units of time, with each phase lasting 15 time units. The specific form is given below.

$$\frac{F(t)}{F^*} = ae^{bt}\mathbf{1}_{0 \leq t < 15} + (d - ct)\mathbf{1}_{15 \leq t < 30} + \mathbf{1}_{30 \leq t \leq 45} \quad (1.16)$$

The first term of Eq(3.41) is an exponential increase in fishing, the second term is a linear decline in relative fishing as initial management practices are applied, and the third term,  $\mathbf{1}_{30 \leq t \leq 45}$ , simply holds the fishing rate at  $F^*$  there after. These three phases are controlled by the four parameters  $a$ ,  $b$ ,  $c$ , and  $d$ . By enforcing that the interface of the phases meet at  $\chi_{max}$  and 1 respectively the relative fishing series is reduced to a two parameter family.

$$a = e^{\log(\chi_{max}) - 15b} \quad b = \frac{1}{t - 15} \log \left( \frac{\chi_{min}}{\chi_{max}} \right) \quad (1.17)$$

$$c = \frac{\chi_{max} - 1}{15 - 1} \quad d = 15c + \chi_{max} \quad (1.18)$$

229 By further specifying  $\chi_{max} = 1.6^x$  and  $\chi_{min} = 0.4^x$  the two parameters  $\chi_{max}$ , and  $\chi_{min}$

can be reduced to the single parameter  $\chi$ . The tuning parameter  $\chi$  then singularly controls contrast that appears in time series data.

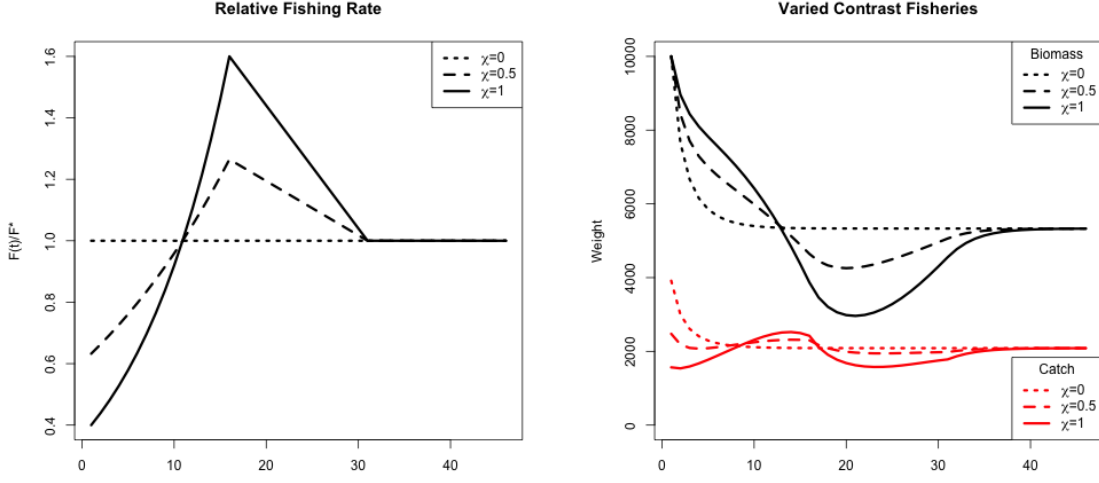


Figure 1.3: (left) Relative fishing with low, medium, and high contrast. (right) Population biomass and catch at each associated level of contrast.

When  $\chi = 0$ , the relative fishing rate is a constant at 1 to create a low contrast simulation environment. As  $\chi$  increases Eq (3.41) induces more and more contrast in the observed index and catch time series until  $\chi = 1$  which produces a high contrast simulation environment. Figure (3.20) demonstrates a spectrum of contrast simulation environments as well as the time series data they induce in the solution of the production model ODE.

## 2.4 Two Parameter Production Model Inference

The simulated mapping results from fitting an intentionally misspecified two parameter production model to index of abundance data that are generated from a more complex three parameter model of productivity. Thus, let  $I_t$  be an index of abundance simulated from the three parameter PT or Schnute production models at time  $t \in \{1, 2, 3, \dots, T\}$ . However the fitted model is specified to be intentionally misspecified so that the fitted model is driven by a two parameter Schaefer, or BH production model respectively.

The observation model for the fitted model is log-normal such that,

$$I_t|q, \sigma^2, \boldsymbol{\theta} \sim LN(qB_t(\boldsymbol{\theta}), \sigma^2). \quad (1.19)$$

$B_t(\boldsymbol{\theta})$  is defined by the solution of the ODEs defined by the Schaefer, or BH models. For

the Schaefer model  $\boldsymbol{\theta} = [r, K]$ , and for the BH model  $\boldsymbol{\theta} = [\alpha, \beta]$ . From the perspective of the fitted model, the observed  $I_t$  are assumed independent conditional on  $q$ ,  $\sigma^2$ ,  $r$ ,  $K$  and the two parameter ODE model for biomass. Thus the log likelihood can be written as

$$\log \mathcal{L}(q, \sigma^2, \boldsymbol{\theta}; I) = -\frac{T}{2} \log(\sigma^2) - \frac{1}{2\sigma^2} \sum_t \log \left( \frac{I_t}{qB_t(\boldsymbol{\theta})} \right)^2. \quad (1.20)$$

In this setting,  $q$  is fixed at the true value of 0.0005 to focus on the inferential effects of model misspecification on biological parameters.  $\sigma^2$  and  $\boldsymbol{\theta}$  are reparameterized to the log scale and fit via MLE. Reparameterizing the parameters to the log scale improves the reliability of optimization, in addition to facilitating the use of Hessian information for estimating MLE standard errors.

Given that the biological parameters enter the likelihood via a nonlinear ODE, and further the parameters themselves are related to each other nonlinearly, the likelihood function can often be difficult to optimize. A hybrid optimization scheme is used to maximize the log likelihood to ensure that a global MLE solution is found. The R package GA ([Scrucca, 2013, 2017](#)) is used to run a genetic algorithm to explore parameter space globally. Optimization periodically jumps into the L-BFGS-B local optimizer to refine optima within a local mode. The scheme functions by searching globally, with the genetic algorithm, across many initial values for starting the local gradient-based optimizer. The genetic algorithm serves to iteratively improve hot starts for the local gradient-based optimizer. Additionally, optimization is only considered to be converged when the optimum results in an invertible Hessian at the found MLE.

## 2.5 Continuous model formulation

An important (and often overlooked) implementation detail is the solution to the ODE which defines the progression of biomass through time. As a statistical model it is of paramount importance that this ODE not only have a solution, but also that the solution be unique. Of primary concern, uniqueness of the ODE solution is necessary for well conditioned inference.

If the form of  $\frac{dB}{dt}$  is at least Lipschitz continuous, then the Cauchy-Lipschitz-Picard theorem provides local existence and uniqueness of  $B(t)$ . Recall from Eq(3.14) that  $\frac{dB}{dt}$  is

separated into a term for biomass production,  $P(B)$ , and a term for removals,  $Z(t)B(t)$ . For determining Lipschitz continuity of  $\frac{dB}{dt}$ , the smallest Lipschitz constant of  $\frac{dB}{dt}$  will be the sum of the constants for each of the terms  $P(B)$  and  $Z(t)B(t)$  separately. Typically any choice of  $P(B)$  will be continuously differentiable, which implies Lipschitz continuity. At a minimum  $Z(t)$  typically contains fishing mortality as a function of time  $F(t)$  to model catch in time as  $C(t) = F(t)B(t)$ .  $Z(t)$  may or may not contain  $M$ , but typically  $M$  is modeled as stationary in time and does not pose a continuity issue, unlike some potential assumptions for  $C(t)$ .

In practice  $C(t)$  is determined by a series of observed, assumed known, catches. Catch observations are typically observed on a quarterly basis, but in practice may not be complete for every quarter (or year) of the modeled period. It is overwhelmingly common to discretize the ODE in time via Euler's method with integration step sizes to match the observation frequency of the modeled data. This is often computationally convenient when the underlying species dynamics are reasonably well behaved, however when the dynamics model is used as a statistical model, with the goal of inferring the behavior of the underlying species dynamics, the regularity of the dynamics are not guaranteed. An implicit assumption of continuity of catch in time provides the necessary regularity for the statistical model. Furthermore a continuous handling of the dynamics provides improved accuracy in evaluating the ODE, particularly when inferring productivity parameters which largely control the regularity of the dynamics.

While there are many ways to handle catch continuity, here I assume that catches accrue linearly between observed catches. This assumption defines the catch function as a piecewise linear function of time, with the smallest Lipschitz constant for the catch term defined by the steepest time segment of the catch function. This assumption represents one of the simplest ways of handling catch, while retaining Lipschitz continuity overall. Furthermore linearly interpolated catch is adequately parsimonious for the typical handling of catches.

## Integration and Stiffness

As previously mentioned, the overwhelming majority of implementations of stock assessment models discretized the ODE using Euler's method with the integration step sized fixed so as to match the observation frequency. In this setting we explore model parameterizations that



explore the full extent of biologically relevant reference points. This exercise produces some combinations of parameters that result in numerically stiff ODEs.

The concept of stiffness in ODEs is hard to precisely characterize. [Wanner and Hairer \(1996, p.2\)](#) describe stiffness in the following pragmatic sense, “Stiff equations are problems for which explicit methods don’t work”. It is hard to make this definition more mathematically precise, but this is a consistent issue for models of fast growing species in the low contrast simulation. Euler’s method, as often implemented, is particularly poorly suited for these stiff regions of parameter space. In these stiff regions it is necessary to integrate the ODE with an implicit integration method.

Several of the most common implicit methods were tried including the Livermore Solver for ODEs (lsode), and the Variable Coefficient ODE Solver (vode) as implemented in the deSolve package of R ([Soetaert et al., 2010](#)). The difference between implicit solvers is negligible, while explicit methods result in wildly varying solutions to the ODE in stiff regions of parameter space. Results shown here are computed using the lsode integration since it runs relatively quickly and has a relatively smaller footprint in system memory.

### 3 Results

#### 3.1 PT/Schaefer

##### An $MSY$ -Optimal Catch History

When  $F(t)$  is held constant at  $F^*$ , as it is in the "low contrast" simulation setting,  $B(t)$  comes to equilibrium as an exponential decay from  $K$  to  $B^*$ . Understanding model misspecification bias is simplified in this setting due to the relative simplicity that this induces in  $B(t)$ . However this simplicity is known to poorly inform estimates of  $r$ , and thus  $F^*$ , due to the limited range of the production function that is observed (Hilborn & Walters, 1992).

Figure (3.21) shows four of the most misspecified example production function fits as compared to the true data generating PT production functions. The rug plots below each set of curves show how the observed biomasses decay exponentially from  $K$  to  $B^*$  in each case. In particular, notice how observations only exist where the PT biomass is greater than  $B^*$ . Due to the leaning of the true PT curves, and the symmetry of the logistic parabola, the logistic curve only observes information about its slope at the origin from data observed on the right portion of the PT curves. The top two panels of Figure (3.21) shows PT data generated such that  $\frac{B^*}{B(0)} > 0.5$ ; in these cases PT is steeper to the right of  $B^*$  than it is on the left, and so the the logistic curve over-estimates  $r$ , and consequently also over-estimates  $F^*$ . The

bottom two panels of Figure (3.21) show PT data generated with  $\frac{B^*}{B(0)} < 0.5$  and where the vice versa phenomena occurs. PT is shallower to the right of  $B^*$  than it is on the left

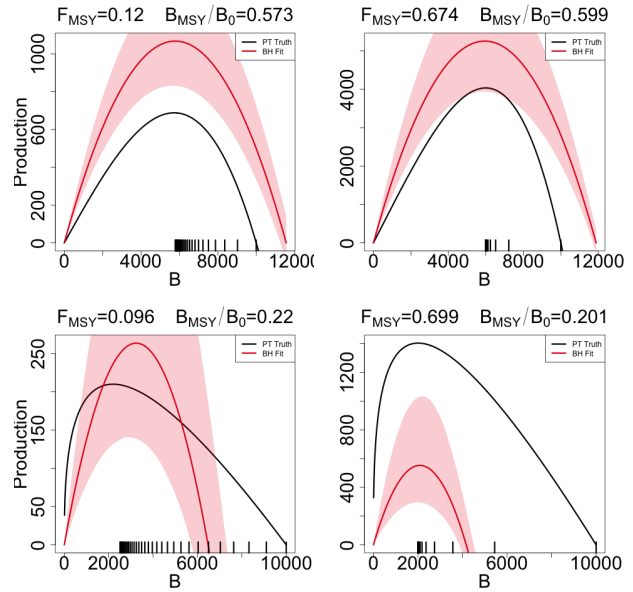


Figure 1.4: A comparison of the true PT production function (in black) and the estimated logistic curve (in red) with 95% CI shown. The examples shown represent the four corners of maximum model misspecification in the simulated RP-space. Observed biomasses are plotted in the rug plots below the curves.

and so the logistic parabola estimate tends to under estimate  $F^*$ .

### Metamodeled Trends

Each point in the space of the RPs  $F^*$  and  $\frac{B^*}{B(0)}$  uniquely identifies a complete PT model with different combinations of parameters values. Recall that when  $\gamma = 2$  for the PT model, the PT curve becomes a parabola and is equivalent to the logistic curve of the Schaefer model. Since the logistic curve is symmetric about  $B^*$ , the Schaefer model must fix the value of  $\frac{B^*}{B(0)}$  at the constant 0.5 for any value of  $F^*$ . So the line through RP space defined by  $\frac{B^*}{B(0)} = 0.5 \quad \forall \quad F^*$ , defines the subset of RP space where  $\gamma = 2$  and where the PT model is equivalent to the Schaefer model. For brevity this subset of RP where  $\frac{B^*}{B(0)} = 0.5$  will be referred to as the ‘‘Schaefer set’’. Thus simulated data that are generated along the Schaefer set will be the only data that are not misspecified relative to the Schaefer model; as PT data are simulated farther and farther away from this line at  $\frac{B^*}{B(0)} = 0.5$  model misspecification of the Schaefer model becomes worse and worse.

While Figure (3.21) demonstrates a real trend in simulation results, individual simulation runs will at best show jittery trends due to the stochastic nature of statistical inference. The GP process metamodel accounts for this stochasticity to focus analysis on the signal in the simulation results. Recall that metamodeling occurs on the scale of the inferred productivity parameters of the restricted production model, by transforming metamodel predictions via Eq. (3.23), metamodeled predictions are obtained for Schaefer RPs. By further subtracting the true data generating PT RPs from the predicted Schaefer RPs at each point in RP space a pattern of inferential RP bias, induced by model misspecification of the Schaefer model, can be seen.

Figure (3.22) shows the pattern of biases the Schaefer model creates when fit to PT data generated at each point of RP space. An equivalent way to think of Figure (3.22) is that since the Schaefer model must estimate RPs in the Schaefer set, the metamodel arrows indicate the mapping that is created by inferring RPs under a misspecified Schaefer model fit to PT data generated at each point over the pictured region.

Since  $\frac{B^*}{B_0}$  must be 0.5 under the Schaefer model, biases in the  $\frac{B^*}{B_0}$  direction must simply map vertically onto the Schaefer set. Due to this simplified RP geometry under the Schaefer

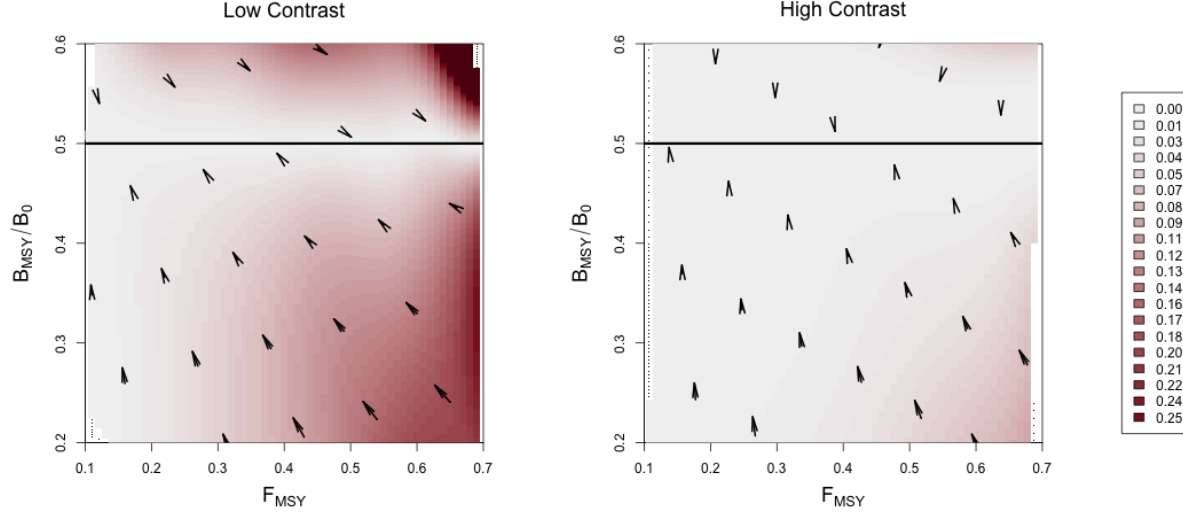


Figure 1.5: Joint bias direction for  $(F^*, \frac{B^*}{B_0})$  estimates under the misspecified Schaefer Model. The intensity of color represents the excess bias relative to the shortest possible mapping. Results in the low contrast setting are shown *left*, and the high contrast setting is shown *right*.

model, the degree of bias in  $\frac{B^*}{B_0}$  estimation is defined solely by the degree of model misspecification irrespective of  $F^*$ . Furthermore, the closest possible point along the Schaefer set that Schaefer model inference could map RPs would be the perfectly vertical mapping. This pattern only contains the strictly necessary bias present in  $\frac{B^*}{B_0}$ , and zero bias in  $F^*$ . Any deviation from this minimal bias pattern is necessarily due to added bias in  $F^*$ .

The two simulation settings shown in Figure (3.22) are identical except for the amount of contrast present in the simulated index. The left panel of Figure (3.22) shows RP biases in the low contrast setting, while the right panel shows the high contrast setting. Notice that in the low contrast setting the RP bias pattern is far from the minimum distance mapping, however when contrast is added the mapping becomes much closer to a minimal bias mapping. In the low contrast setting the observed bias is consistent with the pattern and mechanism described in Figure (3.21), where  $F^*$  is underestimated for data generated below the Schaefer line and overestimated above the Schaefer set. In the high contrast simulation the mapping is nearly minimal distance with the exception of PT data generated with simultaneously low  $\frac{B^*}{B_0}$  and high  $F^*$ .

Figure (6.1) demonstrates how bias in  $F^*$  estimation decreases as contrast is added to

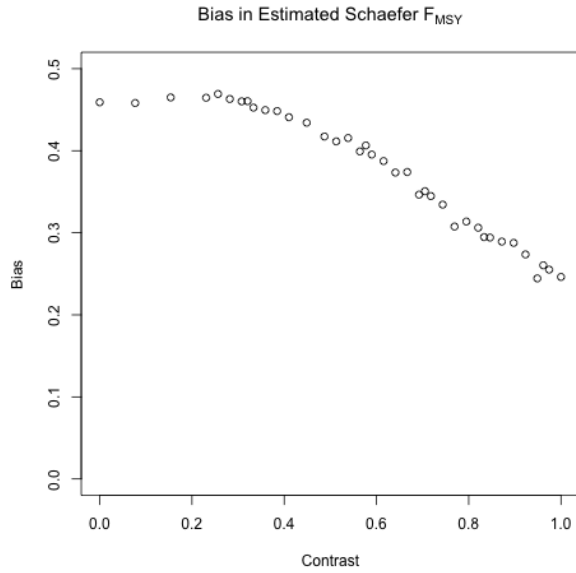


Figure 1.6: Bias in  $F^*$  under the Schaefer model when PT data are generated with increasing contrast so that  $F^*$  and  $\frac{B^*}{B_0}$  are fixed at 0.699 and 0.201 respectively.

PT data as generated in the low  $\frac{B^*}{B_0}$  and high  $F^*$  regime. By including additional contrast  $F^*$  bias is decreased, however parameterizing contrast so as to fully extinguish  $F^*$  bias may require a more complex model of fishing.

## 4 Discussion

Results presented here generally agree with what is known about estimating growth rate parameters (Lee et al., 2012; Conn et al., 2010; Magnusson & Hilborn, 2007). These study's appreciate the role of contrast for estimating growth rates, however they struggle to make generally extensible conclusions since they focus only on a handful of stocks that fall short of forming a random sample of the greater population of possible stock behaviors. The LHS design methods presented here are designed specifically to simulate a representative sample of stocks broadly across the space of possible RPs. Furthermore, the simulation design, taken together with the GP metamodel of productivity parameter estimates, allows this study to control the degree of model misspecification and generalize conclusions about the behavior of productivity estimation within the production model setting presented.

In the presence of contrast,  $F^*$  estimation can enjoy very low bias even for a wide range of poorly specified models; conversely in the absence of contrast  $F^*$  estimation can suffer very large bias even for slightly misspecified models. This pattern is particularly true for inference

under the Schaefer model where the geometry of the restricted RP set isolates estimation failure of  $F^*$  from  $\frac{B^*}{B(0)}$ . While contrast has a similar impact on  $F^*$  estimation under the BH model, the geometry of the BH RP set correlates estimation bias of  $F^*$  and  $\frac{B^*}{B(0)}$ . The GP metamodeling approach reveals a more general pattern that highly informative data sets (high contrast) produces a nearly minimal distance mapping of RPs onto the constrained RP set.

In all cases when model misspecification is removed, even with weakly informative data, RP estimation is unbiased and well estimated. Thus contrast alone is not the only factor leading to inferential failure. Model misspecification is a necessary but not sufficient condition for inducing RP estimation bias. The particular RP bias present depends on the RP geometry of the fitted model and how that geometry is misspecified relative to the data. The RP mapping is then oriented to the RP geometry of the fitted model.

While the relative fishing rate parameterized in Section (5.5) captures a usefully broad spectrum of relevant fishing behaviors, it is still limiting in the amount of information that it can induce. Improved methods for quantifying contrast in fisheries data, and/or methods of discovering more informative fishing behavior, could improve this analysis. In the absence of a maximally informative dataset simulation methods will not fully describe how inference fails, but the methods presented here tell the most complete picture yet, with explicit control of the degree model misspecification, contrast, and a simulation design that allows for uniform representative data generation across biologically meaningful stocks. The results presented here suggest the conjecture that under a maximally informative dataset, RP inference with a two parameter production function will be biased in the direction a shortest distance map from the true RPs onto restricted set of RPs under the two parameter model.

Given the potential for model misspecification of RPs, a minimal distance mapping of RPs represents a best-case scenario where the total bias of RPs, when measured jointly, is minimized. That said, without recognizing the geometry of how two parameter models of productivity limit RP space this may lead to unintuitive implications in RP estimation. For example, due to the shape of the BH RP set a minimal distance mapping ensures that if there is bias in one of  $\frac{B^*}{B_0}$  or  $F^*$ , there will necessarily be bias in the other RP. However under the Schaefer model, since the RP set is a constant in  $\frac{B^*}{B_0}$ , bias in  $F^*$  is not adulterated in the

same way by bias in  $\frac{B^*}{B_0}$  estimation. While models with constant RPs, such as the logistic model  $\frac{B^*}{B_0} = \frac{1}{2}$  or the Fox model  $\frac{B^*}{B_0} = \frac{1}{e}$ , are extremely limited, they can be valuable tools for developing intuition precisely because they isolate RP estimation in their free RPs from the correlated RP biases present in models like the BH or Ricker model.

When one considers the implications of RP bias, overestimation of RPs carries the severe implication of management recommendations potentially leading to overfishing, while underestimation of RP leads to overly conservative management. In this sense, when the true model is not known, the geometry of the BH set together with the metamodeled bias trends makes the BH model a naturally conservative estimator of RPs for most stocks. For most non-BH populations the BH model is likely to make conservative errors in its estimates of  $F^*$  and  $\frac{B^*}{B_0}$ . The one notable exception to the conservatism of the BH model stands for data generated in the Cushing-like regime of Schnute RPs. In this regime the BH model tends to be fairly unbiased overall, however the bias that is present for these populations tends to be overestimation in both RPs, leading to much more severe management consequences for those populations.

The RP bias trends of the Schaefer model demonstrate much less conservatism than the BH overall. For any population with  $\frac{B^*}{B_0} < 0.5$ ,  $\frac{B^*}{B_0}$  will be overestimated. When the population comes from the regime where  $\frac{B^*}{B_0} > 0.5$ ,  $\frac{B^*}{B_0}$  will be under estimated, but  $F^*$  is likely to be overestimated depending on the degree of contrast present in the data. So while the Schaefer model is an intuitive model, it tends to lead to much less conservative RP estimation.

While it is important to recognize these limitations of two parameter models of productivity, we should not solely accept conservatism as a rationale of choosing a BH model of productivity. Increasing the flexibility of the production function by moving toward three parameter models would release the underlying structural limitations (Mangel et al., 2013) that cause these RP biases in the first place. Punt and Cope (2019) considers a suite of possible three parameter curves which could be used instead of current two parameter curves. For all of their benefits, three parameter production functions have their own complicating factors, and the structure present in the Schnute model explored here makes it an intuitive bridge model for developing three parameter models going forward.

- show a schnute fit to data? (Yeakel & Mangel, 2015) Prior



- summary of  $\sigma$  over RP space comparing between models (PT, Schnute, Schnute DD) to show areas of model breakdown.

  - miss-identifying signal for noise.
  - It happens more as the dynamics get more complex.
  - point to the full age structured models.
- show the constrained BH space over a grid of  $M, \kappa, \omega, W_\infty$
- Show that the constrained spaces vary only slightly as compared with the consequences of misspecifying the functional form.
- estimating these other quantities (while they can create quite different Biomass series) can only do so much to improve (expand) RP inference as compared with correctly modeling  $P$ .
- mapping distance as a function of contrast at  $(3.5, 0.5)$
- for LHS grid locations show  $\frac{B^*}{B_0}$  and  $F^*$  biases for grids in  $M \in (0, 0.5)$  For sure in High Contrast, maybe also in Low??.

## 5 Appendix: Inverting $\frac{B^*}{B(0)}$ and $\gamma$ for the PT Model

For brevity let  $\zeta = \frac{B^*}{B(0)}$ .

$$\begin{aligned}\zeta &= \left(\frac{1}{\gamma}\right)^{\frac{1}{\gamma-1}} \\ \zeta &= \gamma \zeta^\gamma \\ \zeta &= \gamma e^{\gamma \log(\zeta)} \\ \zeta \log(\zeta) &= \gamma \log(\zeta) e^{\gamma \log(\zeta)}\end{aligned}$$

The Lambert product logarithm,  $W$ , is defined as the inverse function of  $z = xe^x$  such that  $x = W(z)$ . Applying this definition allows for the isolation of  $\gamma$ .

$$\begin{aligned}\gamma \log(\zeta) &= W(\zeta \log(\zeta)) \\ \gamma &= \frac{W(\zeta \log(\zeta))}{\log(\zeta)}\end{aligned}\tag{1.21}$$

The Lambert product logarithm is a multivalued function with a branch point at  $-\frac{1}{e}$ . The principal branch,  $W_0(z)$ , is defined on  $z \in (-\frac{1}{e}, \infty)$ , and the lower branch,  $W_{-1}(z)$ , is defined on  $z \in (-\frac{1}{e}, 0)$ . Taken individually, each respective branch is analytic, but cannot be expressed in terms of elementary functions.

When  $\zeta \in (0, \frac{1}{e})$  the solution of interest in Eq. (3.24) comes from  $W_0$ . When  $\zeta \rightarrow \frac{1}{e}$ , the Fox Model emerges as  $\gamma \rightarrow 1$ . When  $\zeta \in (\frac{1}{e}, 1)$  the solution of interest comes from  $W_{-1}$ . For the use case presented here, Eq. (3.24) is to be interpreted as,

$$\gamma = \begin{cases} \frac{W_0(\zeta \log(\zeta))}{\log(\zeta)} & \zeta \in (0, \frac{1}{e}) \\ \frac{W_{-1}(\zeta \log(\zeta))}{\log(\zeta)} & \zeta \in (\frac{1}{e}, 1) \end{cases}.\tag{1.22}$$

Prager 2002, Figure(2).

<https://math.stackexchange.com/questions/3004835/is-the-lambert-w-function-analytic-if-not-everywhere-then-on-what-set-is-it-analytic> <https://researchportal.bath.ac.uk/en/publications/algebraic-properties-of-the-lambert-w-function-from-a-result-of-r>



## 490 Chapter 2

## 491 The Schnute Model

## 0.1 Schnute Model

The Schnute production function is a three parameter generalization of many of the most common two parameter production functions (Deriso, 1980; J. Schnute, 1985). It can be written in the following form, with parameters  $\alpha$ ,  $\beta$ , and  $\gamma$ ,

$$P_s(B; [\alpha, \beta, \gamma]) = \alpha B(1 - \beta\gamma B)^{\frac{1}{\gamma}}. \quad (2.1)$$

The BH and Logistic production functions arise when  $\gamma$  is fixed to -1 or 1 respectively. The Ricker model is a limiting case as  $\gamma \rightarrow 0$ . For  $\gamma < -1$  a family of strictly increasing Cushing-like curves arise, culminating in linear production as  $\gamma \rightarrow -\infty$ . These special cases form natural regimes of similarly behaving production functions as seen in Figure (3.16).

The behavior of RP inference under the BH model is of particular interest due to the overwhelming popularity of the BH assumption in fisheries models. Since Schnute production models can represent a quantifiably wide variety of possible productivity behaviors, they present an ideal simulation environment for inquiry of the reliability of inference under the BH assumption.

Under Schnute production, biomass dynamics evolve according to the following ODE,

$$\frac{dB}{dt} = P_s(B; \theta) - (M + F)B. \quad (2.2)$$

This equation largely takes the same form as previously described, except that  $P_s$  is the Schnute production function and natural mortality,  $M$ , is modeled explicitly here. Natural

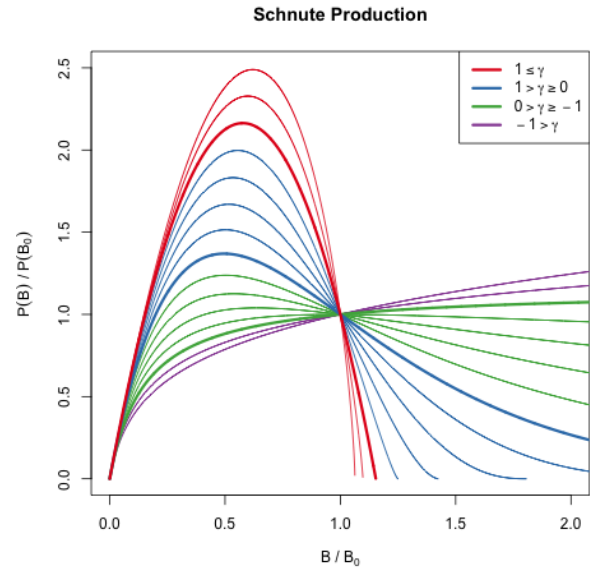


Figure 2.1: The Schnute production function plotted across a variety of parameter values. Regimes of similarly behaving curves are grouped by color.

512 mortality models the instantaneous rate of mortality from all causes outside of fishing. Ex-  
 513 plicitly modeling natural mortality is not only a typical assumption of fisheries models, but  
 514 is also key to the making RPs well defined over the relevant domain of  $\gamma$ .

The derivation of RPs under Eq. (3.26) follows a similar logic as under the PT model. An expression for equilibrium biomass is attained by setting  $\frac{dB}{dt} = 0$  and rearranging the resulting expression to solve for  $B$

$$\bar{B}(F) = \frac{1}{\gamma\beta} \left( 1 - \left( \frac{M+F}{\alpha} \right)^\gamma \right). \quad (2.3)$$

The above expression quickly yields  $B_0$ ,  $B^*$  by evaluation at  $F = 0$  and  $F^*$  respectively,

$$B_0 = \frac{1}{\gamma\beta} \left( 1 - \left( \frac{M}{\alpha} \right)^\gamma \right) \quad (2.4)$$

$$\frac{B^*}{B_0} = \frac{1 - \left( \frac{M+F^*}{\alpha} \right)^\gamma}{1 - \left( \frac{M}{\alpha} \right)^\gamma}. \quad (2.5)$$

Attaining an expression for  $F^*$  requires maximization of equilibrium yield,  $\bar{Y} = F\bar{B}(F)$ , with respect to  $F$ . Analytically maximizing proceeds by differentiating  $\bar{Y}$  to produce

$$\frac{d\bar{Y}}{dF} = \bar{B}(F) + F \frac{d\bar{B}}{dF} \quad (2.6)$$

$$\frac{d\bar{B}}{dF} = -\frac{1}{\beta} \left( \frac{\left( \frac{M+F}{\alpha} \right)^\gamma}{F+M} \right). \quad (2.7)$$

Setting  $\frac{d\bar{Y}}{dF} = 0$ , filling in the expressions for  $\bar{B}(F)$  and  $\frac{d\bar{B}}{dF}$ , then rearranging to solve for  $F^*$  is less yielding here than it was in the case of the PT model. This procedure falls short of providing an analytical solution for  $F^*$  directly in terms of  $\theta$ , but rather shows that  $F^*$  must respect the following expression,

$$0 = \frac{1}{\gamma} - \left( \frac{1}{\gamma} + \frac{F^*}{F^* + M} \right) \left( \frac{F^* + M}{\alpha} \right)^\gamma. \quad (2.8)$$

515 The lack of an analytical solution here is understood. [J. T. Schnute and Richards \(1998,](#)  
 516 [pg. 519\)](#) specifically points out that  $F^*$  cannot be expressed analytically in terms of produc-  
 517 tivity parameters, but rather gives a partial analytical expression for the inverse relationship.

Although parameterized slightly differently, [J. T. Schnute and Richards \(1998\)](#) derives expressions for  $\alpha$  and  $\beta$  as a function of RPs and  $\gamma$ .

Since RPs are left without a closed form expression, computing RPs from productivity parameters amounts to numerically solving the system formed by collecting the expressions (3.32), (3.28), and (3.29).

### Simulation

For the purposed of simulation, it is not necessary to completely know the precise relationships mapping RPs  $\mapsto \theta$  or  $\theta \mapsto$  RPs. Simulation only requires enough knowledge of these mappings to gather a list of  $(\alpha, \beta, \gamma)$  tuples, for data generation under the Schnute model, and the corresponding RPs in some reasonable space-filling design over RP space.

Similarly to [J. T. Schnute and Richards \(1998\)](#), expressions (3.32) and (3.28) are solved for  $\alpha$  and  $\beta$  respectively. This leads to the partial mapping  $(F^*, B_0) \mapsto (\alpha(\cdot, \gamma), \beta(\cdot, \gamma))$  in terms of RPs and  $\gamma$ . By further working with Eq. (3.29), to identify  $\gamma$ , the following system is obtained,

$$\begin{aligned}\alpha &= (M + F^*) \left( 1 + \frac{\gamma F^*}{M + F^*} \right)^{1/\gamma} \\ \beta &= \frac{1}{\gamma B_0} \left( 1 - \left( \frac{M}{\alpha} \right)^\gamma \right) \\ \frac{B^*}{B_0} &= \frac{1 - \left( \frac{M + F^*}{\alpha} \right)^\gamma}{1 - \left( \frac{M}{\alpha} \right)^\gamma}.\end{aligned}\tag{2.9}$$

For a population experiencing natural mortality  $M$ , by fixing  $F^*$ ,  $B_0$ , and  $\frac{B^*}{B_0}$  the above system can fully specify  $\alpha$  and  $\beta$  for a given  $\gamma$ . Notice for a given  $\gamma$  a cascade of closed form solutions for  $\alpha$  and  $\beta$  can be obtained. First  $\alpha(\gamma)$  can be computed, and then  $\beta(\alpha(\gamma), \gamma)$  can be computed. If  $\alpha(\gamma)$  is filled back into the expression for  $\frac{B^*}{B_0}$ , the system collapses into a single onerous expression for  $\frac{B^*}{B_0}(\alpha(\gamma), \gamma)$ . For brevity, define the function  $\zeta(\gamma) = \frac{B^*}{B_0}(\alpha(\gamma), \gamma, F^*, M)$  based on Eq. (3.29).

Inverting  $\zeta(\gamma)$  for  $\gamma$ , and computing the cascade of  $\alpha(\gamma)$ , and then  $\beta(\alpha(\gamma), \gamma)$ , fully defines the Schnute model for a given  $(\frac{F^*}{M}, \frac{B^*}{B_0})$ . However inverting  $\zeta$  accurately is extremely difficult. Inverting  $\zeta$  analytically is not feasible, and numerical methods for inverting  $\zeta$  are unstable

and can be computationally expensive. Rather than numerically invert precise values of  $\zeta(\gamma)$ ,  $\gamma$  is sampled so that the overall simulation design is space filling as described in Section (5.3).

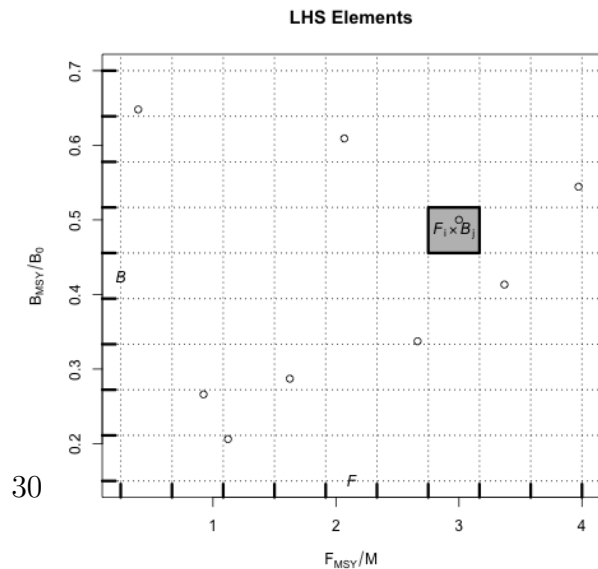
Each design location defines a complete Schnute production model with the given RP values. Indices of abundance are simulated from the Schnute model at each design location, a small amount of residual variation,  $\sigma = 0.01$ , is added to the simulated index, and the data are then fit with a misspecified BH production model. The design at large captures various degrees of model misspecification relative to the BH model, so as to observe the effect of productivity model misspecification upon RP inference.

## 0.2 Latin Hypercube Sampling

The goal of space filling design in this setting is to extend the notion of the random sample (and its desirable parameter estimation properties) across the simulated RP domain so as to represent the simulated space as well as possible (Gramacy, 2020). The simple random sample is the classical approach to unbiased parameter estimation, however simple randomness is patchy, often sampling some regions of design space quite densely, while leaving other regions of design space empty. Space filling designs aim to preserve (or enhance) parameter estimation properties across the simulated domain (Devon Lin & Tang, 2015; Stein, 1987), while constraining samples to be spaced in some notion of spread over the entire space. Latin hypercube sampling (McKay et al., 2000, LHS) is among the most foundational of space filling designs used in computer experiments.

A LHS of size  $n$ , in the 2 dimensional space defined by RPs, distributes samples so as to spread points across a design region in a broadly representative way. A LHS design extends the notion of a univariate random uniform sample across multiple dimensions so that each margin of the design space enjoys a uniform distribution.

LHS designs achieve this notion of uni-





formity by first partitioning each dimension of the design space into regular grids of size  $n$ . By intersecting the grids of each dimension, cells are produced that evenly partition the design space. In two dimensions  $n^2$  cells are produced, from which a total of  $n$  samples are taken. Crucially only one sample is taken from a given element of each grid in each dimension so as to reduce clumping of the  $n$  samples across the design space.

### Schnute Design

Due to the lack of an analytical relationship mapping RPs  $\mapsto \theta$ , analogous to the PT model's Eq. (3.24), producing a LHS design over Schnute RPs requires a more tactful approach. The structured relationship between the RPs and productivity parameters, described in Section (5), allows an approximate LHS to be obtained by a careful navigation of the system of equations seen in Eq. (3.33).

Under the Schnute model, let  $\mathcal{F}$  and  $\mathcal{B}$  represent regular grids on  $\frac{F^*}{M} \in (0.25, 4)$  and  $\frac{B^*}{B_0} \in (0.15, 0.7)$  respectively which can serve as the scaffolding for computing an approximate LHS.

Since it is not practical to invert  $\zeta(\gamma)$ , a uniform sample in  $\frac{B^*}{B_0}$  can be obtained by modeling  $\gamma$  as a random variable, with realization  $\gamma^*$ , and thinking of  $\zeta(\gamma)$  as its cumulative distribution function (CDF). The aim is to model  $\gamma$  as an easily sampled random variable with a CDF that closely approximates  $\zeta$ , so that  $\zeta(\gamma^*) \sim U(\zeta_{min}, 1)$  as closely as possible. There may be many good models for the distribution of  $\gamma$ , but in this setting the

Given  $B_0$ ,  $M$ , and  $F^*$ :

- 1) Draw  $\gamma^* \sim \gamma|F^*, M$ .
- 2) Compute  $\frac{B^*}{B_0} = \zeta(\gamma^*)$
- 3) Compute  $\alpha^* = \alpha(\gamma^*, F^*, M)$
- 4) Compute  $\beta^* = \beta(\alpha^*, \gamma^*, M, B_0)$

Figure 2.3: An outline of the sampling procedure for  $\gamma$  given  $B_0$ ,  $M$ , and  $F^*$ .

following distribution is very effective,

$$\gamma \sim \zeta_{min} \delta(\gamma_{min}) + t(\mu, \sigma, \nu) \mathbf{1}_{\gamma > \gamma_{min}}. \quad (2.10)$$

586 Above,  $t$  is the density of the three pa-  
 587 rameter location-scale family Student's  $t$  dis-  
 588 tribution with location  $\mu$ , scale  $\sigma$ , and de-  
 589 grees of freedom  $\nu$ .  $\mathbf{1}_{\gamma > \gamma_{min}}$  is an indica-  
 590 tor function that serves to truncate the Stu-  
 591 dent's  $t$  distribution at the lower bound  $\gamma_{min}$ .  
 592  $\delta(\gamma_{min})$  is the Dirac delta function evaluated  
 593 at  $\gamma_{min}$ , which is scaled by the known value  
 594  $\zeta_{min}$ ; this places probability mass  $\zeta_{min}$  at  
 595 the point  $\gamma_{min}$ . Since sampling from a Stu-  
 596 dent's  $t$  distribution is readily doable, sam-  
 597 pling from a truncated Student's  $t$  mixture  
 598 only requires slight modification.

Let  $T$  be the CDF of the modeled distri-  
 bution of  $\gamma$ . Since the point  $(\gamma_{min}, \zeta_{min})$  is  
 known from the dynamics of the Schnute model at a given RP, full specification of Eq. (3.34)  
 only requires determining the values for  $\mu$ ,  $\sigma$ , and  $\nu$  which make  $T$  best approximate  $\zeta(\gamma)$ .  
 Thus, the values of  $\mu$ ,  $\sigma$ , and  $\nu$  are chosen by minimizing the  $L^2$  distance between  $T(\gamma)$  and  
 $\zeta(\gamma)$ .

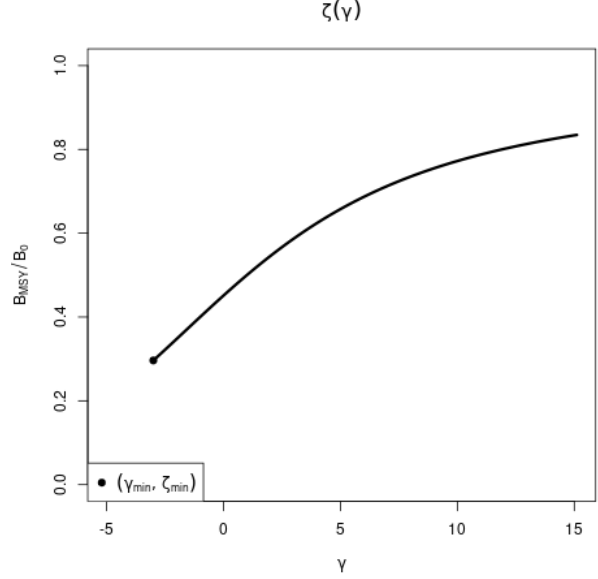


Figure 2.4:  $\zeta(\gamma)$  Plotted for  $F^* = 0.1$  and  $M = 0.2$ . The point  $(\gamma_{min}, \zeta_{min})$  shows the lowest biologically meaningful value of  $\gamma$ ; below which productivity is negative.

$$[\hat{\mu}, \hat{\sigma}, \hat{\nu}] = \arg \min_{[\mu, \sigma, \nu]} \int_{\Gamma} (T(\gamma; \mu, \sigma, \nu) - \zeta(\gamma))^2 d\gamma \quad (2.11)$$

The distribution  $T(\gamma|\hat{\mu}, \hat{\sigma}, \hat{\nu})$  is fit for use in generating  $\gamma^*$  random variates at a specific  $F^*$  and  $M$ . This approximation releases the need to invert  $\zeta$  w.r.t  $\gamma$  by using samples of  $\gamma^*$  values to generate approximately uniform samples of  $\zeta(\gamma^*)$ . By sampling approximately uniform  $\zeta(\gamma^*)$  random variates in this way, and making use of the structure in Eq. (3.33), an approximate LHS sample can be collected via Algorithm (2).

$\frac{F^*}{M}$  is drawn uniformly from  $\mathcal{F}_i$ . Conditioning on the sample of  $F^*$ , and  $M$ ,  $T(\gamma|\hat{\mu}, \hat{\sigma}, \hat{\nu})$  is fit and  $\gamma^*$  is sampled.  $\zeta^*$  is then computed and placed into the appropriate grid element  $\mathcal{B}_j$ . Given  $\gamma^*$ , the cascade  $\alpha(\gamma^*)$ , and  $\beta(\alpha(\gamma^*), \gamma^*)$ , can be computed.

The algorithm continues until all of the de-

sign elements,  $(\frac{F^*}{M}, \zeta^*) \Leftrightarrow (\alpha^*, \beta^*, \gamma^*)$ , have been computed for all  $i \in [1, \dots, n]$ .

## Design Refinement

Since the behavior of RP inference, under misspecified models, will vary in yet-unknown ways, the exact sampling design density may be hard to know a priori. Several factors, including the particular level of observation uncertainty, high variance (i.e. hard to resolve) features of the response surface, or simply "gappy" instantiations of the initial LHS design may necessitate adaptive design refinement, to accurately describe RP biases. Given the temperamental relationship between RPs and productivity parameters in the Schnute model, a recursive refinement algorithm that makes use of the previously described LHS routine, is developed.

While LHS ensures uniformity in the design margins, and a certain degree of spread, it

---

### Algorithm 1 LHS of size $n$ on rectangle $R$ .

---

```

1: procedure  $LHS_n(R)$ 
2:   Define  $n$ -grids  $\mathcal{F}, \mathcal{B} \in R$ 
3:   for each grid element  $i$  do
4:     Draw  $\frac{F^*}{M} \sim Unif(\mathcal{F}_i)$ 
5:     Compute  $[\hat{\mu}, \hat{\sigma}, \hat{\nu}]$  given  $F^*$  &  $M$ 
6:     while  $\mathcal{B}_j$  not sampled do
7:       Draw  $\gamma^* \sim T(\gamma|\hat{\mu}, \hat{\sigma}, \hat{\nu})$ 
8:       Compute  $\zeta^* = \zeta(\gamma^*)$ 
9:       Compute  $j$  such that  $\zeta^* \in \mathcal{B}_j$ 
10:    end while
11:    Compute  $\alpha^* = \alpha(\gamma^*, F^*, M)$ 
12:    Compute  $\beta^* = \beta(\alpha^*, \gamma^*, M, B_0)$ 
13:    Save  $(\frac{F^*}{M}, \zeta^*) \Leftrightarrow (\alpha^*, \beta^*, \gamma^*)$  in  $\mathcal{F}_i \times \mathcal{B}_j$ 
14:  end for
15: end procedure

```

---

is widely recognized that particular LHS instantiations may leave substantive gaps in the simulation design. To correct this, LHS is often paired with design elements of maximin design (Morris & Mitchell, 1995; Devon Lin & Tang, 2015). Maximin designs sample the design space by maximizing the minimum distance between sampled points. This has the advantage of definitionally filling holes in the design, however because no points are ever drawn outside of the design domain, samples tend to clump around edges (particularly corners) of the design domain. Since LHS ensures uniformity in the margins and maximin designs enjoys a certain sense of optimality in how they define and fill gaps (Johnson et al., 1990), the methods are quite complimentary when combined.

Making use of this complimentary relationship, holes in the existing LHS design of RPs are identified based on maximin design principles. New design points are collected based on areas of the RP design space which maximizes the minimum distance between all pairs of points in the current design, based on the following distance function

$$d(\mathbf{x}, \mathbf{x}') = \sqrt{(\mathbf{x} - \mathbf{x}')^T \mathbf{D}^{-1} (\mathbf{x} - \mathbf{x}')} \quad (2.12)$$

$$\mathbf{D} = \mathbf{diag} \left[ \left( \max(\mathcal{F}) - \min(\mathcal{F}) \right)^2, \left( \max(\mathcal{B}) - \min(\mathcal{B}) \right)^2 \right].$$

Above,  $d$  is a scaled distance function that defines the distance between points in the differing scales of  $\frac{B^*}{B_0}$  and  $\frac{F^*}{M}$ .  $\mathbf{D}$  is a diagonal matrix that measures the squared size of the domain in each axis of so as to normalize distances to a common scale.

If  $\mathbf{X}_n$  is the initial design, computed on  $R_{full}$ , let  $\mathbf{x}_a$  be the augmenting point which maximizes the minimum distance between all of the existing design points,

$$\mathbf{x}_a = \underset{\mathbf{x}'}{\operatorname{argmax}} \min \{ d(\mathbf{x}_i, \mathbf{x}') : i = 1, \dots, n \}. \quad (2.13)$$

The point  $\mathbf{x}_a$  is used as an anchor for augmenting  $\mathbf{X}_n$ . An additional  $LHS_{n'}$  (via Algorithm (2)) is collected, adding  $n'$  design points, centered around  $\mathbf{x}_a$ , to the overall design. The augmenting region,  $R_{(\mathbf{x}_a, d_a)}$ , for collecting  $LHS_{n'}$  is defined based on the square centered at  $\mathbf{x}_a$  with side length  $2d_a$ , where  $d_a = \min \{ d(\mathbf{x}_i, \mathbf{x}_a) : i = 1, \dots, n \}$ , in the space defined by the metric  $d$ .

Due to the tendency of maximin sampling to cluster augmenting points on the edges of the design space,  $R_{(x_a, d_a)}$  is truncated by the outer most limits of  $R_{full}$  so as to focus design augmentation within the specified domain of the simulation. Furthermore, since the design space has a nonlinear constraint at low values of  $\frac{B}{B_0}$ , the calculation of  $x_a$  is further truncated based on a convex hull defined by the existing samples in the overall design.

Design refinement then proceeds as follows. An initial design is computed,  $X_n = LHS_n(R_{full})$ , based on an overall simulated region of RPs  $R_{full}$ . The maximin augmenting point,  $x_a$ , is computed at a maximin distance of  $d_a$  from the existing samples. An augmenting design  $X_{n'} = LHS_{n'}(R_{(x_a, d_a)})$  is collected and added to  $X_n$ . Design refinement carries on recursively collecting augmenting designs in this way until the maximin distance falls below the desired level.

### 0.3 Gaussian Process Metamodel

At its core, a metamodel is simply a model of some mapping of inputs to outputs (the mapping itself is typically defined by a computer model). By modeling the mapping with a statistical model (that explicitly defines the relevant features of the mapping) a metamodel defines a specific ontology for the mapping. By simulating examples of the mapping, the inferential infrastructure of the statistical model is used to empirically learn an effective emulation of the mapping within the ontology defined by the statistical model. The predictive infrastructure of the statistical model is then useful as an approximate abstraction of the system itself to better understand the system through further data collection, cheap approximation of the mapping, and/or study of the mapping itself.

In this setting, the aim of metamodeling is to study how well RPs are inferred when typical two parameter models of productivity (Logistic and BH) are misspecified for populations that are actually driven by more complicated dynamics. The simulation design,  $\mathbf{X}$ , provides a sample of different population dynamics that are driven by three parameter production functions broadly in RP space. By simulating index of abundance data from the three parameter model, and fitting those data with the two parameter production model, we observe particular instances of how well RPs are inferred at the given misspecification of the two parameter model relative to the true three parameter production model. By gathering

all of the simulated instances of how RPs are inferred (under the two parameter model), we form a set of example mappings to train a metamodel which represents the mapping of true RPs (under the three parameter model) to estimates of RPs under the misspecified two parameter production model. The metamodel is essentially a surrogate for inference under the misspecified two parameter production model that controls for the specific degree of model misspecification.

A flexible GP model is assumed for the structure of the metamodel to describe the mapping of RPs under misspecified two parameter models of productivity. A GP is a stochastic process generalizing the multivariate normal distribution to an infinite dimensional analog. GP models are often specified primarily through the choice of a covariance (or correlation) function which defines the relationship between locations in the input space. Typically correlation functions are specified so that points closely related in space result in correlated effects in the model. In this setting the inputs to the GP metamodel are the space of reference points which define the simulated three parameter production models.

While index of abundance data are generated from three parameter models, at each design location of the simulation, fitting the restricted two parameter model results in a maximum likelihood estimate (MLE; and associated estimation uncertainty) of each of the productivity parameters (i.e. Schaefer:  $[\log(r), \log(K)]$ , BH:  $[\log(\alpha), \log(\beta)]$ ). To simplify the specification of the metamodel, let  $\mathbf{y}$  be a vector collecting the fitted MLEs for one of the productivity parameters, and let  $\boldsymbol{\omega}$  be a vector of estimates of the estimator variances (via the inverted Fisher information) at each  $\mathbf{y}$ . Each of the fitted productivity parameter estimates are then modeled using independent instances of the following GP metamodel.

$$\begin{aligned}\mathbf{y} &= \beta_0 + \mathbf{X}\boldsymbol{\beta} + \mathbf{v} + \boldsymbol{\epsilon} \\ \mathbf{v} &\sim N_n(\mathbf{0}, \tau^2 \mathbf{R}_\ell) \\ \boldsymbol{\epsilon} &\sim N_n(\mathbf{0}, \boldsymbol{\omega}' \mathbf{I})\end{aligned}\tag{2.14}$$

$\mathbf{X}$  is the  $n \times 2$  LHS design matrix of RPs for each simulated three parameter data generating model as described in Section (5 .3).  $\epsilon$  models independent normally distributed error, which provides an ideal mechanism for propagating uncertainty from inference in the

simulation step into the metamodel. By matching each  $y_i$  with an observed  $\omega_i$  variance term,  $\epsilon$  serves to down weight the influence of each  $y_i$  in proportion to the inferred production model sampling distribution uncertainty. This has the effect of smoothing the GP model in a way similar to the nugget effect (Gramacy & Lee, 2012), although the application here models this effect heterogeneously.

The term,  $\mathbf{v}$ , contains spatially correlated GP effects. The correlation matrix,  $\mathbf{R}_\ell$  describes how RPs close together in the simulation design are more correlated than those that are far away. This spatial effect is modeled with a squared exponential correlation function,

$$R(\mathbf{x}, \tilde{\mathbf{x}}) = \exp \left( \sum_{i=1}^2 \frac{-(x_i - \tilde{x}_i)^2}{2\ell_j^2} \right). \quad (2.15)$$

$R$  has an anisotropic separable form which allows for differing length scales,  $\ell_1$  and  $\ell_2$ , in the different RP axes. The flexibility to model correlations separately in the different RP axes is key due to the differences in the extent of the RP domains marginally. The metamodel parameters  $\beta_0$ ,  $\boldsymbol{\beta}$ ,  $\tau^2$ ,  $\ell_1$  and  $\ell_2$  are fit via MLE against the observations  $\mathbf{y}$ ,  $\mathbf{X}$ , and  $\boldsymbol{\omega}$  from simulation fits.

Fitting the metamodel allows for a full predictive description of inference under the misspecified restricted models. Predictive estimates are obtained via kriging (Cressie, 2015)

$$\hat{y}(\mathbf{x}) = \beta_0 + \mathbf{x}\boldsymbol{\beta} + \mathbf{r}(\mathbf{x})'\mathbf{R}_\ell^{-1}(\mathbf{y} - (\beta_0 + \mathbf{X}\boldsymbol{\beta})) \quad (2.16)$$

$\hat{y}(\mathbf{x})$  is the predicted value of the modeled productivity parameter MLE under the two parameter production model, when the index of abundance is generated from the three parameter production model at RP location  $\mathbf{x}$ .  $\mathbf{r}(\mathbf{x})$  is a vector-valued function of correlation function evaluations for the predictive location  $\mathbf{x}$  against all observations in  $\mathbf{X}$  (i.e.  $\mathbf{r}(\mathbf{x}) = \mathbf{R}(\mathbf{x}, \mathbf{x}_i) \forall \mathbf{x}_i \in \mathbf{X}$ ).

While metamodeling occurs on the inferred productivity parameters of the restricted production model, the metamodel can also be used to build estimates of major biological RPs. For the BH model the relevant transformations for relating productivity parameters with RPs are given in Eqs. (3.29, 3.32) with  $\gamma$  fixed to -1; for the Schaefer model  $\hat{B}^* = \frac{\hat{K}}{2}$  and

711  $\hat{F}^* = \frac{\hat{r}}{2}$ . Applying the metamodel predictive surfaces on the scale of RP estimates allows for  
712 the quantification of estimation bias that is induced by fitting a misspecified two parameter  
713 production model to indices of abundance generated under three parameter productivity.



# 1 Results

## 1.1 Schnute/BH

### Design

Algorithm (1) enforces uniform marginals in  $\frac{F^*}{M}$  directly, as well as the adherence of the overall design to latin squares. Figure (2.5) shows a uniform Q-Q plot for sampled  $\zeta$ , using Algorithm (1), against theoretical uniform quantiles. As evidence by the excellent coherence to the theoretical uniform quantiles, the approximation in Section (5.3) for sampling  $\gamma$  (and therefore  $\zeta(\gamma)$ ), is very effective. Furthermore since numerical inversion of  $\zeta(\gamma)$  is costly and unreliable, the relative speed and accuracy that this approximate LHS sampling method provides is pivotal for the rest of the work presented here.

Similarly to the PT model, the three parameter Schnute model is uniquely identified by each point in the space of  $\frac{F^*}{M}$  and  $\frac{B^*}{B_0}$  RPs. As seen in Figure (2.6), Schnute production has different behaviors in different ranges of RPs space, which are entirely defined by the value of  $\gamma$  (shown in Figure (3.16)). When  $\gamma \geq 1$  the Schnute model produces a family of Logistic-like curves that are increasingly right leaning as  $\gamma$  increases. For  $1 > \gamma \geq 0$ , Schnute production takes a family of left leaning Ricker-like curves that all, at least, approach the x-axis. For  $0 > \gamma > -1$  there are a family of BH-like curves that do not

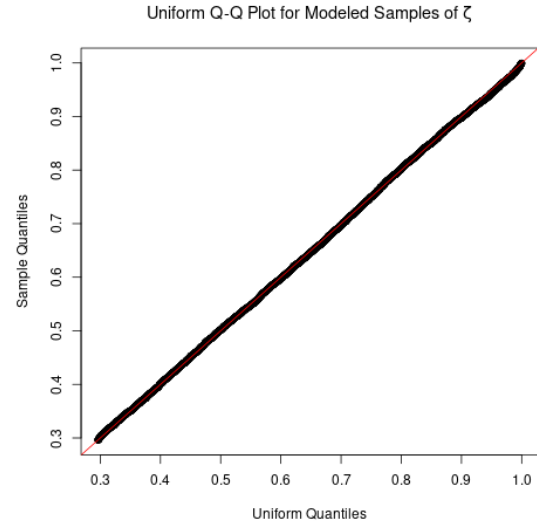


Figure 2.5: Uniform Q-Q plot for  $\zeta$  plotted for  $F^* = 0.1$  and  $M = 0.2$ .

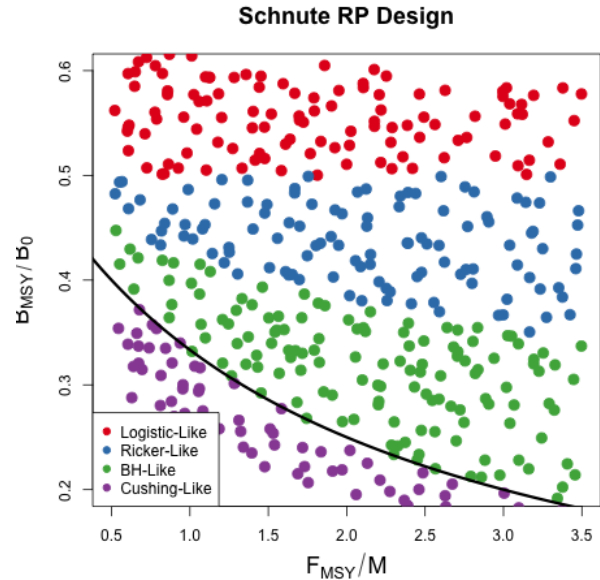


Figure 2.6: A Schnute RP design. Colors indicate different regimes of Schnute production. The black curve shows the BH set.

approach the x-axis but still have decreas-

ing productivity for large biomass stocks. When  $\gamma$  is exactly  $-1$  Schnute reduces to BH production which has asymptoting production for large biomass. Finally when  $-1 > \gamma$  Schnute produces a family of increasing Cushing-like curves that do not asymptote, and produces linear production as  $\gamma \rightarrow -\infty$ .

Modeling index data that are simulated broadly over the theoretical space of RPs with misspecified BH production greatly limits the range of possible RPs that can be inferred. Under BH production the full theoretical space of RPs are limited to the curve  $\frac{B^*}{B_0} = \frac{1}{F^*/M+2}$ . Define the “BH set” as the set of RPs defined by this limited space, i.e. the curve  $\left\{ \left( \frac{F^*}{M}, \frac{B^*}{B_0} \right) \mid \frac{B^*}{B_0} = \frac{1}{F^*/M+2} \right\}$ . as seen in the black curve in Figure (2.6). The farther away from this set that Schnute data are simulated, the worse the BH model is misspecified for those data.

### Metamodeled Trends

Unlike the Schaefer model, the BH set is not a constant in  $\frac{B^*}{B_0}$ . Under the BH model, bias in  $\frac{B^*}{B_0}$  is no longer entirely defined by the degree of model misspecification, but rather the structure of BH RPs allows bias in both  $\frac{B^*}{B_0}$  and  $\frac{F^*}{M}$  to interact as a function of contrast in the data.

**High Contrast** Figure (2.7) shows metamodeled RP bias surfaces for inference under the BH model in the high contrast setting. The (*left*) and (*bottom*) panels focus only on the  $\frac{B^*}{B(0)}$  and  $\frac{F^*}{M}$  components of bias respectively. In these panels bias is shown as relative bias,  $\frac{\widehat{RP}-RP}{RP}$ , similar to a percent error calculation. Where  $RP$  represents the true value of the three parameter RP, and  $\widehat{RP}$  refers to the metamodel estimate.

Figure (2.7, *top-right*) combines the components of bias to show the overall mapping of RPs under BH inference in the high contrast simulation setting. Unlike high contrast RP inference under the Schaefer model, the BH model does shows bias in both RPs here. Despite the bias in  $\frac{B^*}{B(0)}$  and  $\frac{F^*}{M}$  these results are similar to that of the Schaefer model in that the overall mapping of RPs is very nearly a minimal distance mapping onto the constrained set of RPs. The primary difference between Schaefer model and BH RP inference is the geometry of their limited RP spaces. Unlike the Schaefer model the BH set encourages bias

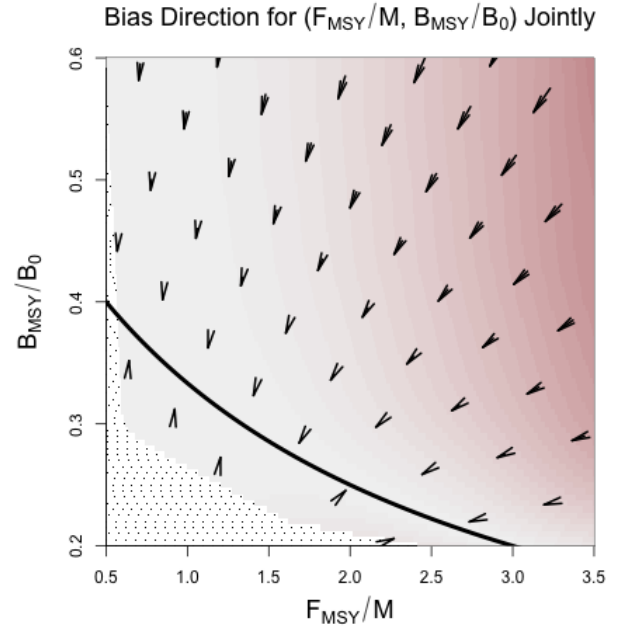
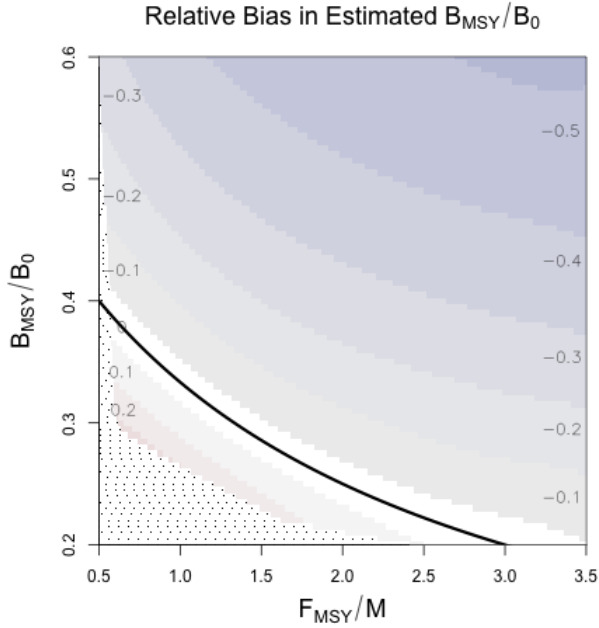
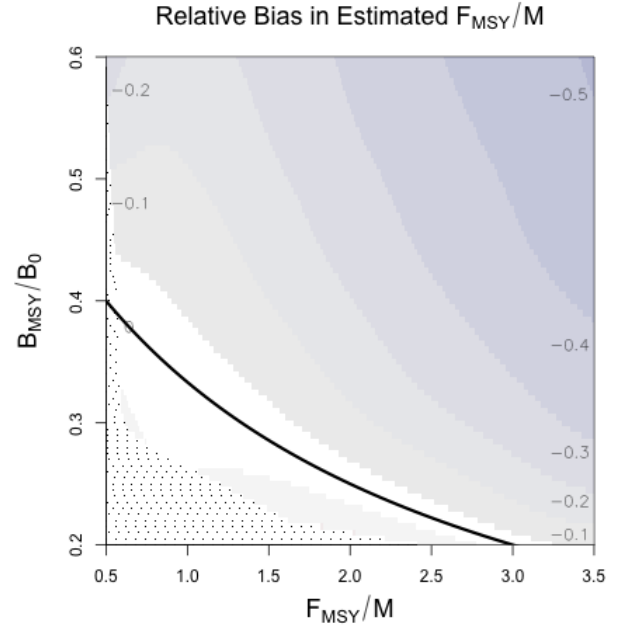
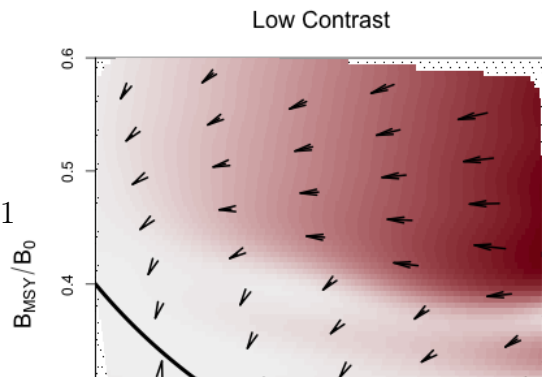


Figure 2.7: Heatplots showing the bias in RP estimation induced by model misspecification of the BH model in the high contrast simulation setting. In all cases the restricted RP-space of the BH set is shown as the black curve. (*left*) Relative bias in  $\frac{B^*}{B(0)}$ . (*top-right*) Bias in RP-space shown directionally. Arrows point from the location where data is generated, toward the location in the BH set where MLE projects estimated RPs. The intensity of color represents the excess bias relative to the shortest possible mapping. (*bottom*) Relative bias in  $F^*$ .



in both RPs for misspecified models even in very well informed setting.

**Low Contrast** Figure (2.8) shows the mapping of RPs in the low contrast simulation setting. Figures (2.8) and (2.7, *top-right*) share a common scale for the inten-



sity of color to facilitate comparison. In Figure (2.8) notice that the mildly misspecified area around the BH set produces mappings onto the BH set which resemble the minimal distance mapping seen in the high contrast setting. The primary difference in this low contrast setting, is the break point around  $\frac{B^*}{B(0)} = 0.4$  above which  $\frac{F^*}{M}$  is sharply underestimated.

The region of RPs where the BH model manages to recover the minimal distance mapping may be considered a “safe regime” of data types that are reasonably well modeled by a BH model. By comparison of Figure (2.8), with Figure (2.6), this safe regime of the BH model occurs for data generated for Cushing-like or BH-like production. While bias of the RPs can still become concerningly large, this region can be considered safe in the sense that even for low contrast data RP estimation under the the BH model recovers the minimal distance mapping.

Outside of this safe regime, RP estimation breaks from the minimal distance mapping at the interface between BH-Like and Ricker-Like regimes of the Schnute model (again see Figure (2.6)). The Ricker model lies along this regime interface, and represents the first model to approach the x-axis for large biomasses as  $\gamma$  increases. This markedly unBH-like productivity in the low information simulation setting breaks MLE inference from the minimal distance mapping and instead maps RPs to extremely low values of  $F^*$ ; consequently  $\frac{B^*}{B(0)}$  is estimated

**Estimated Yield Curves For Poorly Specified BH**

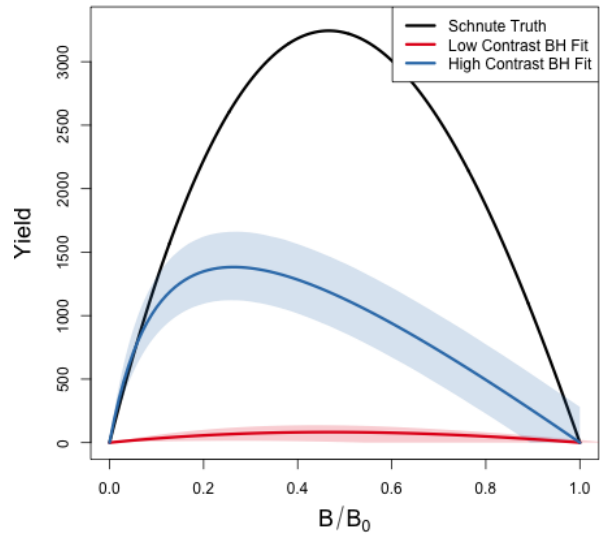


Figure 2.9: Yield curves for data generated with  $\frac{F^*}{M} = 3.48$  and  $\frac{B^*}{B(0)} = 0.48$ .

near the limiting value under the BH (i.e.

$\lim_{F^* \rightarrow 0} \frac{1}{F^*/M+2} = 0.5$ ). Similarly the set of Ricker RPs (as well as the Schaeffer set) include this trivial limiting point in common ( $\frac{F^*}{M} = 0$ ,  $\frac{B^*}{B(0)} = 0.5$ ).

Interestingly, in the high contrast setting this trivial mapping for highly misspecified BH models is not present. This suggests that, under a misspecified BH model, the presence of adequate information in the data to produce reasonable estimates of  $\frac{F^*}{M}$ , drives  $\frac{B^*}{B(0)}$  below 0.5 in accordance with  $\frac{B^*}{B(0)} = \frac{1}{F^*/M+2}$ , even when the true  $\frac{B^*}{B(0)} > 0.5$ . This phenomena balances RP estimation within the constrained BH set as mediated by the information content of the data and the degree of model misspecification. When the information content in the data is too small to drive a compromised RP estimate, inference completely disregards accurate estimation of  $F^*$  in order to better estimate  $\frac{B^*}{B(0)}$  by exploiting the common limiting behavior of the BH set and that of Ricker-like and Logistic-like models.

## 2 Discussion

Results presented here generally agree with what is known about estimating growth rate parameters (Lee et al., 2012; Conn et al., 2010; Magnusson & Hilborn, 2007). These study's appreciate the role of contrast for estimating growth rates, however they struggle to make generally extensible conclusions since they focus only on a handful of stocks that fall short of forming a random sample of the greater population of possible stock behaviors. The LHS design methods presented here are designed specifically to simulate a representative sample of stocks broadly across the space of possible RPs. Furthermore, the simulation design, taken together with the GP metamodel of productivity parameter estimates, allows this study to control the degree of model misspecification and generalize conclusions about the behavior of productivity estimation within the production model setting presented.

In the presence of contrast,  $F^*$  estimation can enjoy very low bias even for a wide range of poorly specified models; conversely in the absence of contrast  $F^*$  estimation can suffer very large bias even for slightly misspecified models. This pattern is particularly true for inference under the Schaeffer model where the geometry of the restricted RP set isolates estimation failure of  $F^*$  from  $\frac{B^*}{B(0)}$ . While contrast has a similar impact on  $F^*$  estimation under the BH model, the geometry of the BH RP set correlates estimation bias of  $F^*$  and  $\frac{B^*}{B(0)}$ . The

GP metamodeling approach reveals a more general pattern that highly informative data sets (high contrast) produces a nearly minimal distance mapping of RPs onto the constrained RP set.

In all cases when model misspecification is removed, even with weakly informative data, RP estimation is unbiased and well estimated. Thus contrast alone is not the only factor leading to inferential failure. Model misspecification is a necessary but not sufficient condition for inducing RP estimation bias. The particular RP bias present depends on the RP geometry of the fitted model and how that geometry is misspecified relative to the data. The RP mapping is then oriented to the RP geometry of the fitted model.

While the relative fishing rate parameterized in Section (5.5) captures a usefully broad spectrum of relevant fishing behaviors, it is still limiting in the amount of information that it can induce. Improved methods for quantifying contrast in fisheries data, and/or methods of discovering more informative fishing behavior, could improve this analysis. In the absence of a maximally informative dataset simulation methods will not fully describe how inference fails, but the methods presented here tell the most complete picture yet, with explicit control of the degree model misspecification, contrast, and a simulation design that allows for uniform representative data generation across biologically meaningful stocks. The results presented here suggest the conjecture that under a maximally informative dataset, RP inference with a two parameter production function will be biased in the direction a shortest distance map from the true RPs onto restricted set of RPs under the two parameter model.

Given the potential for model misspecification of RPs, a minimal distance mapping of RPs represents a best-case scenario where the total bias of RPs, when measured jointly, is minimized. That said, without recognizing the geometry of how two parameter models of productivity limit RP space this may lead to unintuitive implications in RP estimation. For example, due to the shape of the BH RP set a minimal distance mapping ensures that if there is bias in one of  $\frac{B^*}{B_0}$  or  $F^*$ , there will necessarily be bias in the other RP. However under the Schaefer model, since the RP set is a constant in  $\frac{B^*}{B_0}$ , bias in  $F^*$  is not adulterated in the same way by bias in  $\frac{B^*}{B_0}$  estimation. While models with constant RPs, such as the logistic model  $\frac{B^*}{B_0} = \frac{1}{2}$  or the Fox model  $\frac{B^*}{B_0} = \frac{1}{e}$ , are extremely limited, they can be valuable tools for developing intuition precisely because they isolate RP estimation in their free RPs from

the correlated RP biases present in models like the BH or Ricker model.

When one considers the implications of RP bias, overestimation of RPs carries the severe implication of management recommendations potentially leading to overfishing, while underestimation of RP leads to overly conservative management. In this sense, when the true model is not known, the geometry of the BH set together with the metamodeled bias trends makes the BH model a naturally conservative estimator of RPs for most stocks. For most non-BH populations the BH model is likely to make conservative errors in its estimates of  $F^*$  and  $\frac{B^*}{B_0}$ . The one notable exception to the conservatism of the BH model stands for data generated in the Cushing-like regime of Schnute RPs. In this regime the BH model tends to be fairly unbiased overall, however the bias that is present for these populations tends to be overestimation in both RPs, leading to much more severe management consequences for those populations.

The RP bias trends of the Schaefer model demonstrate much less conservatism than the BH overall. For any population with  $\frac{B^*}{B_0} < 0.5$ ,  $\frac{B^*}{B_0}$  will be overestimated. When the population comes from the regime where  $\frac{B^*}{B_0} > 0.5$ ,  $\frac{B^*}{B_0}$  will be under estimated, but  $F^*$  is likely to be overestimated depending on the degree of contrast present in the data. So while the Schaefer model is an intuitive model, it tends to lead to much less conservative RP estimation.

While it is important to recognize these limitations of two parameter models of productivity, we should not solely accept conservatism as a rationale of choosing a BH model of productivity. Increasing the flexibility of the production function by moving toward three parameter models would release the underlying structural limitations (Mangel et al., 2013) that cause these RP biases in the first place. Punt and Cope (2019) considers a suite of possible three parameter curves which could be used instead of current two parameter curves. For all of their benefits, three parameter production functions have their own complicating factors, and the structure present in the Schnute model explored here makes it an intuitive bridge model for developing three parameter models going forward.

- [show a schnute fit to data?](#) (Yeakel & Mangel, 2015) Prior

- 894 • summary of  $\sigma$  over RP space comparing between models (PT, Schnute, Schnute DD)

895 to show areas of model breakdown.

  - 896 – miss-identifying signal for noise.
  - 897 – It happens more as the dynamics get more complex.
  - 898 – point to the full age structured models.
- 899 • show the constrained BH space over a grid of  $M, \kappa, \omega, W_\infty$
- 900 • Show that the constrained spaces vary only slightly as compared with the consequences

901 of misspecifying the functional form.
- 902 • estimating these other quantities (while they can create quite different Biomass series)

903 can only do so much to improve (expand) RP inference as compared with correctly

904 modeling  $P$ .
- 905 • mapping distance as a function of contrast at (3.5, 0.5)
- 906 • for LHS grid locations show  $\frac{B^*}{B_0}$  and  $F^*$  biases for grids in  $M \in (0, 0.5)$  For sure in High

907 Contrast, maybe also in Low??.



## 908 Chapter 3

### 909 A Delay Differential Model

910     • Introduction

- 911             – piggy back intro off of simpleModel
- 912             – problem statement and motivation
- 913             – introduce reference point and management decision making
- 914             – new dynamics of cohorting.

915     • Methods

- 916             – state and describe model
- 917             – Reference Point Derivation
- 918             – layout data generation/space filling problem
- 919             – how far to get the math for inputting into CAS
- 920             – method of CAS.
- 921             – describe and plot  $\zeta$ .
- 922             – constrained BH space (method for visualizing)
- 923             – appendix for RP CAS calculation

924     • Results

- 925     • summary of  $\sigma$  over RP space comparing between models (PT, Schnute, Schnute DD)
- 926         to show areas of model breakdown.
- 927             – miss-identifying signal for noise.
- 928             – It happens more as the dynamics get more complex.
- 929             – point to the full age structured models.
- 930     • Show that the constrained spaces vary only slightly as compared with the consequences
- 931         of misspecifying the functional form.
- 932     • ?Discussion?

- 933 • summary of  $\sigma$  over RP space comparing between models (PT, Schnute, Schnute DD)
- 934 to show areas of model breakdown.
- 935     – miss-identifying signal for noise.
- 936     – It happens more as the dynamics get more complex.
- 937     – point to the full age structured models.
- 938 • show the constrained BH space over a grid of  $M, \kappa, \omega, W_\infty$
- 939 • Show that the constrained spaces vary only slightly as compared with the consequences
- 940 of misspecifying the functional form.
- 941 • estimating these other quantities (while they can create quite different Biomass series)
- 942 can only do so much to improve (expand) RP inference as compared with correctly
- 943 modeling  $P$ .

# 1 Introduction

- the delay model: [J. Schnute \(1985\)](#) [J. Schnute \(1987\)](#) [Fournier and Doonan \(1987\)](#).
- discrete: [Hilborn and Walters \(1992, pg. 334\)](#)
- [Walters \(2020\)](#)
- automatic accounting for cohort cycles

## 2 Methods

### 2.1 Delay Differential Model

Age structured fisheries models typically assume [Von Bertalanffy \(1938, VB\)](#) growth in length with age. To model weight the assumption of VB growth in length is composed with a power law relating length to weight,  $w = al^b$ . Since  $b$  is usually  $\sim 3$  this composition of assumed functional forms typically results in a monotonically increasing sigmoidal curve of weight with age. When  $b \leq 1$  weight at age takes a VB-like form with  $b = 1$  resulting in an exact correspondence of simultaneous VB-growth in length and weight.

The delay model slightly abridges these relationships by directly assuming VB growth in weight as follows,

$$w(a) = w_{\infty}(1 - e^{-\kappa(a-a_0)}). \quad (3.1)$$

$\kappa$  is a parameter that controls the instantaneous rate of individual growth (in weight) with age.  $w_{\infty}$  is the maximum weight of individuals in the population, and  $w(a)$  is the average

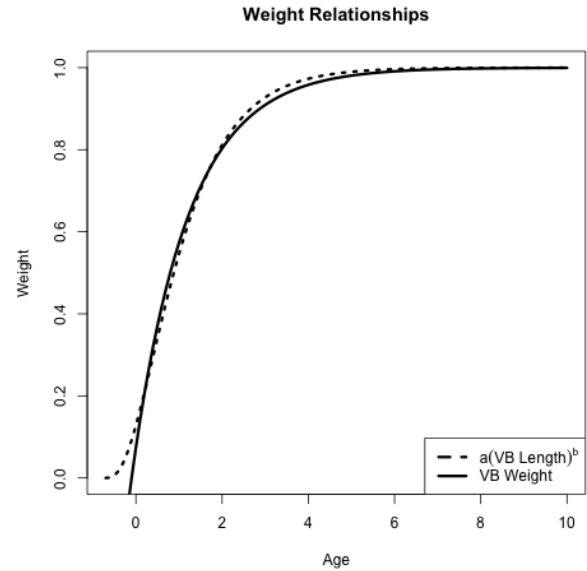


Figure 3.1: The typical composition of allometric weight ( $b = 3$ ) with VB growth in length, as approximated by VB growth in weight directly.

weight of an individual at age  $a$ . The parameter  $a_0$  controls the age at which individuals are assumed to have zero weight; by letting  $a_0 < 0$  this allows fish of age zero to have positive weight. Rather than taking a sigmoidally increasing function, VB growth directly in weight results in an monotonically increasing curve that asymptotes with a strictly decreasing growth rate with age. (only a good approximation for older ages where growth begins to decline)

Together with VB growth, the delay model is derived from the assumption that both natural mortality and fishing selectivity are separately proportional to a common heavyside step function with age. That is to say, before a threshold age of selectivity,  $a_s$ , the population is assumed not to experience any mortality whatsoever, but all fish older than  $a_s$  experience the same rate of natural mortality. Simultaneously all fish older than  $a_s$  are equally vulnerable to fishing (i.e. knife edge selectivity at age  $a_s$ ), although fishing effort may vary from through time.

Walters (2020) shows that within these assumptions the following delay differential system of equations exactly models the population dynamics of the total exploitable biomass  $B(t)$  and number of individuals  $N(t)$  through time.

$$\frac{dB}{dt} = w(a_s)R(B; \theta) + \kappa [w_\infty N - B] - (M + F)B \quad (3.2)$$

$$\frac{dN}{dt} = R(B; \theta) - (M + F)N \quad (3.3)$$

This formulation separates the number of individuals in the population from the biomass of the population. The dynamics of  $N$ , as seen in Eq (3.3), are very similar to that of the production models previously presented, however the role of the production function is now filled by a "recruitment" function,  $R(B)$ , which describes the number of new individuals recruiting into the exploitable population as a function of exploitable biomass. In turn, the biomass dynamics are coupled to the numbers dynamics by the assumption of VB growth with growth parameters appearing in Eq (3.2), converting population numbers into biomass and accounting for the growth of biomass with age.

Eq (3.2) of the above model expands the notion of biomass production into the processes of recruitment, individual growth, and maturity. The term  $w(a_s)R(B; \theta)$  represents the

987 biomass of new recruits; with  $w(a_s)$  representing the weight of individuals at the age of  
 988 maturity,  $a_s$ , and  $R(B; \theta)$  representing the number of new recruits entering the exploitable  
 989 population at time  $t$ . The negative term,  $(M + F)B$ , represents all causes of mortality as  
 990 it is applied to biomass. Finally, the term  $\kappa[w_\infty N - B]$  accounts for the net growth of the  
 991 existing biomass by discounting the limiting maximal individual growth rate by metabolic  
 992 weight loss proportional to  $B(t)$ . This term, together with the delay structure in  $R$ , provides  
 993 the major computational savings of the delay differential setting, as compared with full age  
 994 structured models, by automatically keeping track of changes in the mean size and growth  
 995 associated with changes in recruitment as cohorts mature into the population.

Often a BH functional form is assumed for the stock recruitment relationship, but any adequately flexible family of functions may model this relationship. For the sake of evaluating the adequacy of assumed BH recruitment the simulation setting below is derived for the delay model under the assumption of the generalized three parameter Schnute recruitment as follows.

$$R(B; [\alpha, \beta, \gamma]') = \alpha B(t - a_s)(1 - \beta \gamma B(t - a_s))^{\frac{1}{\gamma}} \quad (3.4)$$

996 The parameters  $\theta' = [\alpha, \beta, \gamma]$  function similarly in this setting as previously described in  
 997 Section (??). That said, since the delay model explicitly parses out growth in it's dynamics,  
 998 these parameters only describe the net processes of larval production, and maturation into  
 999 the population, where as the production model used these parameters to also model the net  
 1000 effects of growth on biomass production. The  $\gamma$  parameter generalizes the family to model  
 1001 varying degrees of decreasing recruitment for large biomasses as  $\gamma$  increases. The Schnute  
 1002 function is exactly equivalent to BH recruitment at the special case when  $\gamma = -1$ , it passes  
 1003 through the Ricker model as  $\gamma \rightarrow 0$ , and Logistic recruitment occurs when  $\gamma = 1$ .

1004 Since the delay model assumes knife edge selectivity, at age  $a_s$ , the term  $B(t - a_s)$  appears  
 1005 in  $R$ . That is to say fish recruiting into the exploitable population are the result of larval  
 1006 production of biomass  $a_s$  time units in the past. This is because fishing selectivity is only  
 1007 assumed to occur for fish that are at least  $a_s$  time units old and thus fish younger than  $a_s$   
 1008 are not exploitable. This waiting period requires that new recruits be the result of spawning

1009 biomass  $a_s$  time units in the past. Modeling maturity in this way results in dynamics  
 1010 equations which are a system of delay differential equations as opposed to the simple ODEs  
 1011 that arise in the production model setting.

1012  $\sim$  interpretation of recruitment (larval production, recruitment) [growth external] vs.  
 1013 production (larval production, recruitment, growth)

1014 • general structure: [Walters \(2020\)](#) [Hilborn and Walters \(1992, pg. 334\)](#)

1015 • growth: [Von Bertalanffy \(1938\)](#)

1016 • recruitment: [J. Schnute \(1985\)](#); [J. T. Schnute and Richards \(1998\)](#)

## 1017 2.2 Reference Points

1018 Deriving reference points for the delay model under Schnute recruitment is conceptually  
 1019 similar to the production model setting. The additional nonlinear VB growth assumptions  
 1020 along side Schnute recruitment quickly make the expressions look somewhat unweildy, al-  
 1021 though analytical solutions can still be derived for most of the same quantities (although  
 1022 complicated by growth parameters).

Starting from Eqs. (3.2) and (3.3), setting both  $\frac{dB}{dt}$  and  $\frac{dN}{dt}$  simultaneously equal to zero, and solving for  $B$  and  $N$  as a function of fishing, gives the equilibrium biomass and numbers equations.

$$\bar{B}(F) = \frac{1}{\beta\gamma} \left( 1 - \left( \frac{(F+M)(F+M+\kappa)}{\alpha w(a_s)(F+M+\frac{\kappa w_\infty}{w(a_s)})} \right)^\gamma \right) \quad (3.5)$$

$$\bar{N}(F) = \frac{\alpha \bar{B}(F)(1 - \beta\gamma \bar{B}(F))^{1/\gamma}}{F+M} \quad (3.6)$$

1023 Eq. (3.6) is just  $\frac{R(\bar{B})}{F+M}$ , and is coupled to  $\bar{B}(F)$  where most of the dynamics appear. Eq.  
 1024 (3.5) resembles Eq (3.27) from the simple production model setting although the growth  
 1025 parameters  $\kappa$ ,  $w_\infty$  and  $w(a_s)$ , make slight adjustments to the balance of the maximum rate  
 1026 of recruitment and mortality rate to give an expression for equilibrium biomass that accounts  
 1027 for the factors of individual growth.

Expressions for  $B_0$  and  $B^*$  are attained by evaluating  $\bar{B}(F)$  at  $F = 0$  and  $F = F^*$  respectively. Calculation of  $F^*$  typically involves maximization of equilibrium yield,  $\bar{Y} = F\bar{B}(F)$ . While it was not possible to analytically maximize  $\bar{Y}$ , stable numerical solutions for calculating  $F^*$  were obtained by numerically solving for the roots of the analytical derivative of equilibrium yield with respect to  $F$ . Below a greatly simplified expression for  $\frac{d\bar{Y}}{dF}$  is shown; the substitution  $Z = F + M$  (total mortality rate) has been made to produce a more compact expression.

$$\frac{d\bar{Y}}{dF} = \frac{1}{\beta\gamma} \left[ 1 - \left( \frac{Z(Z + \kappa)}{\alpha w(a_s)(Z + \frac{\kappa w_\infty}{w(a_s)})} \right)^\gamma - \left( \frac{\gamma F}{\alpha w(a_s)} \right) \left( \frac{Z(Z + \kappa)}{\alpha w(a_s)(Z + \frac{\kappa w_\infty}{w(a_s)})} \right)^{\gamma-1} \left( 1 + \frac{\left( \frac{\kappa w_\infty}{w(a_s)} \right) \left( \kappa - \frac{\kappa w_\infty}{w(a_s)} \right)}{\left( Z + \frac{\kappa w_\infty}{w(a_s)} \right)^2} \right) \right] \quad (3.7)$$

$F^*$  is calculated as the numerical root, w.r.t.  $F$ , of the above expression. The numerical root is calculated using the base R uniroot function which employs a derivative free search given by [Brent \(1973\)](#).

### BH Constraint

In the simple production model the BH constrained RPs are fixed to  $\frac{1}{x+2}$ . In the delay differential modeling setting the constrained BH RP set is complicated the growth parameters  $a_s$  and  $\kappa$ . Under BH recruitment these parameters of the delay model slightly influence this relationship as seen in Figure (3.13). That said, the influence of  $a_s$  and  $\kappa$  on RPs is still largely limited to a confined region of reference point space which resembles the  $\frac{1}{x+2}$  form. In fact the confined region of RPs is bounded above by  $\frac{1}{x+2}$ . In Figure (3.13) notice that for high values of  $\kappa$  and small values of  $a_s$  (red region) the BH RP space converges to  $\frac{1}{x+2}$  as derived in the simple production model setting. The opposite limit with low values of  $\kappa$  and high values  $a_s$

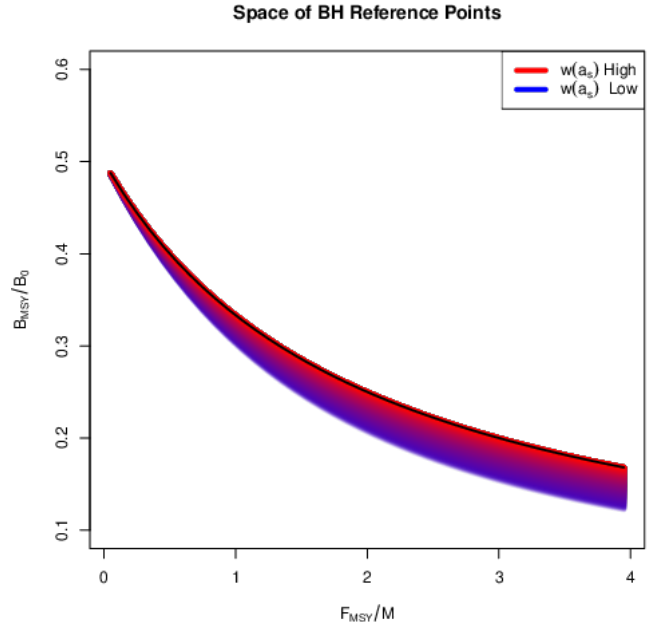


Figure 3.2: The space of BH RPs for the delay model as a function of  $\kappa$  and  $a_s$ . The RP space is plotted for  $80 \times 80$  combinations of  $\kappa \in [0.1, 2]$  and  $a_s \in [0.1, 10]$ . The color drawn is the resulting value of  $w(a_s)$  mapped between blue and red.  $\frac{1}{x+2}$  is plotted in black for reference.



1055 (blue region) depresses RPs away from  $\frac{1}{x+2}$ .

## 1056 2 .3 Delay Differential Integration

1057 The delay model belongs to a class of differential equations known as delay differential  
1058 equations (DDE). The delay arises from the  $B(t - a_s)$  terms found in the recruitment  
1059 function. Solving DDEs require special care which depends on the nature of the time delay.  
1060 The addition of time-varying delays, many different delays, or very small delays (delays  
1061 below the step size of the numerical integrator) results in some of the more challenging  
1062 settings for solving DDEs. However with a single stationary model of the age of selectivity,  
1063 the delay model in this setting represents one of the most straight forward DDE structures.  
1064 The most numerically challenging case presented here arises in the case of the limiting  
1065 production model when  $a_s \rightarrow 0$  while  $\kappa \rightarrow \infty$ . That said the limiting production model can  
1066 be approximated for values of  $a_s \approx 0.1$ , and it was straightforward to ensure that the step  
1067 size of the integrator remained reasonably below 0.1.

1068 The DDE presented here is integrated with the initial values fixed at  $B_0$  and  $N_0$  as given  
1069 by Eqs. (3.5) and (3.6) with  $F = 0$  at any given configuration of  $\theta$  and growth parameters.  
1070 The system given in Eqs. (3.2) and (3.3) are then solved numerically using the implicit  
1071 Livermore Solver (lsode) as implemented in the `dede` function of the R package `deSolve`  
1072 (Soetaert et al., 2010). The `dede` solver provides many methods for integrating DDEs, but  
1073 lsode was chosen because it is an implicit method that runs relatively quickly with a relatively  
1074 smaller footprint in system memory as compared with other methods. The radau method  
1075 was also tried in more computationally challenging settings with good results (albeit running  
1076 more slowly than lsode). Ultimately the simulated parameter space did not produce DDEs  
1077 that require the more expensive radau integrator to solve accurately.

## 1078 2 .4 Simulation Design

1079 Similarly as previously described in Section (5 ) the relationship between RPs  $\mapsto \theta$  cannot be  
1080 fully expressed analytically for the Schnute delay model. However, just as in the production  
1081 model setting, simulation only requires enough knowledge of these mappings to gather a list  
1082 of  $(\alpha, \beta, \gamma)$  tuples and the corresponding RPs in some reasonable space-filling design over

1083 RP space.

1084 In the delay model a partial mapping for  $(F^*, B_0) \mapsto (\alpha(\cdot, \gamma), \beta(\cdot, \cdot, \gamma))$  can be derived  
 1085 analytically in terms of RPs and  $\gamma$ . The substitution  $Z^* = F^* + M$  is made where  $F^*$  and  
 1086  $M$  appear together to produce a more compact expression.

$$\alpha = \left[ \left( \frac{Z^*(Z^* + \kappa)}{w(a_s)(Z^* + \frac{\kappa w_\infty}{w(a_s)})} \right)^\gamma + \left( \frac{\gamma F^*}{w(a_s)} \right) \left( \frac{Z^*(Z^* + \kappa)}{w(a_s)(Z^* + \frac{\kappa w_\infty}{w(a_s)})} \right)^{\gamma-1} \left( 1 + \frac{\left( \frac{\kappa w_\infty}{w(a_s)} \right) \left( \kappa - \frac{\kappa w_\infty}{w(a_s)} \right)}{(Z^* + \frac{\kappa w_\infty}{w(a_s)})^2} \right) \right]^{\frac{1}{\gamma}} \quad (3.8)$$

$$\beta = \frac{1}{\gamma B_0} \left( 1 - \left( \frac{M(M + \kappa)}{\alpha w(a_s)(M + \frac{\kappa w_\infty}{w(a_s)})} \right)^\gamma \right) \quad (3.9)$$

Above Eq. (3.8) results from setting Eq. (3.31) equal to zero and solving for  $\alpha$ , and Eq. (3.9) results from solving the  $\bar{B}(0)$  expression, as derived from Eq. (3.5), for  $\beta$ . The system is completed by further working with the  $\frac{\bar{B}(F^*)}{\bar{B}(0)}$  expression, as seen below, to identify  $\gamma$ .

$$\frac{B^*}{B_0} = \frac{1 - \left( \frac{(F^* + M)(F^* + M + \kappa)}{\alpha w(a_s)(F^* + M + \frac{\kappa w_\infty}{w(a_s)})} \right)^\gamma}{1 - \left( \frac{M(M + \kappa)}{\alpha w(a_s)(M + \frac{\kappa w_\infty}{w(a_s)})} \right)^\gamma} \quad (3.10)$$

1087 The system formed by collecting Eqs. (3.8), (3.9), and (3.10) can be navigated similarly  
 1088 to Eq. (3.33) in the Schnute production model setting. For a population experiencing  
 1089 natural mortality  $M$ , VB growth with paramters  $\kappa$  and  $w_\infty$ , and age of selectivity  $a_s$  the  
 1090 above system can fully specify  $\alpha$  and  $\beta$  for a given  $\gamma$ , by fixing  $F^*$ ,  $B_0$ , and  $\frac{B^*}{B_0}$ . For a given  $\gamma$   
 1091 a cascade of closed form solutions for  $\alpha$  and  $\beta$  can be obtained, just as in Section (5 ). First  
 1092  $\alpha(\gamma)$  can be computed, and then  $\beta(\alpha(\gamma), \gamma)$  can be computed. If  $\alpha(\gamma)$  is filled back into the  
 1093 expression for  $\frac{B^*}{B_0}$ , the system collapses into a single onerous expression for  $\frac{B^*}{B_0}(\alpha(\gamma), \gamma)$ . For  
 1094 brevity, define the function  $\zeta(\gamma) = \frac{B^*}{B_0}(\alpha(\gamma), \gamma, F^*, M)$  based on Eq. (3.10).

1095 Again rather than inverting  $\zeta(\gamma)$  for  $\gamma$ ,  $\gamma$  is the sampled so that the overall simulation  
 1096 design is space filling as described in Section (5 .3). Given the sampled  $\gamma$ , the cascade of  
 1097  $\alpha(\gamma)$ , and then  $\beta(\alpha(\gamma), \gamma)$ , can be computed, and the Schnute delay model is fully defined  
 1098 by a given  $(\frac{F^*}{M}, \frac{B^*}{B_0})$ . While conceputally this framing is similar to the Schnute production  
 1099 model, the analytical expressions are more complex, and numerically trecherous, since growth  
 1100 parameters appear explicitly here. Other ways of navigating the RPs  $\mapsto \theta$  system are possible,

1101 but for the sake of numerical stability this strategy has proven the most reliably accurate by  
 1102 limiting exposure to numerical error propagation.

1103 Each design location defines a complete Schnute delay differential model with the given  
 1104 RP values. Indices of abundance are simulated from the Schnute model at each design  
 1105 location, a small amount of residual variation,  $\sigma = 0.01$ , is added to the simulated index,  
 1106 and the data are then fit with a misspecified BH model. The design captures various degrees  
 1107 of model misspecification relative to the BH model, so as to observe the effect of recruitment  
 1108 misspecification upon RP inference.

1109 point to catch, and LHS design, and Metamodel.

## 1110 2 .5 Parmeter Estimation

- 1111 • I use B only here
- 1112 • quick statement of inference, and reference to previous section

Let  $I_t$ ,  $t \in \{1, 2, 3, \dots, T\}$ , be a series of indicies of abundance, proportional to biomass, as simulated from the Schnute Delay model. These data are modelled with the following log-normal observation model that has been intentionally constrained to BH recruitment,

$$I_t \sim LN(qB_t(\boldsymbol{\theta}, \boldsymbol{\phi}), \sigma^2). \quad (3.11)$$

1113  $B_t(\boldsymbol{\theta}, \boldsymbol{\phi})$  is the biomass solution of the BH constrained DDE system. The BH constraint  
 1114 isimplemented by fixing  $\gamma = -1$  so that  $\boldsymbol{\theta}' = [\alpha, \beta, \gamma = -1]$ .  $\boldsymbol{\phi}$  is a vector of growth and  
 1115 maturity parameters,  $\boldsymbol{\phi}' = [\kappa, w_\infty, a_0, a_s]$ . The nuisance parameter  $q$  models the proportion-  
 1116 ality constant of the index with process biomass, and  $\sigma^2$  models residual variation of the  
 1117 index.

1118 In this setting,  $\boldsymbol{\phi}$  and  $q$  are fixed to focus on the inferential affects of model misspecifi-  
 1119 cation on recruitment parameters and RPs. Without an explicite mechanism for the delay  
 1120 model to incorporate age data, under the BH model  $\boldsymbol{\phi}$  is not well informed and would typically  
 1121 be estimated externally for data limited stocks. Under BH recruitment  $\boldsymbol{\phi}$  can only slightly  
 1122 impact RPs as seen in Figure (3.13).

1123  $\sigma^2$  and  $\theta$  are reparameterized to the log scale and fit via MLE. Reparameterizing the

1124 parameters to the log scale improves the reliability of optimization, in addition to facili-  
 1125 tating the use of Hessian information for estimating MLE standard errors. Given that the  
 1126 biological parameters enter the likelihood via a nonlinear differential equation, and further  
 1127 the parameters themselves are related to each other nonlinearly, the likelihood function can  
 1128 often be difficult to optimize. A hybrid optimization scheme is used to maximize the log  
 1129 likelihood to ensure that a global MLE solution is found. The R package GA (Scrucca, 2013,  
 1130 2017) is used to run a genetic algorithm to explore parameter space globally. Optimization  
 1131 periodically jumps into the L-BFGS-B local optimizer to refine optima within a local mode.  
 1132 The scheme functions by searching globally, with the genetic algorithm, across many initial  
 1133 values for starting the local gradient-based optimizer. The genetic algorithm serves to iter-  
 1134 atively improve hot starts for the local gradient-based optimizer. Additionally, optimization  
 1135 is only considered to be converged when the optimum results in an invertible Hessian at the  
 1136 found MLE.

- 1137 • fixed  $M = 0.2$ ,  $a_0 = -1$ ,  $w_\infty = 1$
- 1138 • play with  $\kappa$  and age of selectivity  $a_s$

## 1139 Numbers Indices

While not utilized here, age structured models may commonly model indices as proportional  
 to numbers rather than (or simultaiously to) biomass. When solving the DDE, Eq. (3.3)  
 points out that the full DDE solution will expose a numbers solution simultaneously with  
 a biomass solution that may be used for these purposes. These solutions are often quite  
 similar since the main driver of process behavior comes from the form of  $R$  which is shared  
 among  $N$  and  $B$ . However, it is common on the west coast of the US that indices derived  
 from commercial fisheries are measured as weights while indices derived from recreational  
 fisheries are often measured as counts. If a numbers index,  $J_t$ , is observed alongside the  
 previously mentioned biomass index, the following likelihood component is often added as a  
 conditionally independent component of the likelihood,

$$J_t \sim LN(pN_t(\boldsymbol{\theta}, \boldsymbol{\phi}), \tau^2). \quad (3.12)$$

1140  $N_t(\boldsymbol{\theta}, \boldsymbol{\phi})$  is the numbers solution of the DDE system.  $\boldsymbol{\theta}$  and  $\boldsymbol{\phi}$  are the productivity and  
 1141 growth parameters shared in common with the biomass component.  $p$  and  $\tau^2$  are then the  
 1142 analogous proportionality constant and residual variation of the numbers index respectively.

## 1143 2.6 GP Metamodel

1144 point to catch, and LHS design, and Metamodel.

## 1145 3 Results

1146 Figure (3.3) shows three hypothetical  
 1147 individual-growth/maturity curves that span  
 1148 a wide range of RPs. As seen in Figure  
 1149 (3.13), the larger values of  $w(a_s)$  correspond  
 1150 to less dramatic growth with the red curve  
 1151 demonstrating the simple (no growth) pro-  
 1152 duction model limit ( $a_s \rightarrow 0$  and  $\kappa \rightarrow \infty$ ).  
 1153 The cases with smaller  $w(a_s)$  values (blue  
 1154 and purple curves) correspond to more dra-  
 1155 matic growth behaviors, with the blue curve  
 1156 where  $a_s = 2$  and  $\kappa = 0.1$  representing the  
 1157 most dramatic growth shown here.

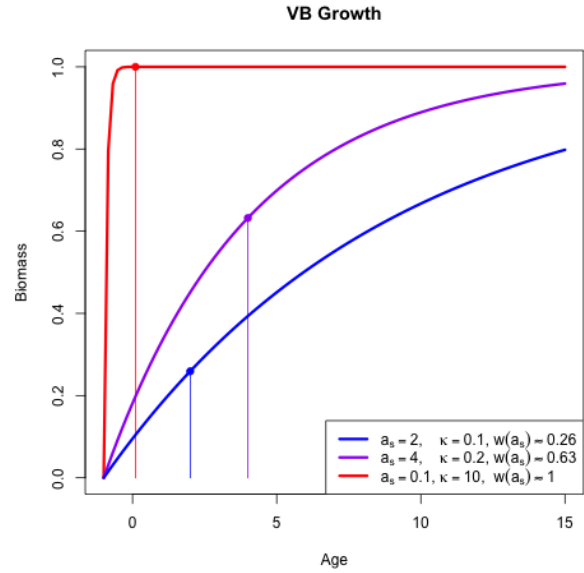


Figure 3.3: Three hypothetical individual-growth curves, showing  $w(a_s)$  on each curve.

1158 Figure (3.4) demonstrates a range of biomass dynamics that the Schnute delay model  
 1159 can display under a spectrum of growth behaviors with fishing held consistent at  $F_{MSY}$ . The  
 1160 three special cases of  $\gamma = -1$  (BH),  $\gamma \rightarrow 0$  (Ricker), and  $\gamma = 1$  (Logistic) recruitment are  
 1161 shown in each of the above shown growth configurations. Notice under the most dramatic  
 1162 growth ( $a_s = 2$  and  $\kappa = 0.1$ ) setting, biomass of the Logistic model comes into equilibrium  
 1163 at  $B_{MSY}$  as an oscillating curve. This effect occurs here due to the Logistic model's steeply  
 1164 right leaning yield curve interacting with the lag in selectivity upon the sudden onset of  
 1165 fishing; this produces a shock that oscillates over the steepest regions of the yield curve. One  
 1166 may also observe these oscillations under the Ricker model by exaggerating the  $a_s$  lag as well  
 1167 as the steepness of the Ricker curve. The BH model may also demonstrate these oscillations,

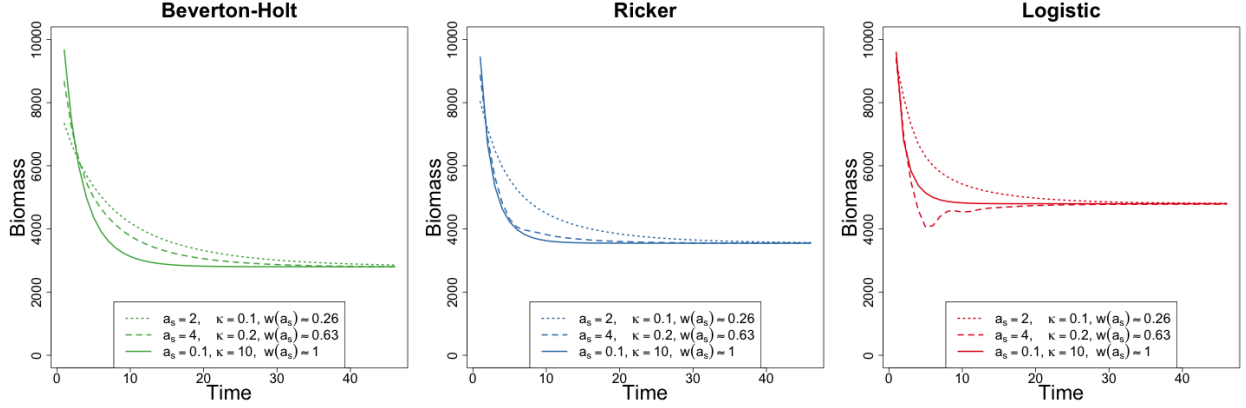


Figure 3.4: Biomass dynamics of BH (*left*), Ricker (*center*), and Logistic (*right*) delay differential models in the low contrast simulation setting. In all cases  $\alpha = 1.2$  and  $\beta$  is chosen so that each model shares the same  $B_{MSY}$  within each given  $\gamma$ .

in a heavily lagged setting, by shocking the population over the steepest portion of its yield curve (a sudden release in fishing applied to a heavily fished population at low equilibrium biomass).

Figure (3.5) shows the range of RPs that can be modeled with each of the BH, Ricker, and Logistic recruitments over the spectrum of individual-growth/maturity models simulated here. Notice that the more dramatic the growth, the further the RP curve lies from the simple production model, but each recruitment model reacts differently under each of the given growth parameters. The Ricker and BH RP-spaces are qualitatively similar in shape with more dramatic growth settings decreasing  $\frac{B_{MSY}}{B_0}$  relative to the simple production model setting. The Logistic model on the other hand increases  $\frac{B_{MSY}}{B_0}$  relative to the simple production model setting as growth parameters become more dramatic. It is also worth noting that the Ricker model's RPs are much less influenced by growth parameters as compared with that of the BH or Logistic model.

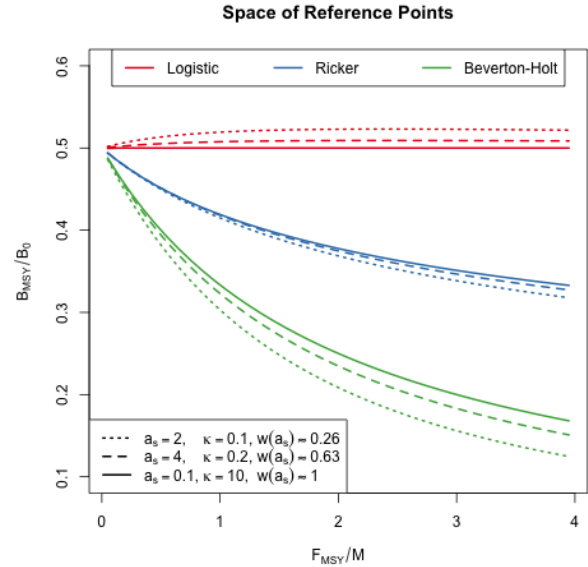


Figure 3.5: Restricted RP-space under each recruitment models, with each growth curve.

1187 **3 .1 Simple Production Model Limit**

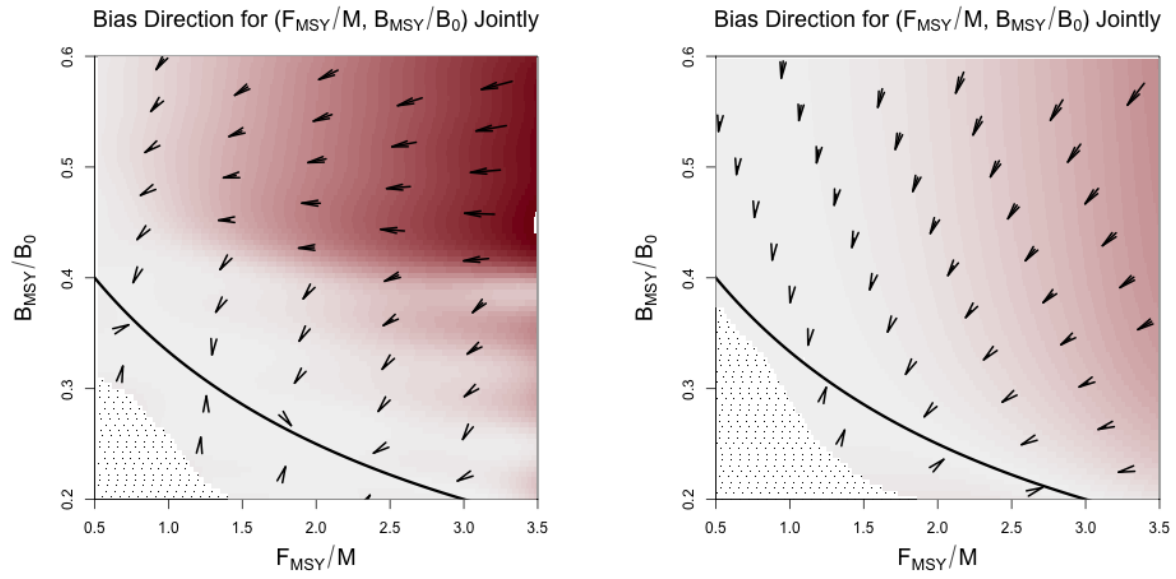


Figure 3.6:

- 1188 • Reiterate from simple case





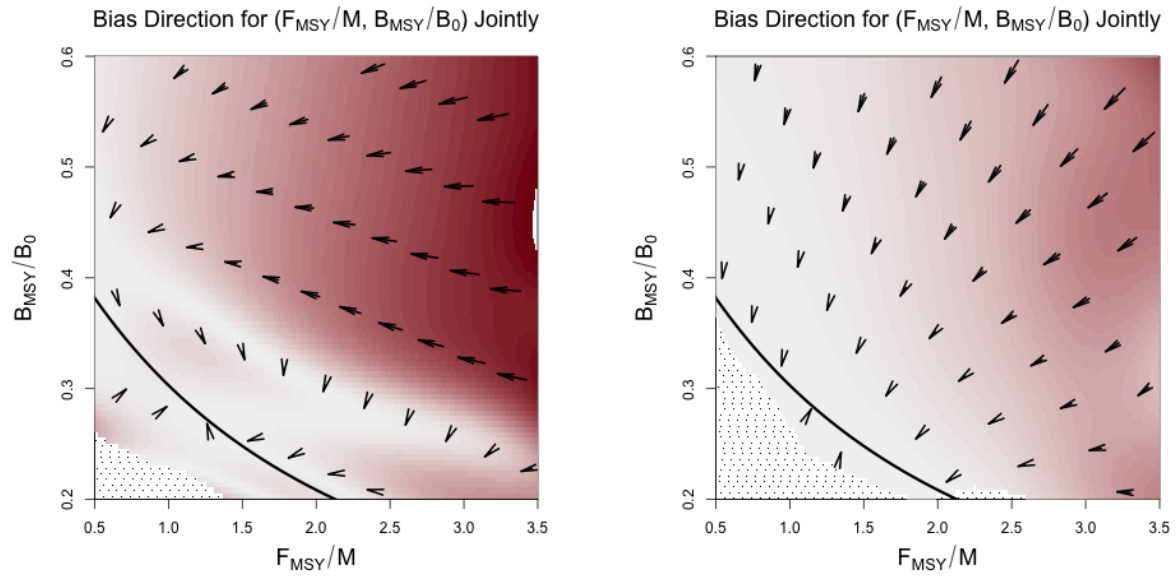


Figure 3.7:

1191 **3 .4 Ocillatory Growth Influence**

1192 maybe an appendix

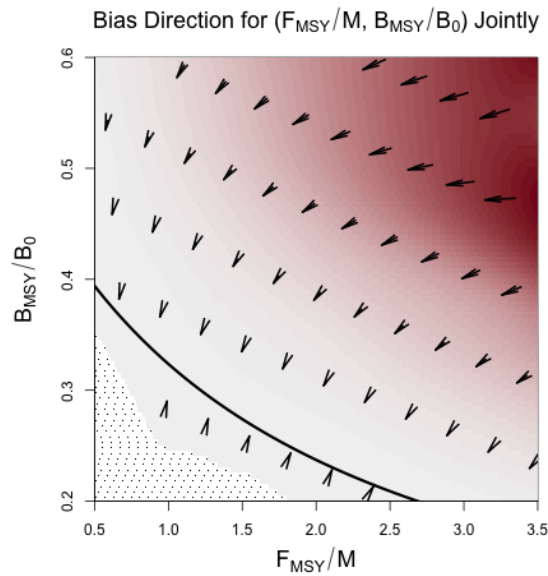


Figure 3.8:

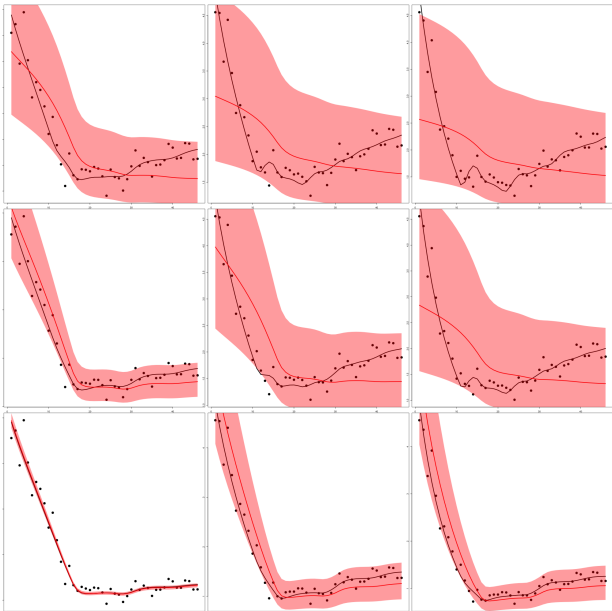


Figure 3.9:

- 1193 • Selectivity and Growth cannot account for misspecification of Recruitment.

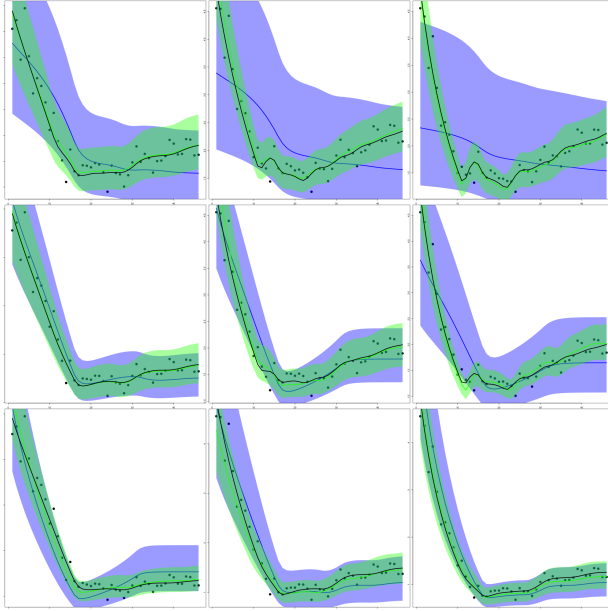


Figure 3.10:

- Selectivity and Growth are influenced by the proper specification of recruitment. If properly specified Selectivity and Growth can be estimated, along with all three parameters of the Schnute model.

- show production model limit (contrast

- $a_s \rightarrow 0$ : instant maturity

- $\kappa \rightarrow \infty$ : recruit as an adult ()

- describe second order shapes of growth/maturity (and cause)

- weight of recruits => scaling biomass ( $q$ ,  $\beta$ , and  $w_\infty$ )

- 

- describe RP bias

- flat

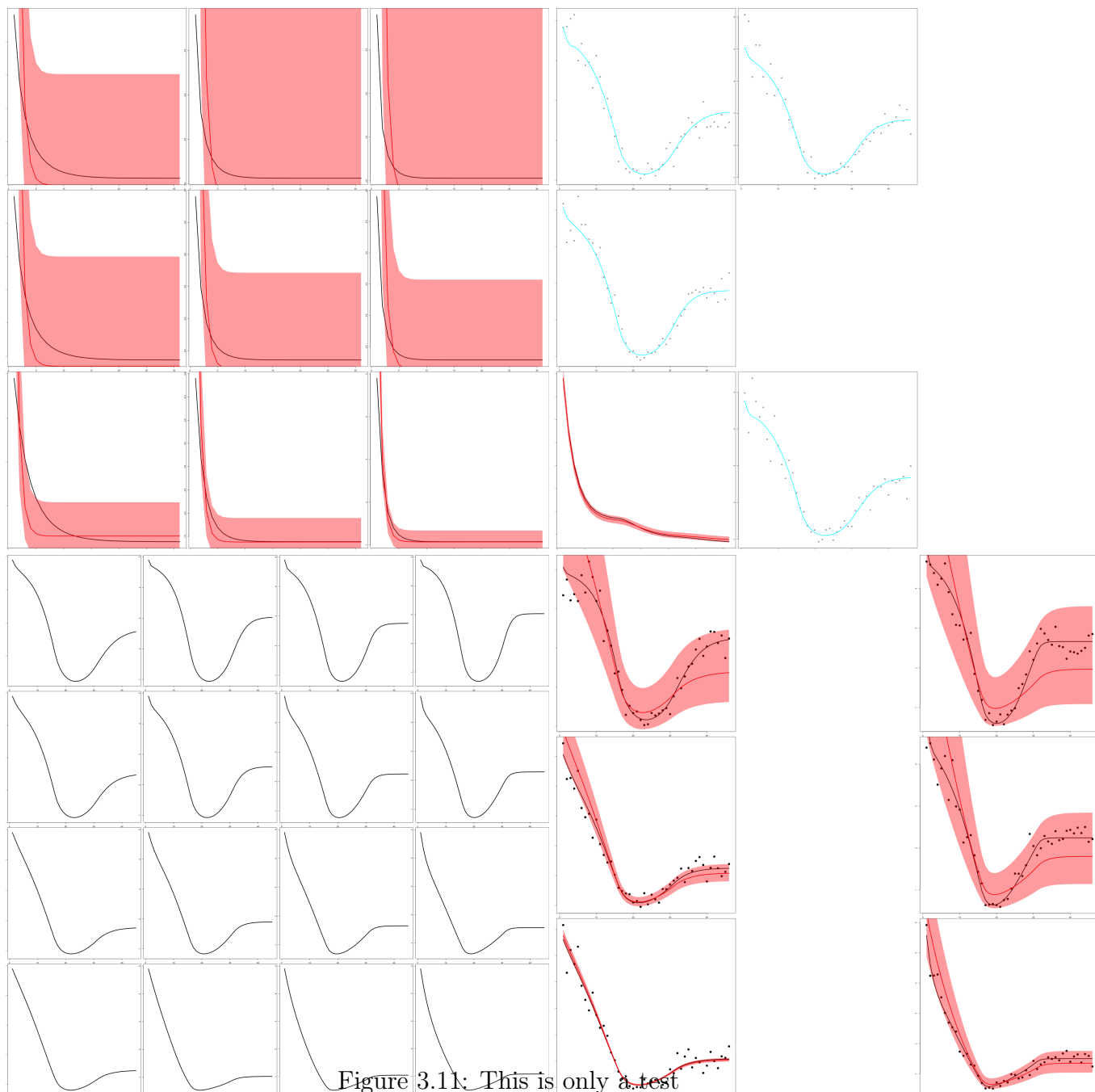


Figure 3.11: This is only a test

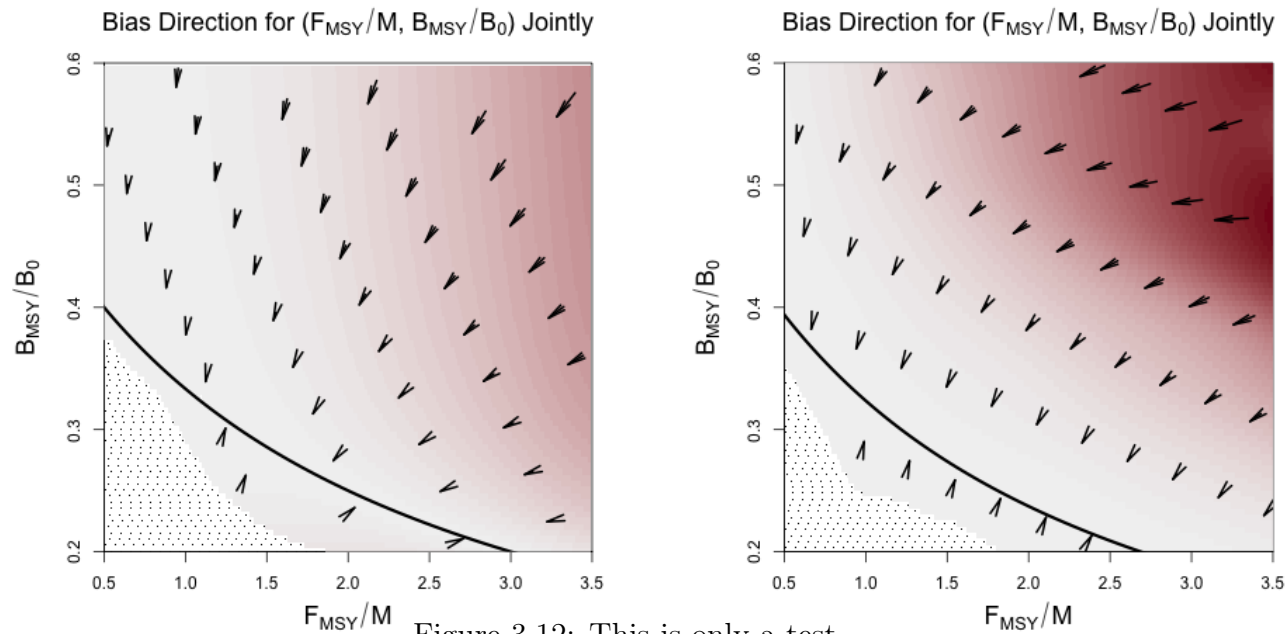


Figure 3.12: This is only a test

1205

why not here?

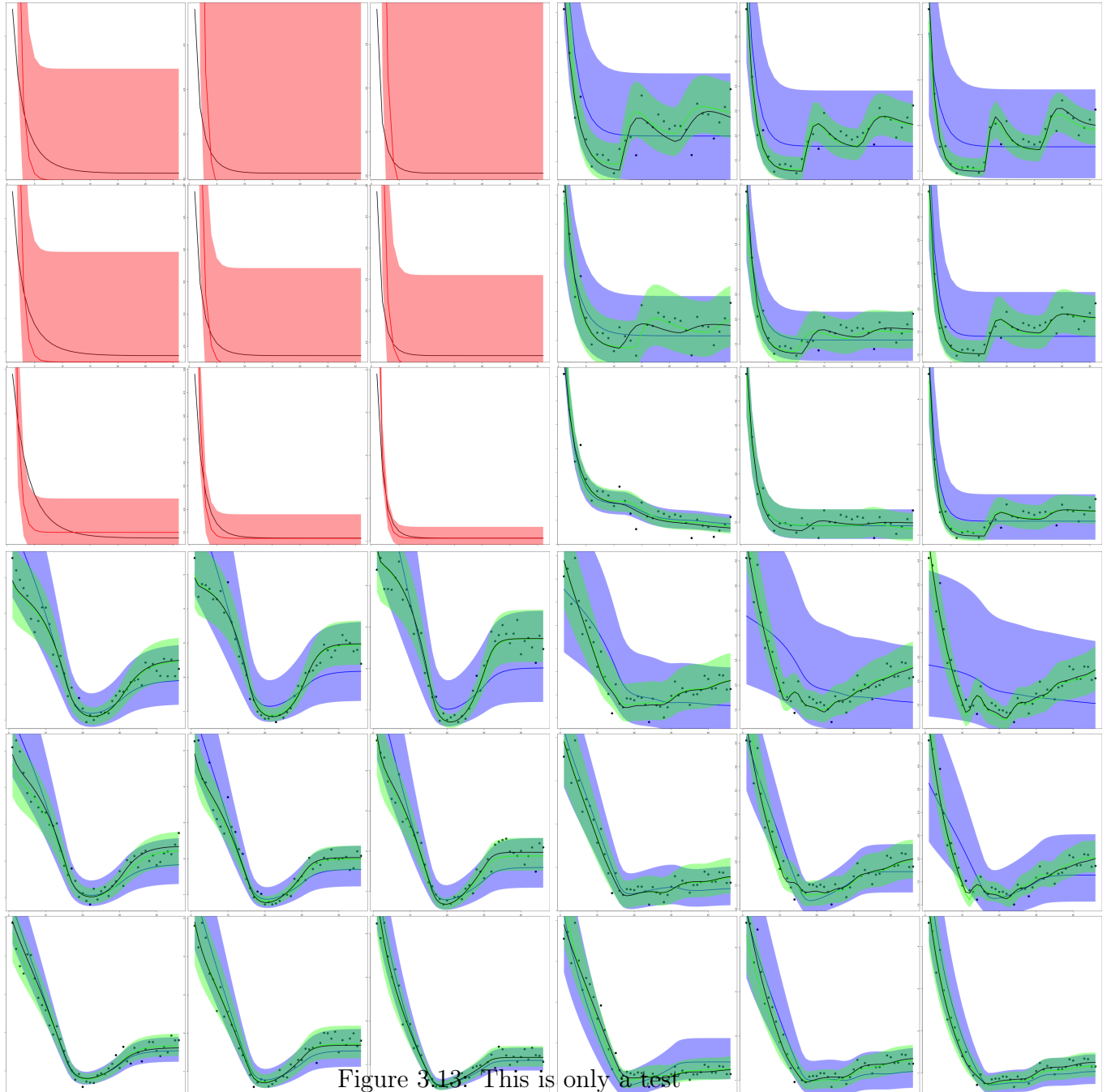


Figure 3.13. This is only a test

## 4 Introduction

The most fundamental model in modern fisheries management is the surplus-production model. These models focus on modeling population growth via nonlinear parametric ordinary differential equations (ODE). Key management quantities called reference points (RPs) are commonly derived from the ODE equilibrium equations and depend upon the parameterization of biomass production. Two-parameter forms of the production function have been shown to limit the theoretical domain of RPs (Mangel et al., 2013). The limited RP-space of two parameter models are a major source of model misspecification for RPs and thus induce bias in RP estimation. The behavior of RP estimation bias is not well understood and as a result often underappreciated. A metamodeling approach is developed here to describe RP biases and explore mechanisms of model failure under the most common two parameter models.

Data for a typical surplus-production model comes in the form of an index of abundance through time which is assumed to be proportional to the reproducing biomass for the population of interest. The index is often observed alongside a variety of other known quantities, but at a minimum, each observed index will be observed in the presence of some known catch for the period. Figure (3.14) shows the classic Namibian Hake dataset exemplifying the form.

Indices are assumed to have multiplicative log-normal errors, and thus the following observation model arises naturally,

$$I_t = qB_te^\epsilon \quad \epsilon \sim N(0, \sigma^2). \quad (3.13)$$

Above  $q$  is often referred to as the “catchability parameter”; it serves as the proportionality constant mapping between the observed index of abundance and biomass.  $\sigma^2$  models residual variation. Biologically speaking  $q$  and  $\sigma^2$  are often treated as nuisance parameters with the “biological parameters” entering the model through a process model on biomass.

Biomass is assumed to evolve as an ODE; in this case I focus on the following form

$$\frac{dB}{dt} = P(B(t); \boldsymbol{\theta}) - Z(t)B(t). \quad (3.14)$$

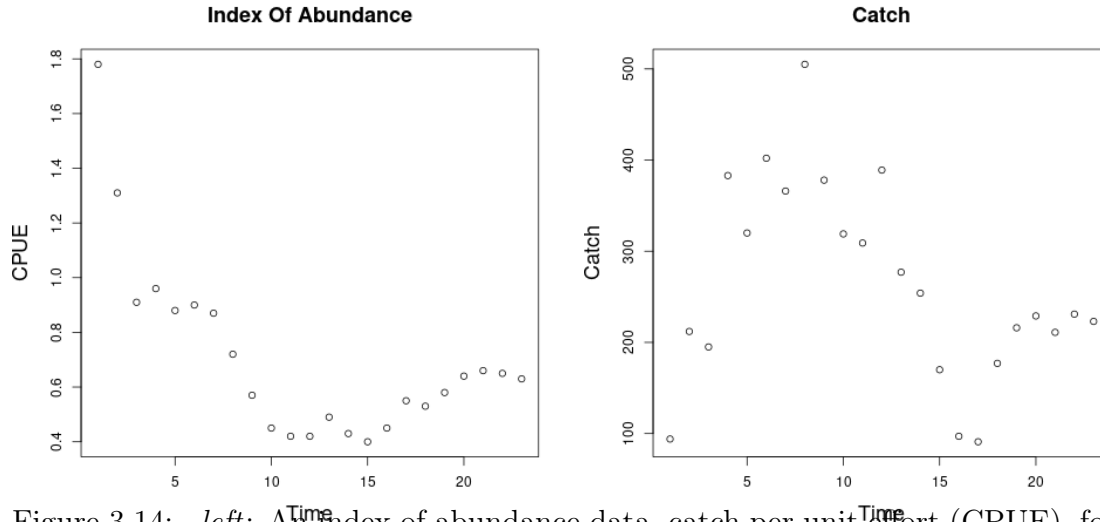


Figure 3.14: *left*: An index of abundance data, catch per unit effort (CPUE), for Namibian Hake from 1965 to 1987 (Hilborn & Mangel, 1997). *right*: The associated catch data for Namibian Hake over the same time period.

Here biomass is assumed to change in time by two processes, net production of biomass into the population,  $P(B)$ , and various sources of biomass removal,  $Z$ , from the population.

Firstly, the population grows through a production function,  $P(B)$ . Production in this setting is defined as the net biomass increase due to all reproduction and maturation processes. The production function is assumed to be a parametric (generally non-linear) function relating the current biomass of the population to an aggregate production of biomass.

Secondly, the population decreases as biomass is removed by various sources that are assumed to remove biomass linearly with biomass. Above,  $Z(t)$ , is an aggregate rate of removal. When the fishing rate,  $F(t)$ , is the only source of removal  $Z(t) = F(t)$ , however often models will also included other linear terms in  $Z(t)$ . Commonly the rate of “natural mortality”,  $M$ , is also included as an additional term so that  $Z(t) = M + F(t)$ .

From a management perspective a major goal of modeling is to accurately infer a quantity known as *maximum sustainable yield* (MSY). One could maximize simple yield at a particular moment in time (and only for that moment) by fishing all available biomass in that moment. This strategy is penny-wise but pound-foolish (not to mention ecologically devastating) since it doesn’t leave biomass in the population to reproduce in the future. We seek to fish in a way that allows (or even encourages) future productivity in the population. This is accomplished by maximizing the equilibrium level of catch over time. Equilibrium yield is considered by



replacing the steady state biomass ( $\bar{B}$ ) in the assumed form for catch, so that  $\bar{Y} = F\bar{B}(F)$ , where  $\bar{\cdot}$  indicates a value at steady state. MSY is found by maximizing  $\bar{Y}(F)$  with respect to  $F$ , and  $F^*$  is the fishing rate at MSY. Going forward let  $*$  decorate any value derived under the condition of MSY.

Fisheries are very often managed based upon reference points which serve as simplified heuristic measures of population behavior. The mathematical form of RPs depends upon the model assumptions through the production function. While a number of different RPs exist which describe the population in different (but related) ways, the most common RPs revolve around the concept of MSY (or robust ways of measuring MSY (Hilborn, 2010; Punt et al., 2016)). Here the focus is primarily on the RPs  $\frac{B^*}{B(0)}$  and  $F^*$  ( $\frac{F^*}{M}$  when appropriate) for their pervasive use in modern fisheries (Punt & Cope, 2019).

$F^*$  is the afore mentioned fishing rate which results in MSY.  $\frac{B^*}{B(0)}$  is the depletion of the stock at MSY. That is to say  $\frac{B^*}{B(0)}$  describes the fraction of the unfished population biomass that will remain in the equilibrium at MSY. In general  $F^* \in \mathbb{R}^+$  and  $\frac{B^*}{B(0)} \in (0, 1)$ , however under the under the assumption of a two parameter production function production models will be structurally unable to capture the full theoretical range of RPs.

Many of the most commonly used production functions depend only on two parameters. For example, the Schaefer model depends only on the biological parameters  $r$  and  $K$ , and limits RP inference so that under the Schaefer model  $\left(F^*, \frac{B^*}{B(0)}\right) \in \left(\mathbb{R}^+, \frac{1}{2}\right)$ . The two parameter Fox model (Fox Jr., 1970) limits  $\left(F^*, \frac{B^*}{B(0)}\right) \in \left(\mathbb{R}^+, \frac{1}{e}\right)$ . Similarly the two parameter Cushing (Cushing, 1971), Beverton-Holt (Beverton & Holt, 1957, BH) and Ricker (Ricker, 1954) production functions do not model the full theoretical space of RPs (Mangel et al., 2013; Yeakel & Mangel, 2015).

The bias-variance trade-off (Ramasubramanian & Singh, 2017) makes it clear that the addition of a third parameter in the production function will necessarily reduce estimation bias. However the utility of this bias reduction is still under debate because the particular mechanisms and behavior (direction and magnitude) of these biases for key management quantities are not fully understood or described. Lee et al. (2012) provides some evidence that estimation of productivity parameters are dependent on biomass contrast as well as model specification. Conn et al. (2010) comes to similar conclusions via calibration modeling

1277 techniques. These studies indicate important factors that contribute to inferential failure.  
 1278 However they do not offer mechanisms of model failure, nor do their experimental designs  
 1279 allow for the control of different types of model misspecification.

1280 In this study I consider the behavior of inference when index data are simulated from  
 1281 three parameter PT and Schnute production models, but the simulated data are fit using  
 1282 intentionally misspecified two parameter logistic or BH production models. The work begins  
 1283 with a derivation of RPs under the three parameter models. A method is then presented  
 1284 for generating simulation designs based on the parametric form of RPs which serves as a  
 1285 control on the nature of simulated model misspecification. Finally a Gaussian Process (GP)  
 1286 metamodel ([Gramacy, 2020](#)) is constructed for exploration and analysis of RP biases.

1287 A key insight of this approach is that bias is considered broadly across RP-space to  
 1288 uncover patterns and correlations between RPs. The GP metamodel is explicit about trade-  
 1289 offs between RPs so as to inform the full utility of reducing bias, as well as to suggest  
 1290 mechanisms for understanding what causes bias. Further, the effect of contrast on estimation  
 1291 is considered together with model misspecification.

## 1292 5 Methods

### 1293 5.1 Pella-Tomlinson Model

The three parameter Pella-Tomlinson (PT) family has a convenient form that includes, among others ([Fox Jr., 1970](#); [Rankin & Lemos, 2015](#)), the logistic production function as a special case. PT production function is parameterized so that  $\boldsymbol{\theta} = [r, K, \gamma]$  and the family takes the following form,

$$P_p(B; [r, K, \gamma]) = \frac{rB}{\gamma - 1} \left( 1 - \left( \frac{B}{K} \right)^{(\gamma-1)} \right). \quad (3.15)$$

1294  $\gamma$  is a parameter which breaks PT out of the  
 1295 restrictive symmetry of the logistic curve. In gen-  
 1296 eral  $\gamma \in (1, \infty)$ , with the logistic model appear-  
 1297 ing in the special case of  $\gamma = 2$ , and the Fox  
 1298 model appearing as a limiting case as  $\gamma \rightarrow 1$ . The  
 1299 parameter  $r$  controls the maximum reproductive  
 1300 rate of the population in the absence of compe-  
 1301 tition for resources (i.e. the slope of production  
 1302 function at the origin).  $K$  is the so called "car-  
 1303 rying capacity" of the population. In this con-  
 1304 text the carrying capacity can be formally stated  
 1305 as steady state biomass in the absence of fishing  
 1306 (i.e.  $\bar{B}(0) = K$ ). In Figure (3.15) PT recruitment  
 1307 is shown for a range of parameter values so as to  
 1308 demonstrate the various recruitment shapes that  
 1309 can be achieved by PT recruitment.

1310 While the form of the PT curve produces  
 1311 some limitations (Fletcher, 1978), importantly  
 1312 the introduction of a third parameter allows enough flexibility to fully describe the space  
 1313 of reference points used in management. To see this, the reference points are analytically  
 1314 derived for the PT model below.

### 1315 PT Reference Points

1316 With  $B(t)$  representing biomass at time  $t$ , under PT production, the dynamics of biomass  
 1317 are defined by the following ODE,

$$\frac{dB}{dt} = \frac{rB}{\gamma - 1} \left( 1 - \left( \frac{B}{K} \right)^{\gamma-1} \right) - FB. \quad (3.16)$$

An expression for the equilibrium biomass is attained by setting Eq (3.16) equal to zero,  
 and rearranging the resulting equation to solve for  $B$ . Thinking of the result as a function

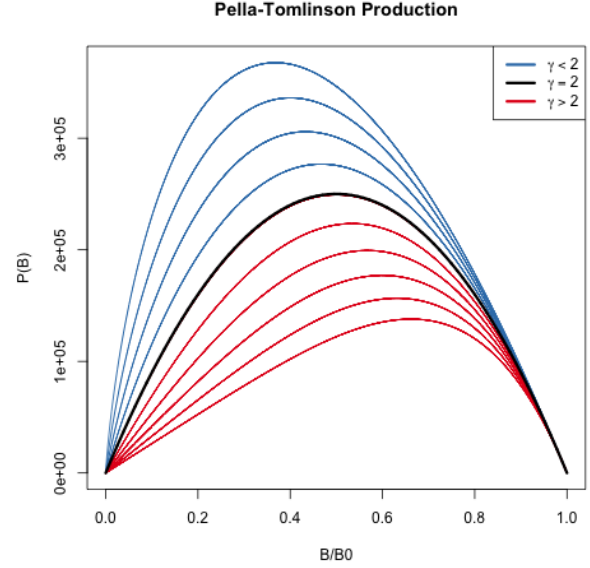


Figure 3.15: The Pella-Tomlinson production function plotted across a variety of parameter values. The special cases of Logistic production is shown in black, and the left-leaning and right-leaning regimes are shown in blue and red respectively.

of  $F$  gives,

$$\bar{B}(F) = K \left( 1 - \frac{F(\gamma - 1)}{r} \right)^{\frac{1}{(\gamma-1)}}. \quad (3.17)$$

At this point it is convenient to notice that  $\bar{B}(0) = K$ . The expression for  $B^*$  is given by evaluating Eq (3.17) at  $F^*$ . To get an expression for  $F^*$ , the equilibrium yield is maximized with respect to  $F$ ,

$$F^* = \operatorname{argmax}_F F \bar{B}(F). \quad (3.18)$$

In the case of PT production this maximization can be done analytically, by differentiating the equilibrium yield with respect to  $F$  as follows,

$$\frac{d\bar{Y}}{dF} = \bar{B}(F) + F \frac{d\bar{B}}{dF} \quad (3.19)$$

$$\frac{d\bar{B}}{dF} = -\frac{K}{r} \left( 1 - \frac{F(\gamma - 1)}{r} \right)^{\frac{1}{\gamma-1} - 1}. \quad (3.20)$$

Setting Eq (3.19) equal to 0, substituting  $\bar{B}(F)$  and  $\frac{d\bar{B}}{dF}$  by Equations (3.17) and (3.20) respectively, and solving for  $F$  produces the following expression for the fishing rate required to produce MSY,

$$F^* = \frac{r}{\gamma} \quad (3.21)$$

Plugging the above expression for  $F^*$  back into Eq (3.17) gives the following expression for biomass at MSY,

$$B^* = K \left( \frac{1}{\gamma} \right)^{\frac{1}{\gamma-1}}. \quad (3.22)$$

The above derived expressions for  $\bar{B}(0)$ ,  $B^*$ , and  $F^*$  can then be used to build a specific analytical form for the biological reference points in terms of only productivity parameters.

$$F^* = \frac{r}{\gamma} \qquad \frac{B^*}{\bar{B}(0)} = \left( \frac{1}{\gamma} \right)^{\frac{1}{\gamma-1}} \quad (3.23)$$

## 1321 Simulation

Generating simulated indices of abundance from the PT model requires inverting the relationship between  $\left(F^*, \frac{B^*}{B(0)}\right)$ , and  $(r, \gamma)$ . It is not generally possible to analytically invert this relationship for many three parameter production functions (Punt & Cope, 2019; J. T. Schnute & Richards, 1998). Most three parameter production functions lead to RPs that require expensive numerical methods to invert; more over the numerical inversion procedure can often be unstable. That said, for the case of PT this relationship is analytically invertible, and leads to the following relationship

$$r = \gamma F^* \qquad \gamma = \frac{W\left(\frac{B^*}{B(0)} \log\left(\frac{B^*}{B(0)}\right)\right)}{\log\left(\frac{B^*}{B(0)}\right)}. \quad (3.24)$$

1322 Above  $W$  is the Lambert product logarithm function. More details about this derivation,  
1323 and the Lambert product logarithm, are given in Appendix (7 ).

1324 Using Eq. (3.24) to obtain production parameters, a PT production model can be fully  
1325 defined for any combination of the RPs  $F^*$  and  $\frac{B^*}{B(0)}$ . Since  $K$  does not enter the RP  
1326 calculation its value is fixed arbitrarily at 10000.

1327 Indices of abundance are simulated from the three parameter PT production model  
1328 broadly over the space of  $F^*$  and  $\frac{B^*}{B(0)}$  via a space filling design as described in Section  
1329 (5 .3). A small amount of residual variation,  $\sigma = 0.01$ , is added to the simulated index, and  
1330 these data are then fit with a Schaefer model, at various degrees of misspecification, so as to  
1331 observe the effect of productivity model misspecification upon RP inference.

## 1332 5 .2 Schnute Model

The Schnute production function is a three parameter generalization of many of the most common two parameter production functions (Deriso, 1980; J. Schnute, 1985). It can be written in the following form, with parameters  $\alpha$ ,  $\beta$ , and  $\gamma$ ,

$$P_s(B; [\alpha, \beta, \gamma]) = \alpha B(1 - \beta\gamma B)^{\frac{1}{\gamma}}. \quad (3.25)$$

The BH and Logistic production functions arise when  $\gamma$  is fixed to -1 or 1 respectively. The Ricker model is a limiting case as  $\gamma \rightarrow 0$ . For  $\gamma < -1$  a family of strictly increasing Cushing-like curves arise, culminating in linear production as  $\gamma \rightarrow -\infty$ . These special cases form natural regimes of similarly behaving production functions as seen in Figure (3.16).

The behavior of RP inference under the BH model is of particular interest due to the overwhelming popularity of the BH assumption in fisheries models. Since Schnute production models can represent a quantifiably

wide variety of possible productivity behaviors, they present an ideal simulation environment for inquiry of the reliability of inference under the BH assumption.

Under Schnute production, biomass dynamics evolve according to the following ODE,

$$\frac{dB}{dt} = P_s(B; \theta) - (M + F)B. \quad (3.26)$$

This equation largely takes the same form as previously described, except that  $P_s$  is the Schnute production function and natural mortality,  $M$ , is modeled explicitly here. Natural mortality models the instantaneous rate of mortality from all causes outside of fishing. Explicitly modeling natural mortality is not only a typical assumption of fisheries models, but is also key to the making RPs well defined over the relevant domain of  $\gamma$ .

The derivation of RPs under Eq. (3.26) follows a similar logic as under the PT model. An expression for equilibrium biomass is attained by setting  $\frac{dB}{dt} = 0$  and rearranging the resulting expression to solve for  $B$

$$\bar{B}(F) = \frac{1}{\gamma\beta} \left( 1 - \left( \frac{M + F}{\alpha} \right)^\gamma \right). \quad (3.27)$$

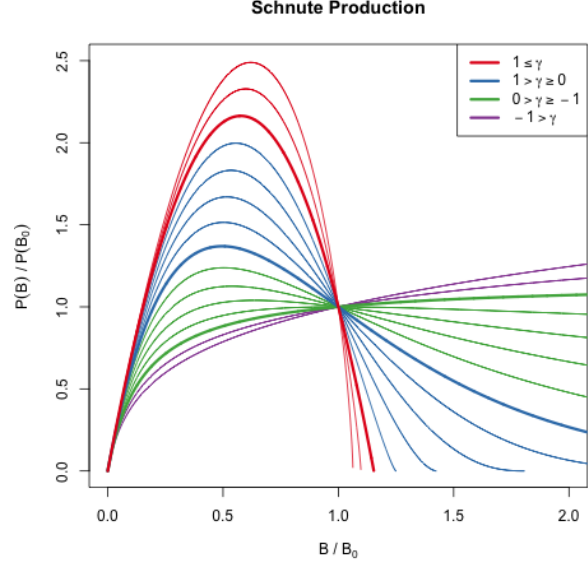


Figure 3.16: The Schnute production function plotted across a variety of parameter values. Regimes of similarly behaving curves are grouped by color.

The above expression quickly yields  $B_0$ ,  $B^*$  by evaluation at  $F = 0$  and  $F^*$  respectively,

$$B_0 = \frac{1}{\gamma\beta} \left( 1 - \left( \frac{M}{\alpha} \right)^\gamma \right) \quad (3.28)$$

$$\frac{B^*}{B_0} = \frac{1 - \left( \frac{M+F^*}{\alpha} \right)^\gamma}{1 - \left( \frac{M}{\alpha} \right)^\gamma}. \quad (3.29)$$

Attaining an expression for  $F^*$  requires maximization of equilibrium yield,  $\bar{Y} = F\bar{B}(F)$ , with respect to  $F$ . Analytically maximizing proceeds by differentiating  $\bar{Y}$  to produce

$$\frac{d\bar{Y}}{dF} = \bar{B}(F) + F \frac{d\bar{B}}{dF} \quad (3.30)$$

$$\frac{d\bar{B}}{dF} = -\frac{1}{\beta} \left( \frac{\left( \frac{M+F}{\alpha} \right)^\gamma}{F+M} \right). \quad (3.31)$$

Setting  $\frac{d\bar{Y}}{dF} = 0$ , filling in the expressions for  $\bar{B}(F)$  and  $\frac{d\bar{B}}{dF}$ , then rearranging to solve for  $F^*$  is less yielding here than it was in the case of the PT model. This procedure falls short of providing an analytical solution for  $F^*$  directly in terms of  $\theta$ , but rather shows that  $F^*$  must respect the following expression,

$$0 = \frac{1}{\gamma} - \left( \frac{1}{\gamma} + \frac{F^*}{F^* + M} \right) \left( \frac{F^* + M}{\alpha} \right)^\gamma. \quad (3.32)$$

The lack of an analytical solution here is understood. [J. T. Schnute and Richards \(1998](#), pg. 519) specifically points out that  $F^*$  cannot be expressed analytically in terms of productivity parameters, but rather gives a partial analytical expression for the inverse relationship. Although parameterized slightly differently, [J. T. Schnute and Richards \(1998\)](#) derives expressions for  $\alpha$  and  $\beta$  as a function of RPs and  $\gamma$ .

Since RPs are left without a closed form expression, computing RPs from productivity parameters amounts to numerically solving the system formed by collecting the expressions (3.32), (3.28), and (3.29).

## Simulation

For the purposed of simulation, it is not necessary to completely know the precise relationships mapping RPs  $\mapsto \theta$  or  $\theta \mapsto$  RPs. Simulation only requires enough knowledge of these

1365 mappings to gather a list of  $(\alpha, \beta, \gamma)$  tuples, for data generation under the Schnute model,  
 1366 and the corresponding RPs in some reasonable space-filling design over RP space.

Similarly to [J. T. Schnute and Richards \(1998\)](#), expressions (3.32) and (3.28) are solved for  $\alpha$  and  $\beta$  respectively. This leads to the partial mapping  $(F^*, B_0) \mapsto (\alpha(\cdot, \gamma), \beta(\cdot, \cdot, \gamma))$  in terms of RPs and  $\gamma$ . By further working with Eq. (3.29), to identify  $\gamma$ , the following system is obtained,

$$\begin{aligned}\alpha &= (M + F^*) \left( 1 + \frac{\gamma F^*}{M + F^*} \right)^{1/\gamma} \\ \beta &= \frac{1}{\gamma B_0} \left( 1 - \left( \frac{M}{\alpha} \right)^\gamma \right) \\ \frac{B^*}{B_0} &= \frac{1 - \left( \frac{M + F^*}{\alpha} \right)^\gamma}{1 - \left( \frac{M}{\alpha} \right)^\gamma}.\end{aligned}\tag{3.33}$$

1367 For a population experiencing natural mortality  $M$ , by fixing  $F^*$ ,  $B_0$ , and  $\frac{B^*}{B_0}$  the above  
 1368 system can fully specify  $\alpha$  and  $\beta$  for a given  $\gamma$ . Notice for a given  $\gamma$  a cascade of closed  
 1369 form solutions for  $\alpha$  and  $\beta$  can be obtained. First  $\alpha(\gamma)$  can be computed, and then  
 1370  $\beta(\alpha(\gamma), \gamma)$  can be computed. If  $\alpha(\gamma)$  is filled back into the expression for  $\frac{B^*}{B_0}$ , the system  
 1371 collapses into a single onerous expression for  $\frac{B^*}{B_0}(\alpha(\gamma), \gamma)$ . For brevity, define the function  
 1372  $\zeta(\gamma) = \frac{B^*}{B_0}(\alpha(\gamma), \gamma, F^*, M)$  based on Eq. (3.29).

1373 Inverting  $\zeta(\gamma)$  for  $\gamma$ , and computing the cascade of  $\alpha(\gamma)$ , and then  $\beta(\alpha(\gamma), \gamma)$ , fully defines  
 1374 the Schnute model for a given  $(\frac{F^*}{M}, \frac{B^*}{B_0})$ . However inverting  $\zeta$  accurately is extremely difficult.  
 1375 Inverting  $\zeta$  analytically is not feasible, and numerical methods for inverting  $\zeta$  are unstable  
 1376 and can be computationally expensive. Rather than numerically invert precise values of  $\zeta(\gamma)$ ,  
 1377  $\gamma$  is sampled so that the overall simulation design is space filling as described in Section (5  
 1378 .3).

1379 Each design location defines a complete Schnute production model with the given RP  
 1380 values. Indices of abundance are simulated from the Schnute model at each design location,  
 1381 a small amount of residual variation,  $\sigma = 0.01$ , is added to the simulated index, and the data  
 1382 are then fit with a misspecified BH production model. The design at large captures various  
 1383 degrees of model misspecification relative to the BH model, so as to observe the effect of  
 1384 productivity model misspecification upon RP inference.



### 5.3 Latin Hypercube Sampling

The goal of space filling design in this setting is to extend the notion of the random sample (and its desirable parameter estimation properties) across the simulated RP domain so as to represent the simulated space as well as possible (Gramacy, 2020). The simple random sample is the gold standard of classical unbiased parameter estimation, however simple randomness is patchy, often sampling some regions of design space quite densely, while leaving other regions of design space empty. Space filling designs aim to preserve (or enhance) parameter estimation properties across the simulated domain (Devon Lin & Tang, 2015; Stein, 1987), while constraining samples to be spaced in some notion of spread over the entire space. Latin hypercube sampling (McKay et al., 2000, LHS) is among the most foundational of space filling designs used in computer experiments.

A LHS of size  $n$ , in the 2 dimensional space defined by RPs, distributes samples so as to spread points across a design region in a broadly representative way. A LHS design extends the notion of a univariate random uniform sample across multiple dimensions so that each margin of the design space enjoys a uniform distribution.

LHS designs achieve this notion of uniformity by first partitioning each dimension of the design space into regular grids of size  $n$ . By intersecting the grids of each dimension, cells are produced that evenly partition the design space. In two dimensions  $n^2$  cells are produced, from which a total of  $n$  samples are taken. Crucially only one sample is taken from a given element of each grid in each dimension so as to reduce clumping of the  $n$  samples across the design space.

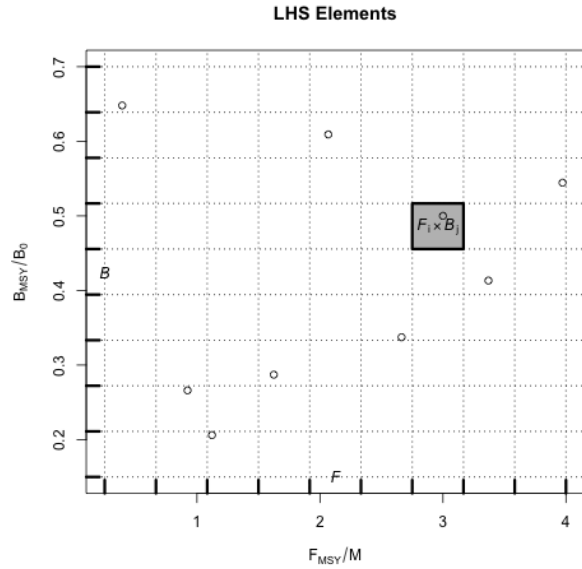


Figure 3.17: LHS grids. Intersecting  $\mathcal{F}$  and  $\mathcal{B}$  produces  $n^2$  cells; a particular cell  $\mathcal{F}_i \times \mathcal{B}_j$  is shown in grey. Maybe just show points.

## 1414 PT Design

1415 Letting  $\mathcal{F}$  and  $\mathcal{B}$  be regular grids, of size  $n = 100$ , on  $F^* \in (0.1, 0.7)$  and  $\frac{B^*}{B_0} \in (0.2, 0.6)$   
 1416 respectively, a LHS design of size 100 is collected among the cells produced by  $\mathcal{F} \times \mathcal{B}$ .

1417 Each of the sampled LHS design locations represent a unique PT model with the sampled  
 1418 RP values. Since the relationship mapping RPs analytically to productivity parameters can  
 1419 be found for the PT model, LHS designs the the PT model are computed directly in RP  
 1420 space and Eq. (3.24) is used to map the sampled RP design locations to PT productivity  
 1421 parameters.

## 1422 Schnute Design

1423 Due to the lack of an analytical relationship mapping RPs  $\mapsto \theta$ , analogous to the PT model's  
 1424 Eq. (3.24), producing a LHS design over Schnute RPs requires a more tactful approach. The  
 1425 structured relationship between the RPs and productivity parameters, described in Section  
 1426 (5 ), allows an approximate LHS to be obtained by a careful navigation of the system of  
 1427 equations seen in Eq. (3.33).

1428 Under the Schnute model, let  $\mathcal{F}$  and  $\mathcal{B}$   
 1429 represent regular grids on  $\frac{F^*}{M} \in (0.25, 4)$  and  
 1430  $\frac{B^*}{B_0} \in (0.15, 0.7)$  respectively which can serve  
 1431 as the scaffolding for computing an approx-  
 1432 imate LHS

Given  $B_0$ ,  $M$ , and  $F^*$ :

- 1) Draw  $\gamma^* \sim \gamma|F^*, M$ .
- 2) Compute  $\frac{B^*}{B_0} = \zeta(\gamma^*)$
- 3) Compute  $\alpha^* = \alpha(\gamma^*, F^*, M)$
- 4) Compute  $\beta^* = \beta(\alpha^*, \gamma^*, M, B_0)$

Since it is not practical to invert  $\zeta(\gamma)$ ,  
 a uniform sample in  $\frac{B^*}{B_0}$  can be obtained by  
 modeling  $\gamma$  as a random variable, with real-  
 ization  $\gamma^*$ , and thinking of  $\zeta(\gamma)$  as its cumu-  
 lative distribution function (CDF). The aim  
 is to model  $\gamma$  as an easily sampled random

variable with a CDF that closely approximates  $\zeta$ , so that  $\zeta(\gamma^*) \sim U(\zeta_{min}, 1)$  as closely as  
 possible. There may be many good models for the distribution of  $\gamma$ , but in this setting the

Figure 3.18: An outline of the sampling pro-  
 cedure for  $\gamma$  given  $B_0$ ,  $M$ , and  $F^*$ .

following distribution is very effective,

$$\gamma \sim \zeta_{min} \delta(\gamma_{min}) + t(\mu, \sigma, \nu) \mathbf{1}_{\gamma > \gamma_{min}}. \quad (3.34)$$

1433 Above,  $t$  is the density of the three pa-  
 1434 rameter location-scale family Student's  $t$  dis-  
 1435 tribution with location  $\mu$ , scale  $\sigma$ , and de-  
 1436 grees of freedom  $\nu$ .  $\mathbf{1}_{\gamma > \gamma_{min}}$  is an indica-  
 1437 tor function that serves to truncate Stu-  
 1438 dent's  $t$  distribution at the lower bound  $\gamma_{min}$ .  
 1439  $\delta(\gamma_{min})$  is the Dirac delta function evaluated  
 1440 at  $\gamma_{min}$ , which is scaled by the known value  
 1441  $\zeta_{min}$ ; this places probability mass  $\zeta_{min}$  at  
 1442 the point  $\gamma_{min}$ . Since sampling from Stu-  
 1443 dent's  $t$  distribution is readily doable, sam-  
 1444 pling from a truncated Student's  $t$  mixture  
 1445 only requires slight modification.

Let  $T$  be the CDF of the modeled distri-  
 bution of  $\gamma$ . Since the point  $(\gamma_{min}, \zeta_{min})$  is  
 known from the dynamics of the Schnute model at a given RP, full specification of Eq. (3.34)  
 only requires determining the values for  $\mu$ ,  $\sigma$ , and  $\nu$  which make  $T$  best approximate  $\zeta(\gamma)$ .  
 Thus, the values of  $\mu$ ,  $\sigma$ , and  $\nu$  are chosen by minimizing the  $L^2$  distance between  $T(\gamma)$  and  
 $\zeta(\gamma)$ .

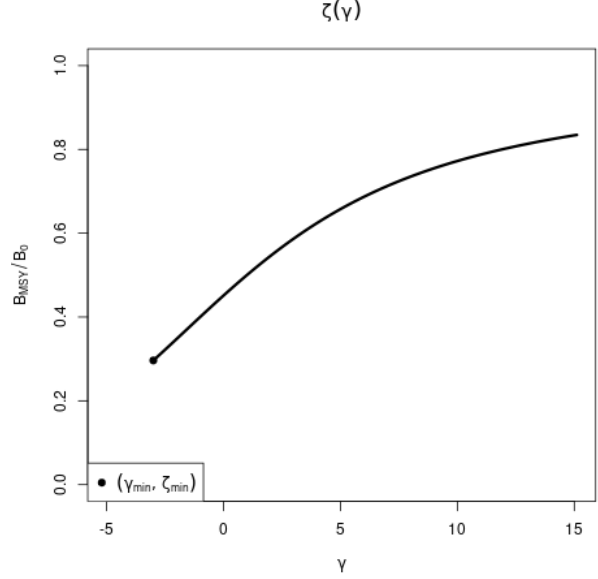


Figure 3.19:  $\zeta(\gamma)$  Plotted for  $F^* = 0.1$  and  $M = 0.2$ . The point  $(\gamma_{min}, \zeta_{min})$  shows the lowest biologically meaningful value of  $\gamma$ ; below which productivity is negative.

$$[\hat{\mu}, \hat{\sigma}, \hat{\nu}] = \arg \min_{[\mu, \sigma, \nu]} \int_{\Gamma} (T(\gamma; \mu, \sigma, \nu) - \zeta(\gamma))^2 d\gamma \quad (3.35)$$

1446 Fitting the distribution  $T(\gamma|\hat{\mu}, \hat{\sigma}, \hat{\nu})$  for  
 1447 use generating  $\gamma^*$  values at a specific  $F^*$  and  
 1448  $M$  releases the need to invert  $\zeta$ .  $T(\gamma|\hat{\mu}, \hat{\sigma}, \hat{\nu})$ ,  
 1449 together with the structure in Eq. (3.33),  
 1450 allows for the collection of an approximate  
 1451 LHS sample via the algorithm seen in Algo-  
 1452 rithm (2).

1453  $\frac{F^*}{M}$  is drawn uniformly from  $\mathcal{F}_i$ . Con-  
 1454 ditioning on the sample of  $F^*$ , and  $M$ ,  
 1455  $T(\gamma|\hat{\mu}, \hat{\sigma}, \hat{\nu})$  is fit and  $\gamma^*$  is sampled.  $\zeta^*$  is  
 1456 then computed and placed into the appropri-  
 1457 ate grid element  $\mathcal{B}_j$ . Given  $\gamma^*$ , the cascade  
 1458  $\alpha(\gamma^*)$ , and  $\beta(\alpha(\gamma^*), \gamma^*)$ , can be computed.  
 1459 The algorithm continues until all of the de-  
 1460 sign elements,  $(\frac{F^*}{M}, \zeta^*) \Leftrightarrow (\alpha^*, \beta^*, \gamma^*)$ , have  
 1461 been computed for all  $i \in [1, \dots, n]$ .

---

**Algorithm 2** LHS of size  $n$  on rectangle  $R$ .

---

```

1: procedure  $LHS_n(R)$ 
2:   Define  $n$ -grids  $\mathcal{F}, \mathcal{B} \in R$ 
3:   for each grid element  $i$  do
4:     Draw  $\frac{F^*}{M} \sim Unif(\mathcal{F}_i)$ 
5:     Compute  $[\hat{\mu}, \hat{\sigma}, \hat{\nu}]$  given  $F^*$  &  $M$ 
6:     while  $\mathcal{B}_j$  not sampled do
7:       Draw  $\gamma^* \sim T(\gamma|\hat{\mu}, \hat{\sigma}, \hat{\nu})$ 
8:       Compute  $\zeta^* = \zeta(\gamma^*)$ 
9:       Compute  $j$  such that  $\zeta^* \in \mathcal{B}_j$ 
10:    end while
11:    Compute  $\alpha^* = \alpha(\gamma^*, F^*, M)$ 
12:    Compute  $\beta^* = \beta(\alpha^*, \gamma^*, M, B_0)$ 
13:    Save  $(\frac{F^*}{M}, \zeta^*) \Leftrightarrow (\alpha^*, \beta^*, \gamma^*)$  in  $\mathcal{F}_i \times \mathcal{B}_j$ 
14:  end for
15: end procedure

```

---

## 1462 Design Refinement

1463 Since the behavior of RP inference, under misspecified models, will vary in yet-unknown  
 1464 ways, the exact sampling design density may be hard to know a priori. Several factors,  
 1465 including the particular level of observation uncertainty, high variance (i.e. hard to resolve)  
 1466 features of the response surface, or simply "gappy" instantiations of the initial LHS design  
 1467 may necessitate adaptive design refinement, to accurately describe RP biases. Given the  
 1468 temperamental relationship between RPs and productivity parameters in the Schnute model,  
 1469 a recursive refinement algorithm, that makes use of the previously described LHS routine, is  
 1470 developed.

1471 While LHS ensures uniformity in the design margins, and a certain degree of spread, it  
 1472 is widely recognized that particular LHS instantiations may leave substantive gaps in the  
 1473 simulation design. To correct this, LHS is often paired with design elements of maximin

1474 design (Morris & Mitchell, 1995; Devon Lin & Tang, 2015). Maximin designs sample the  
 1475 design space by maximizing the minimum distance between sampled points. This has the  
 1476 advantage of definitionally filling holes in the design, however because no points are ever  
 1477 drawn outside of the design domain, samples tend to clump around edges (particularly  
 1478 corners) of the design domain. Since LHS ensures uniformity in the margins and maximin  
 1479 designs enjoys a certain sense of optimality in how they define and fill gaps (Johnson et al.,  
 1480 1990), the methods are quite complimentary when combined.

Making use of this complimentary relationship, holes in the existing LHS design of RPs are identified based on maximin design principles. New design points are collected based on areas of the RP design space which maximizes the minimum distance between all pairs of points in the current design, based on the following distance function

$$d(\mathbf{x}, \mathbf{x}') = \sqrt{(\mathbf{x} - \mathbf{x}')^T \mathbf{D}^{-1} (\mathbf{x} - \mathbf{x}')} \quad (3.36)$$

$$\mathbf{D} = \text{diag} \left[ (\max(\mathcal{F}) - \min(\mathcal{F}))^2, (\max(\mathcal{B}) - \min(\mathcal{B}))^2 \right].$$

1481 Above,  $d$  is a scaled distance function that defines the distance between points in the  
 1482 differing scales of  $\frac{B^*}{B_0}$  and  $\frac{F^*}{M}$ .  $\mathbf{D}$  is a diagonal matrix that measures the squared size of the  
 1483 domain in each axis of so as to normalize distances to a common scale.

If  $\mathbf{X}_n$  is the initial design, computed on  $R_{full}$ , let  $\mathbf{x}_a$  be the augmenting point which maximizes the minimum distance between all of the existing design points,

$$\mathbf{x}_a = \underset{\mathbf{x}'}{\operatorname{argmax}} \min \{d(\mathbf{x}_i, \mathbf{x}') : i = 1, \dots, n\}. \quad (3.37)$$

1484 The point  $\mathbf{x}_a$  is used as an anchor for augmenting  $\mathbf{X}_n$ . An additional  $LHS_{n'}$  (via  
 1485 Algorithm (2)) is collected, adding  $n'$  design points, centered around  $\mathbf{x}_a$ , to the overall  
 1486 design. The augmenting region,  $R_{(x_a, d_a)}$ , for collecting  $LHS_{n'}$  is defined based on the square  
 1487 centered at  $\mathbf{x}_a$  with side length  $2d_a$ , where  $d_a = \min \{d(\mathbf{x}_i, \mathbf{x}_a) : i = 1, \dots, n\}$ , in the space  
 1488 defined by the metric  $d$ .

1489 Due to the tendency of maximin sampling to cluster augmenting points on the edges of  
 1490 the design space,  $R_{(x_a, d_a)}$  is truncated by the outer most limits of  $R_{full}$  so as to focus design

1491 augmentation within the specified domain of the simulation. Furthermore, since the design  
 1492 space has a nonlinear constraint at low values of  $\frac{B^*}{B_0}$ , the calculation of  $x_a$  is further truncated  
 1493 based on a convex hull defined by the existing samples in the overall design.

1494 Design refinement then proceeds as follows. An initial design is computed,  $X_n = LHS_n(R_{full})$ ,  
 1495 based on an overall simulated region of RPs  $R_{full}$ . The maximin augmenting point,  $x_a$ , is  
 1496 computed at a maximin distance of  $d_a$  from the existing samples. An augmenting design  
 1497  $X_{n'} = LHS_{n'}(R_{(x_a, d_a)})$  is collected and added to  $X_n$ . Design refinement carries on recursively  
 1498 collecting augmenting designs in this way until the maximin distance falls below the desired  
 1499 level.

## 1500 5 .4 Gaussian Process Metamodel

1501 At its core, a metamodel is simply a model of some mapping of inputs to outputs (the  
 1502 mapping itself is typically defined by a computer model). By modeling the mapping with a  
 1503 statistical model (that explicitly defines the relevant features of the mapping) a metamodel  
 1504 defines a specific ontology for the mapping. By simulating examples of the mapping, the  
 1505 inferential infrastructure of the statistical model is used to empirically learn an effective  
 1506 emulation of the mapping within the ontology defined by the statistical model. The pre-  
 1507 dictive infrastructure of the statistical model is then useful as an approximate abstraction  
 1508 of the system itself to better understand the system through further data collection, cheap  
 1509 approximation of the mapping, and/or study of the mapping itself.

1510 In this setting, the aim of metamodeling is to study how well RPs are inferred when typical  
 1511 two parameter models of productivity (Logistic and BH) are misspecified for populations  
 1512 that are actually driven by more complicated dynamics. The simulation design,  $\mathbf{X}$ , provides  
 1513 a sample of different population dynamics that are driven by three parameter production  
 1514 functions broadly in RP space. By simulating index of abundance data from the three  
 1515 parameter model, and fitting those data with the two parameter production model, we  
 1516 observe particular instances of how well RPs are inferred at the given misspecification of the  
 1517 two parameter model relative to the true three parameter production model. By gathering  
 1518 all of the simulated instances of how RPs are inferred (under the two parameter model),  
 1519 we form a set of example mappings to train a metamodel which represents the mapping

1520 of true RPs (under the three parameter model) to estimates of RPs under the misspecified  
 1521 two parameter production model. The metamodel is essentially a surrogate for inference  
 1522 under the misspecified two parameter production model that controls for the specific degree  
 1523 of model misspecification.

1524 A flexible GP model is assumed for the structure of the metamodel to describe the map-  
 1525 ping of RPs under misspecified two parameter models of productivity. A GP is a stochastic  
 1526 process generalizing the multivariate normal distribution to an infinite dimensional analog.  
 1527 GP models are often specified primarily through the choice of a covariance (or correlation)  
 1528 function which defines the relationship between locations in the input space. Typically corre-  
 1529 lation functions are specified so that points closely related in space result in correlated effects  
 1530 in the model. In this setting the inputs to the GP metamodel are the space of reference points  
 1531 with define the simulated three parameter production models.

While index of abundance data are generated from three parameter models, at each  
 design location of the simulation, fitting the restricted two parameter model results in a  
 maximum likelihood estimate (MLE; and associated estimation uncertainty) of each of the  
 productivity parameters (i.e. Schaefer:[ $\log(r)$ ,  $\log(K)$ ], BH:[ $\log(\alpha)$ ,  $\log(\beta)$ ]). To simplify  
 the specification of the metamodel, let  $\mathbf{y}$  be a vector collecting the fitted MLEs for one of  
 the productivity parameters, and let  $\boldsymbol{\omega}$  be a vector of estimates of the estimator variances  
 (via the inverted Fisher information) at each  $\mathbf{y}$ . Each of the fitted productivity parameter  
 estimates are then modeled using independent instances of the following GP metamodel.

$$\begin{aligned}\mathbf{y} &= \beta_0 + \mathbf{X}\boldsymbol{\beta} + \mathbf{v} + \boldsymbol{\epsilon} \\ \mathbf{v} &\sim N_n(\mathbf{0}, \tau^2 \mathbf{R}_\ell) \\ \boldsymbol{\epsilon} &\sim N_n(\mathbf{0}, \boldsymbol{\omega}'\mathbf{I})\end{aligned}\tag{3.38}$$

1532  $\mathbf{X}$  is the  $n \times 2$  LHS design matrix of RPs for each simulated three parameter data  
 1533 generating model as described in Section (5 .3).  $\epsilon$  models independent normally distributed  
 1534 error, which provides an ideal mechanism for propagating uncertainty from inference in the  
 1535 simulation step into the metamodel. By matching each  $\mathbf{y}_i$  with an observed  $\omega_i$  variance term,  
 1536  $\epsilon$  serves to down weight the influence of each  $\mathbf{y}_i$  in proportion to the inferred production model

1537 sampling distribution uncertainty. This has the effect of smoothing the GP model in a way  
 1538 similar to the nugget effect (Gramacy & Lee, 2012), although the application here models  
 1539 this effect heterogeneously.

The term,  $\mathbf{v}$ , contains spatially correlated GP effects. The correlation matrix,  $\mathbf{R}_\ell$  describes how RPs close together in the simulation design are more correlated than those that are far away. This spatial effect is modeled with a squared exponential correlation function,

$$R(\mathbf{x}, \tilde{\mathbf{x}}) = \exp \left( \sum_{i=1}^2 \frac{-(x_i - \tilde{x}_i)^2}{2\ell_j^2} \right). \quad (3.39)$$

1540  $R$  has an anisotropic separable form which allows for differing length scales,  $\ell_1$  and  $\ell_2$ ,  
 1541 in the different RP axes. The flexibility to model correlations separately in the different  
 1542 RP axes is key due to the differences in the extent of the RP domains marginally. The  
 1543 metamodel parameters  $\beta_0$ ,  $\boldsymbol{\beta}$ ,  $\tau^2$ ,  $\ell_1$  and  $\ell_2$  are fit via MLE against the observations  $\mathbf{y}$ ,  $\mathbf{X}$ ,  
 1544 and  $\boldsymbol{\omega}$  from simulation fits.

1545 Fitting the metamodel allows for a full predictive description of inference under the  
 1546 misspecified restricted models. Predictive estimates are obtained via kriging (Cressie, 2015)

$$\hat{y}(\mathbf{x}) = \beta_0 + \mathbf{x}\boldsymbol{\beta} + \mathbf{r}(\mathbf{x})'\mathbf{R}_\ell^{-1}(\mathbf{y} - (\beta_0 + \mathbf{X}\boldsymbol{\beta})) \quad (3.40)$$

1547  $\hat{y}(\mathbf{x})$  is the predicted value of the modeled productivity parameter MLE under the two  
 1548 parameter production model, when the index of abundance is generated from the three  
 1549 parameter production model at RP location  $\mathbf{x}$ .  $\mathbf{r}(\mathbf{x})$  is a vector-valued function of correlation  
 1550 function evaluations for the predictive location  $\mathbf{x}$  against all observations in  $\mathbf{X}$  (i.e.  $\mathbf{r}(\mathbf{x}) =$   
 1551  $\mathbf{R}(\mathbf{x}, \mathbf{x}_i) \forall \mathbf{x}_i \in \mathbf{X}$ ).

1552 While metamodeling occurs on the inferred productivity parameters of the restricted  
 1553 production model, the metamodel can also be used to build estimates of major biological  
 1554 RPs. For the BH model the relevant transformations for relating productivity parameters  
 1555 with RPs are given in Eqs. (3.29, 3.32) with  $\gamma$  fixed to -1; for the Schaefer model  $\hat{B}^* = \frac{\hat{K}}{2}$  and  
 1556  $\hat{F}^* = \frac{\hat{r}}{2}$ . Applying the metamodel predictive surfaces on the scale of RP estimates allows for  
 1557 the quantification of estimation bias that is induced by fitting a misspecified two parameter



1558 production model to indices of abundance generated under three parameter productivity.

## 1559 5 .5 Catch

1560 It is known that contrast in the observed index and catch time series can effect inference  
1561 on the productivity parameters (Hilborn & Walters, 1992). In this setting contrast refers  
1562 to changes in the long term trends of index data. Figure (3.20, *right*) demonstrates an  
1563 example of biomass that includes contrast induced by catch. It is not well understood how  
1564 contrast may factor into inferential failure induced by model misspecification. Thus catch is  
1565 parameterized so as to allow for a spectrum of possible contrast simulation settings.

1566 Catch is parameterized so that  $F(t)$  can be controlled with respect to  $F^*$ . Recall that  
1567 catch is assumed to be proportional to biomass, so that  $C(t) = F(t)B(t)$ . To control  $F(t)$   
1568 with respect to  $F^*$ ,  $C(t)$  is specified by defining the quantity  $\frac{F(t)}{F^*}$  as the relative fishing rate.  
1569  $B(t)$  is defined by the solution of the ODE, and  $F^*$  is defined by the biological parameters  
1570 of the model. By defining  $\frac{F(t)}{F^*}$ , catch can then be written as  $C(t) = F^* \left( \frac{F(t)}{F^*} \right) B(t)$ .

1571 Intuitively  $\frac{F(t)}{F^*}$  describes the fraction of  $F^*$  that  $F(t)$  is specified to for the current  $B(t)$ .  
1572 When  $\frac{F(t)}{F^*} = 1$ ,  $F(t)$  will be held at  $F^*$ , and the solution of the ODE brings  $B(t)$  into  
1573 equilibrium at  $B^*$ . When  $\frac{F(t)}{F^*}$  is held constant in time biomass comes to equilibrium as an  
1574 exponential decay from  $K$  approaching  $B^*$ . When  $\frac{F(t)}{F^*} < 1$ ,  $F(t)$  is lower than  $F^*$  and  $B(t)$  is  
1575 pushed toward  $\bar{B} > B^*$ . Contrarily, when  $\frac{F(t)}{F^*} > 1$ ,  $F(t)$  is higher than  $F^*$  and  $B(t)$  is pushed  
1576 toward  $\bar{B} < B^*$ ; the precise values of  $\bar{B}$  can be calculated from the steady state biomass  
1577 equations provided above and depend upon the specific form of the production function.

For the simulations presented here, a family of fishing behaviors are considered where the fishing rate accelerates as technology and fishing techniques improve rapidly until management practices are applied, which ultimately brings fishing into equilibrium at  $F^*$ . This is parameterized as three distinct phases, over a total of 45 units of time, with each phase lasting 15 time units. The specific form is given below.

$$\frac{F(t)}{F^*} = ae^{bt}\mathbf{1}_{0 \leq t < 15} + (d - ct)\mathbf{1}_{15 \leq t < 30} + \mathbf{1}_{30 \leq t \leq 45} \quad (3.41)$$

The first term of Eq(3.41) is an exponential increase in fishing, the second term is a linear

decline in relative fishing as initial management practices are applied, and the third term,  $\mathbf{1}_{30 \leq t \leq 45}$ , simply holds the fishing rate at  $F^*$  there after. These three phases are controlled by the four parameters  $a$ ,  $b$ ,  $c$ , and  $d$ . By enforcing that the interface of the phases meet at  $\chi_{max}$  and 1 respectively the relative fishing series is reduced to a two parameter family.

$$a = e^{\log(\chi_{max}) - 15b} \quad b = \frac{1}{t - 15} \log \left( \frac{\chi_{min}}{\chi_{max}} \right) \quad (3.42)$$

$$c = \frac{\chi_{max} - 1}{15 - 1} \quad d = 15c + \chi_{max} \quad (3.43)$$

1578 By further specifying  $\chi_{max} = 1.6^\chi$  and  $\chi_{min} = 0.4^\chi$  the two parameters  $\chi_{max}$ , and  $\chi_{min}$   
 1579 can be reduced to the single parameter  $\chi$ . The tuning parameter  $\chi$  then singularly controls  
 1580 contrast that appears in time series data.

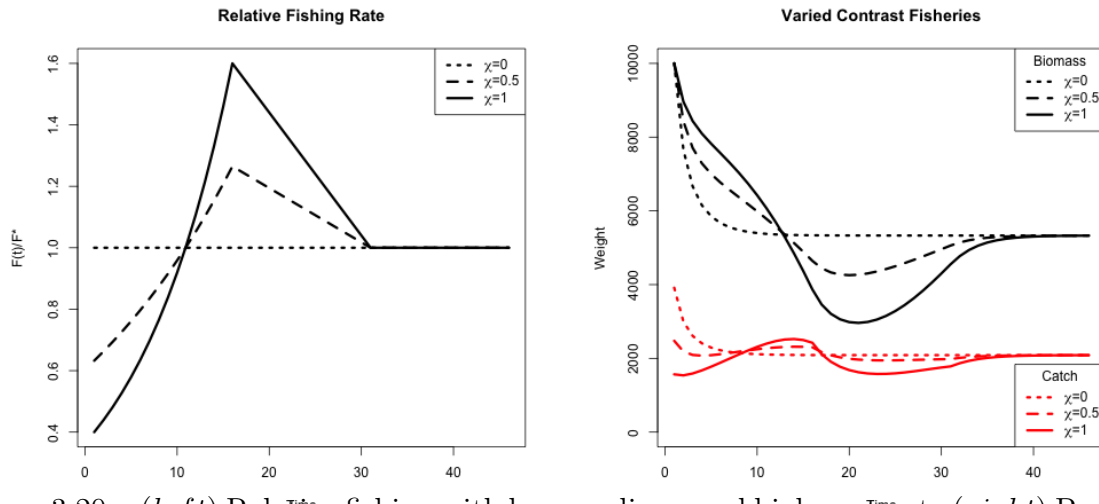


Figure 3.20: (left) Relative fishing with low, medium, and high contrast. (right) Population biomass and catch at each associated level of contrast.

1581 When  $\chi = 0$ , the relative fishing rate is a constant at 1 to create a low contrast simulation  
 1582 environment. As  $\chi$  increases Eq (3.41) induces more and more contrast in the observed index  
 1583 and catch time series until  $\chi = 1$  which produces a high contrast simulation environment.  
 1584 Figure (3.20) demonstrates a spectrum of contrast simulation environments as well as the  
 1585 time series data they induce in the solution of the production model ODE.

## 5.6 Two Parameter Production Model Inference

The simulated mapping results from fitting an intentionally misspecified two parameter production model to index of abundance data that are generated from a more complex three parameter model of productivity. Thus, let  $I_t$  be an index of abundance simulated from the three parameter PT or Schnute production models at time  $t \in \{1, 2, 3, \dots, T\}$ . However the fitted model is specified to be intentionally misspecified so that the fitted model is driven by a two parameter Schaefer, or BH production model respectively.

The observation model for the fitted model is log-normal such that,

$$I_t|q, \sigma^2, \boldsymbol{\theta} \sim LN(qB_t(\boldsymbol{\theta}), \sigma^2). \quad (3.44)$$

$B_t(\boldsymbol{\theta})$  is defined by the solution of the ODEs defined by the Schaefer, or BH models. For the Schaefer model  $\boldsymbol{\theta} = [r, K]$ , and for the BH model  $\boldsymbol{\theta} = [\alpha, \beta]$ . From the perspective of the fitted model, the observed  $I_t$  are assumed independent conditional on  $q$ ,  $\sigma^2$ ,  $r$ ,  $K$  and the two parameter ODE model for biomass. Thus the log likelihood can be written as

$$\log \mathcal{L}(q, \sigma^2, \boldsymbol{\theta}; I) = -\frac{T}{2} \log(\sigma^2) - \frac{1}{2\sigma^2} \sum_t \log \left( \frac{I_t}{qB_t(\boldsymbol{\theta})} \right)^2. \quad (3.45)$$

In this setting,  $q$  is fixed at the true value of 0.0005 to focus on the inferential effects of model misspecification on biological parameters.  $\sigma^2$  and  $\boldsymbol{\theta}$  are reparameterized to the log scale and fit via MLE. Reparameterizing the parameters to the log scale improves the reliability of optimization, in addition to facilitating the use of Hessian information for estimating MLE standard errors.

Given that the biological parameters enter the likelihood via a nonlinear ODE, and further the parameters themselves are related to each other nonlinearly, the likelihood function can often be difficult to optimize. A hybrid optimization scheme is used to maximize the log likelihood to ensure that a global MLE solution is found. The R package GA ([Scrucca, 2013](#), [2017](#)) is used to run a genetic algorithm to explore parameter space globally. Optimization periodically jumps into the L-BFGS-B local optimizer to refine optima within a local mode. The scheme functions by searching globally, with the genetic algorithm, across many initial

values for starting the local gradient-based optimizer. The genetic algorithm serves to iteratively improve hot starts for the local gradient-based optimizer. Additionally, optimization is only considered to be converged when the optimum results in an invertible Hessian at the found MLE.

## 5.7 Continuous model formulation

An important (and often overlooked) implementation detail is the solution to the ODE which defines the progression of biomass through time. As a statistical model it is of paramount importance that this ODE not only have a solution, but also that the solution be unique.

If the form of  $\frac{dB}{dt}$  is at least Lipschitz continuous, then the Cauchy-Lipschitz-Picard theorem provides local existence and uniqueness of  $B(t)$ . Recall from Eq(3.14) that  $\frac{dB}{dt}$  is separated into a term for biomass production,  $P(B)$ , and a term for removals,  $Z(t)B(t)$ . For determining Lipschitz continuity of  $\frac{dB}{dt}$ , the smallest Lipschitz constant of  $\frac{dB}{dt}$  will be the sum of the constants for each of the terms  $P(B)$  and  $Z(t)B(t)$  separately. Typically any choice of  $P(B)$  will be continuously differentiable, which implies Lipschitz continuity. At a minimum  $Z(t)$  typically contains fishing mortality as a function of time  $F(t)$  to model catch in time as  $C(t) = F(t)B(t)$ .  $Z(t)$  may or may not contain  $M$ , but typically  $M$  is modeled as stationary in time and does not pose a continuity issue, unlike some potential assumptions for  $C(t)$ .

In practice  $C(t)$  is determined by a series of observed, assumed known, catches. Catch observations are typically observed on a quarterly basis, but in practice may not be complete for every quarter of the modeled period. It is overwhelmingly common to discretized the ODE via Euler's method with integration step sizes to match the observation frequency of the modeled data. This is often convenient but can present several issues. This strategy often pushes the assumption of catch continuity under the rug, but for regularity of the statistical model an implicit assumption of continuity of the catches is required. While mechanistically at the finest scale fishers must only catch discrete packets of biomass (i.e. individual fish), it is sensible to consider catches as accruing in a continuous way. Furthermore any assumption of continuity will be required to be at least Lipschitz continuous for the required regularity of the model.

Here I assume catches accrue linearly between observed catches. This assumption defines

1634 the catch function as a piecewise linear function of time, with the smallest Lipschitz constant  
1635 for the catch term defined by the steepest segment of the catch function. This assumption  
1636 represents one of the simplest ways of handling catch, while retaining Lipschitz continuity  
1637 overall. Furthermore linearly interpolated catch is adequately parsimonious for the typical  
1638 handling of catches.

## 1639 **Integration and Stiffness**

1640 As previously mentioned, the overwhelming majority of implementations of population dy-  
1641 namics models discretized the ODE using Euler's method with the integration step sized  
1642 fixed so as to match the observation frequency. In this setting we explore model parameter-  
1643 izations that explore the full extent of biologically relevant reference points. This exercise  
1644 produces some combinations of parameters that result in numerically stiff ODEs.

1645 The concept of stiffness in ODEs is hard to precisely characterize. [Wanner and Hairer](#)  
1646 ([1996](#), p.2) describe stiffness in the following pragmatic sense, "Stiff equations are problems  
1647 for which explicit methods don't work". It is hard to make this definition more mathemati-  
1648 cally precise, but this a consistent issue for models of fast growing species in the low contrast  
1649 simulation. Euler's method, as often implemented, is particularly poorly suited for these  
1650 stiff regions of parameter space. In these stiff regions it is necessary to integrate the ODE  
1651 with an implicate integration method.

1652 Several of the most common implicate methods were tried including the Livermore Solver  
1653 for ODEs (lsode), and the Variable Coefficient ODE Solver (vode) as implemented in the  
1654 deSolve package of R ([Soetaert et al., 2010](#)). The difference between implicit solvers is  
1655 negligible, while explicit methods result in wildly varying solutions to the ODE in stiff  
1656 regions of parameter space. Results shown here are computed using the lsode integration  
1657 since it runs relatively quickly and has a relatively smaller footprint in system memory.

## 6 Results

### 6.1 PT/Schaefer

#### An $MSY$ -Optimal Catch History

When  $F(t)$  is held constant at  $F^*$ , as it is in the "low contrast" simulation setting,  $B(t)$  comes to equilibrium as an exponential decay from  $K$  to  $B^*$ . Understanding model misspecification bias is simplified in this setting due to the relative simplicity that this induces in  $B(t)$ . However this simplicity is known to poorly inform estimates of  $r$ , and thus  $F^*$ , due to the limited range of the production function that is observed (Hilborn & Walters, 1992).

Figure (3.21) shows four of the most misspecified example production function fits as compared to the true data generating PT production functions. The rug plots below each set of curves show how the observed biomasses decay exponentially from  $K$  to  $B^*$  in each case. In particular, notice how observations only exist where the PT biomass is greater than  $B^*$ . Due to the leaning of the true PT curves, and the symmetry of the logistic parabola, the logistic curve only observes information about its slope at the

origin from data observed on the right portion of the PT curves. The top two panels of Figure (3.21) shows PT data generated such that  $\frac{B^*}{B(0)} > 0.5$ ; in these cases PT is steeper to the right of  $B^*$  than it is on the left, and so the the logistic curve over-estimates  $r$ , and consequently also over-estimates  $F^*$ . The bottom two panels of Figure (3.21) show PT

data generated with  $\frac{B^*}{B(0)} < 0.5$  and where the vice versa phenomena occurs. PT is shallower

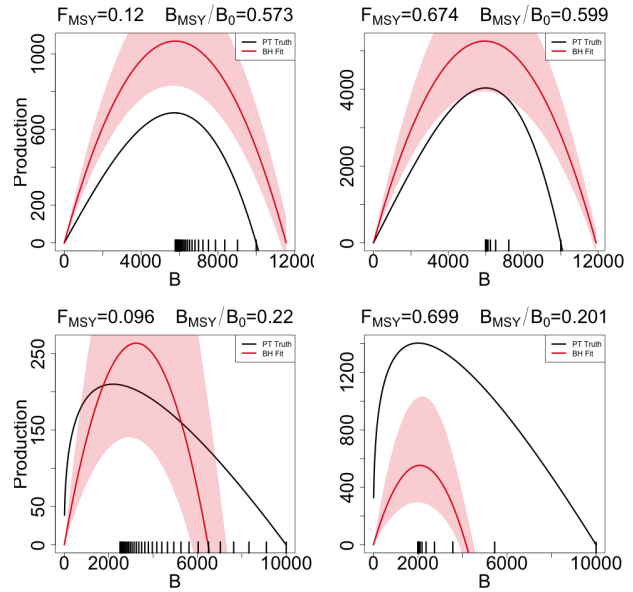


Figure 3.21: A comparison of the true PT production function (in black) and the estimated logistic curve (in red) with 95% CI shown. The examples shown represent the four corners of maximum model misspecification in the simulated RP-space. Observed biomasses are plotted in the rug plots below the curves.

1687 to the right of  $B^*$  than it is on the left and so the logistic parabola estimate tends to under  
 1688 estimate  $F^*$ .

## 1689 **Metamodeled Trends**

1690 Each point in the space of the RPs  $F^*$  and  $\frac{B^*}{B(0)}$  uniquely identifies a complete PT model  
 1691 with different combinations of parameters values. Recall that when  $\gamma = 2$  for the PT model,  
 1692 the PT curve becomes a parabola and is equivalent to the logistic curve of the Schaefer  
 1693 model. Since the logistic curve is symmetric about  $B^*$ , the Schaefer model must fix the  
 1694 value of  $\frac{B^*}{B(0)}$  at the constant 0.5 for any value of  $F^*$ . So the line through RP space defined  
 1695 by  $\frac{B^*}{B(0)} = 0.5 \quad \forall \quad F^*$ , defines the subset of RP space where  $\gamma = 2$  and where the PT model  
 1696 is equivalent to the Schaefer model. For brevity this subset of RP were  $\frac{B^*}{B(0)} = 0.5$  will be  
 1697 referred to as the ‘‘Schaefer set’’. Thus simulated data that are generated along the Schaefer  
 1698 set will be the only data that are not misspecified relative to the Schaefer model; as PT data  
 1699 are simulated farther and farther away from this line at  $\frac{B^*}{B(0)} = 0.5$  model misspecification of  
 1700 the Schaefer model becomes worse and worse.

1701 While Figure (3.21) demonstrates a real trend in simulation results, individual simulation  
 1702 runs will at best show jittery trends due to the stochastic nature of statistical inference. The  
 1703 GP process metamodel accounts for this stochasticity to focus analysis on the signal in the  
 1704 simulation results. Recall that metamodeling occurs on the scale of the inferred productivity  
 1705 parameters of the restricted production model, by transforming metamodel predictions via  
 1706 Eq. (3.23), metamodeled predictions are obtained for Schaefer RPs. By further subtracting  
 1707 the true data generating PT RPs from the predicted Schaefer RPs at each point in RP space  
 1708 a pattern of inferential RP bias, induced by model misspecification of the Schaefer model,  
 1709 can be seen to be seen.

1710 Figure (3.22) shows the pattern of biases the Schaefer model creates when fit to PT data  
 1711 generated at each point of RP space. An equivalent way to think of Figure (3.22) is that since  
 1712 the Schaefer model must estimate RPs in the Schaefer set, the metamodel arrows indicate  
 1713 the mapping that is created by inferring RPs under a misspecified Schaefer model fit to PT  
 1714 data generated at each point over the pictured region.

1715 Since  $\frac{B^*}{B_0}$  must be 0.5 under the Schaefer model, biases in the  $\frac{B^*}{B_0}$  direction must simply

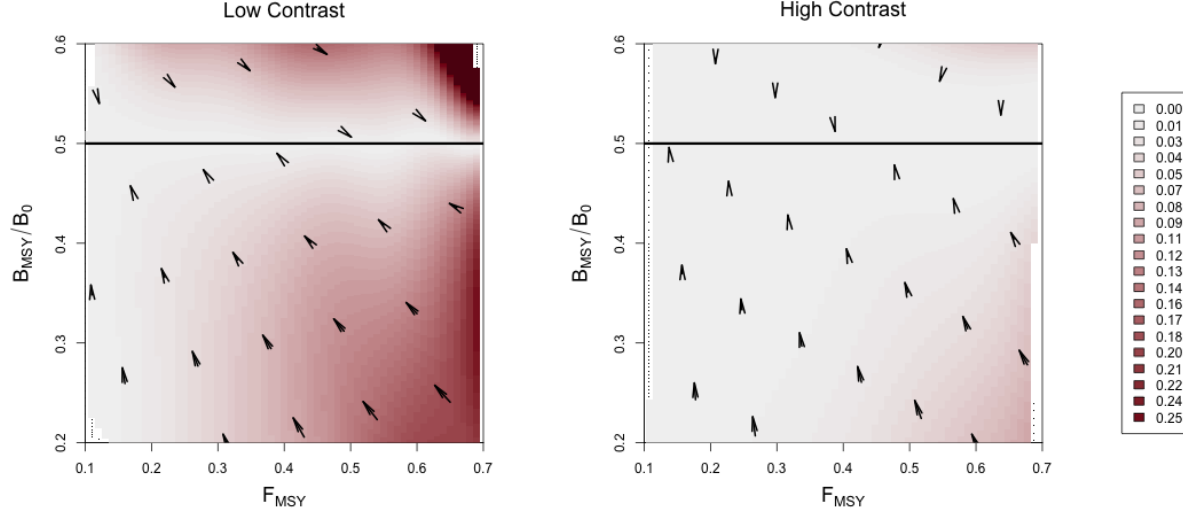


Figure 3.22: Joint bias direction for  $(F^*, \frac{B^*}{B_0})$  estimates under the misspecified Schaefer Model. The intensity of color represents the excess bias relative to the shortest possible mapping. Results in the low contrast setting are shown *left*, and the high contrast setting is shown *right*.

map vertically onto the Schaefer set. Due to this simplified RP geometry under the Schaefer model, the degree of bias in  $\frac{B^*}{B_0}$  estimation is entirely defined solely by the degree of model misspecification irrespective of  $F^*$ . Furthermore, the closest possible point along the Schaefer set that Schaefer model inference could map RPs would be the perfectly vertical mapping. This pattern only contains the strictly necessary bias present in  $\frac{B^*}{B_0}$ , and zero bias in  $F^*$ . Any deviation from this minimal bias pattern necessarily to be due to added bias in  $F^*$ .

The two simulation settings shown in Figure (3.22) are identical except for the amount of contrast present in the simulated index. The left panel of Figure (3.22) shows RP biases in the low contrast setting, while the right panel shows the high contrast setting. Notice that in the low contrast setting the RP bias pattern is far from the minimum distance mapping, however when contrast is added the mapping becomes much closer to a minimal bias mapping. In the low contrast setting the observed bias is consistent with the pattern and mechanism described in Figure (3.21), where  $F^*$  is underestimated for data generated below the Schaefer line and overestimated above the Schaefer set. In the high contrast simulation the mapping is nearly minimal distance with the exception of PT data generated with simultaneously low  $\frac{B^*}{B_0}$  and high  $F^*$ .



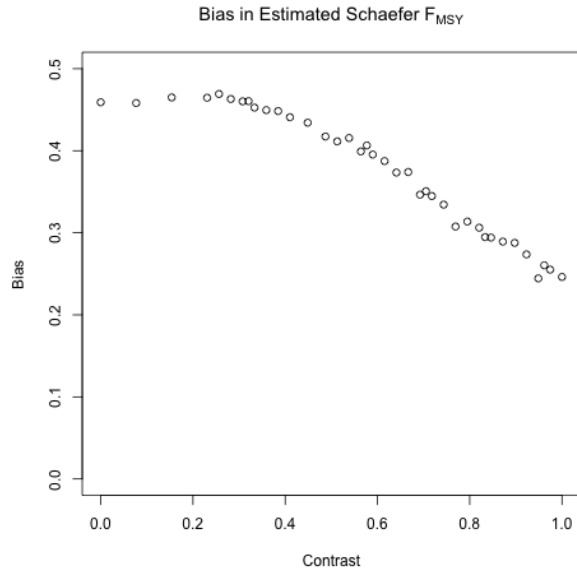


Figure 3.23: Bias in  $F^*$  under the Schaefer model when PT data are generated with increasing contrast so that  $F^*$  and  $\frac{B^*}{B_0}$  are fixed at 0.699 and 0.201 respectively.

1732 Figure (6 .1) demonstrates how bias in  $F^*$  estimation decreases as contrast is added to  
 1733 PT data as generated in the low  $\frac{B^*}{B_0}$  and high  $F^*$  regime. By including additional contrast  
 1734  $F^*$  bias is decreased, however parameterizing contrast so as to fully extinguish  $F^*$  bias may  
 1735 require a more complex model of fishing.

- 1736 • summary of  $\sigma$  over RP space comparing between models (PT, Schnute, Schnute DD)
- 1737 to show areas of model breakdown.
- 1738 – miss-identifying signal for noise.
- 1739 – It happens more as the dynamics get more complex.
- 1740 – point to the full age structured models.
- 1741 • show the constrained BH space over a grid of  $M, \kappa, \omega, W_\infty$
- 1742 • Show that the constrained spaces vary only slightly as compared with the consequences
- 1743 of misspecifying the functional form.
- 1744 • estimating these other quantities (while they can create quite different Biomass series)
- 1745 can only do so much to improve (expand) RP inference as compared with correctly
- 1746 modeling  $P$ .
- 1747 • mapping distance as a function of contrast at (3.5, 0.5)
- 1748 • for LHS grid locations show  $\frac{B^*}{B_0}$  and  $F^*$  biases for grids in  $M \in (0, 0.5)$  For sure in High
- 1749 Contrast, maybe also in Low??.

## 1750 7 Appendix: Inverting $\frac{B^*}{B(0)}$ and $\gamma$ for the PT Model

For brevity let  $\zeta = \frac{B^*}{B(0)}$ .

$$\begin{aligned}\zeta &= \left(\frac{1}{\gamma}\right)^{\frac{1}{\gamma-1}} \\ \zeta &= \gamma \zeta^\gamma \\ \zeta &= \gamma e^{\gamma \log(\zeta)} \\ \zeta \log(\zeta) &= \gamma \log(\zeta) e^{\gamma \log(\zeta)}\end{aligned}$$

The Lambert product logarithm,  $W$ , is defined as the inverse function of  $z = xe^x$  such that  $x = W(z)$ . Applying this definition allows for the isolation of  $\gamma$ .

$$\begin{aligned}\gamma \log(\zeta) &= W(\zeta \log(\zeta)) \\ \gamma &= \frac{W(\zeta \log(\zeta))}{\log(\zeta)}\end{aligned}\tag{3.46}$$

1751 The Lambert product logarithm is a multivalued function with a branch point at  $-\frac{1}{e}$ . The  
1752 principal branch,  $W_0(z)$ , is defined on  $z \in (-\frac{1}{e}, \infty)$ , and the lower branch,  $W_{-1}(z)$ , is  
1753 defined on  $z \in (-\frac{1}{e}, 0)$ . Taken individually, each respective branch is analytic, but cannot  
1754 be expressed in terms of elementary functions.

1755 When  $\zeta \in (0, \frac{1}{e})$  the solution of interest in Eq. (3.24) comes from  $W_0$ . When  $\zeta \rightarrow \frac{1}{e}$ , the  
1756 Fox Model emerges as  $\gamma \rightarrow 1$ . When  $\zeta \in (\frac{1}{e}, 1)$  the solution of interest comes from  $W_{-1}$ . For  
1757 the use case presented here, Eq. (3.24) is to be interpreted as,

$$\gamma = \begin{cases} \frac{W_0(\zeta \log(\zeta))}{\log(\zeta)} & \zeta \in (0, \frac{1}{e}) \\ \frac{W_{-1}(\zeta \log(\zeta))}{\log(\zeta)} & \zeta \in (\frac{1}{e}, 1) \end{cases}.\tag{3.47}$$

1758 Prager 2002, Figure(2).

1759 [https://math.stackexchange.com/questions/3004835/is-the-lambert-w-function-analytic-](https://math.stackexchange.com/questions/3004835/is-the-lambert-w-function-analytic-if-not-everywhere-then-on-what-set-is-it-an)  
1760 [if-not-everywhere-then-on-what-set-is-it-an](https://math.stackexchange.com/questions/3004835/is-the-lambert-w-function-analytic-if-not-everywhere-then-on-what-set-is-it-an) [https://researchportal.bath.ac.uk/en/publications/algebraic-](https://researchportal.bath.ac.uk/en/publications/algebraic-properties-of-the-lambert-w-function-from-a-result-of-r)  
1761 [properties-of-the-lambert-w-function-from-a-result-of-r](https://researchportal.bath.ac.uk/en/publications/algebraic-properties-of-the-lambert-w-function-from-a-result-of-r)



# References

- Beverton, R. J., & Holt, S. J. (1957). *On the dynamics of exploited fish populations* (Vol. 11). Springer Science & Business Media.
- Brent, R. P. (1973). Chapter 4: An Algorithm with Guaranteed Convergence for Finding a Zero of a Function. In *Algorithms for minimization without derivatives*. Courier Corporation.
- Conn, P. B., Williams, E. H., & Shertzer, K. W. (2010). When can we reliably estimate the productivity of fish stocks? *Canadian Journal of Fisheries and Aquatic Sciences*, 67(3), 511–523.
- Cressie, N. (2015). *Statistics for spatial data*. John Wiley & Sons.
- Cushing, D. H. (1971, May). The Dependence of Recruitment on Parent Stock in Different Groups of Fishes. *ICES Journal of Marine Science*, 33(3), 340–362. Retrieved 2023-06-03, from <https://doi.org/10.1093/icesjms/33.3.340> doi: 10.1093/icesjms/33.3.340
- Deriso, R. B. (1980, February). Harvesting Strategies and Parameter Estimation for an Age-Structured Model. *Canadian Journal of Fisheries and Aquatic Sciences*, 37(2), 268–282. Retrieved 2020-05-13, from <https://www.nrcresearchpress.com/doi/abs/10.1139/f80-034> doi: 10.1139/f80-034
- Devon Lin, C., & Tang, B. (2015). Latin Hypercubes and Space-filling Designs. In *Handbook of Design and Analysis of Experiments*.
- Fletcher, R. I. (1978). On the restructuring of the Pella-Tomlinson system. *Fish. Bull*, 76(3), 515–521.
- Fournier, D. A., & Doonan, I. J. (1987). A length-based stock assessment method utilizing a generalized delay-difference model. *Canadian Journal of Fisheries and Aquatic*

- Sciences*, 44(2), 422–437. (Publisher: NRC Research Press Ottawa, Canada)
- Fox Jr., W. W. (1970). An Exponential Surplus-Yield Model for Optimizing Exploited Fish Populations. *Transactions of the American Fisheries Society*, 99(1), 80–88. Retrieved 2022-02-17, from <https://onlinelibrary.wiley.com/doi/abs/10.1577/1548-8659%281970%2999%3C80%3AAESMFO%3E2.0.CO%3B2> (\_eprint: <https://onlinelibrary.wiley.com/doi/pdf/10.1577/1548-8659%281970%2999%3C80%3AAESMFO%3E2.0.CO%3B2>) doi: 10.1577/1548-8659(1970)99<80:AESMFO>2.0.CO;2
- Gramacy, R. B. (2020). *Surrogates: Gaussian process modeling, design, and optimization for the applied sciences*. Chapman and Hall/CRC.
- Gramacy, R. B., & Lee, H. K. (2012). Cases for the nugget in modeling computer experiments. *Statistics and Computing*, 22(3), 713–722. (Publisher: Springer)
- Hilborn, R. (2010). Pretty good yield and exploited fishes. *Marine Policy*, 34(1), 193–196. (Publisher: Elsevier)
- Hilborn, R., & Mangel, M. (1997). *The Ecological Detective: Confronting Models with Data*. Princeton University Press.
- Hilborn, R., & Walters, C. J. (1992). Quantitative Fisheries, Stock Assessment: Choice Dynamics, and Uncertainty Chapman and Hall. *New York*.
- Johnson, M. E., Moore, L. M., & Ylvisaker, D. (1990). Minimax and maximin distance designs. *Journal of statistical planning and inference*, 26(2), 131–148. (Publisher: Elsevier)
- Lee, H.-H., Maunder, M. N., Piner, K. R., & Methot, R. D. (2012, August). Can steepness of the stock–recruitment relationship be estimated in fishery stock assessment models? *Fisheries Research*, 125-126, 254–261. Retrieved 2022-01-29, from <https://linkinghub.elsevier.com/retrieve/pii/S0165783612001099> doi: 10.1016/j.fishres.2012.03.001
- Magnusson, A., & Hilborn, R. (2007). What makes fisheries data informative? *Fish and Fisheries*, 8(4), 337–358. (Publisher: Wiley Online Library)
- Mangel, M., MacCall, A. D., Brodziak, J., Dick, E., Forrest, R. E., Pourzand, R., & Ralston, S. (2013, April). A perspective on steepness, reference points, and stock assessment.

- 1817 *Canadian Journal of Fisheries and Aquatic Sciences*, 70(6), 930–940. Retrieved 2019-  
1818 07-03, from <https://www.nrcresearchpress.com/doi/10.1139/cjfas-2012-0372>  
1819 doi: 10.1139/cjfas-2012-0372
- 1820 McKay, M. D., Beckman, R. J., & Conover, W. J. (2000). A comparison of three methods  
1821 for selecting values of input variables in the analysis of output from a computer code.  
1822 *Technometrics*, 42(1), 55–61. (Publisher: Taylor & Francis)
- 1823 Morris, M. D., & Mitchell, T. J. (1995, February). Exploratory designs for computa-  
1824 tional experiments. *Journal of Statistical Planning and Inference*, 43(3), 381–402. Re-  
1825 trieved 2023-05-28, from [https://www.sciencedirect.com/science/article/pii/](https://www.sciencedirect.com/science/article/pii/S037837589400035T)  
1826 [037837589400035T](https://www.sciencedirect.com/science/article/pii/S037837589400035T) doi: 10.1016/0378-3758(94)00035-T
- 1827 Punt, A. E., Butterworth, D. S., Moor, C. L. d., Oliveira, J. A. A. D., & Haddon, M. (2016).  
1828 Management strategy evaluation: best practices. *Fish and Fisheries*, 17(2), 303–334.  
1829 Retrieved 2018-12-13, from [https://onlinelibrary.wiley.com/doi/abs/10.1111/](https://onlinelibrary.wiley.com/doi/abs/10.1111/faf.12104)  
1830 [faf.12104](https://onlinelibrary.wiley.com/doi/abs/10.1111/faf.12104) doi: 10.1111/faf.12104
- 1831 Punt, A. E., & Cope, J. M. (2019, September). Extending integrated stock assessment mod-  
1832 els to use non-depensatory three-parameter stock-recruitment relationships. *Fisheries*  
1833 *Research*, 217, 46–57. Retrieved 2019-07-19, from [http://www.sciencedirect.com/](http://www.sciencedirect.com/science/article/pii/S0165783617301819)  
1834 [science/article/pii/S0165783617301819](http://www.sciencedirect.com/science/article/pii/S0165783617301819) doi: 10.1016/j.fishres.2017.07.007
- 1835 Ramasubramanian, K., & Singh, A. (2017). *Machine learning using R* (No. 1). Springer.
- 1836 Rankin, P. S., & Lemos, R. T. (2015, October). An alternative surplus production  
1837 model. *Ecological Modelling*, 313, 109–126. Retrieved 2022-02-11, from [https://](https://www.sciencedirect.com/science/article/pii/S0304380015002732)  
1838 [www.sciencedirect.com/science/article/pii/S0304380015002732](https://www.sciencedirect.com/science/article/pii/S0304380015002732) doi: 10.1016/  
1839 [j.ecolmodel.2015.06.024](https://www.sciencedirect.com/science/article/pii/S0304380015002732)
- 1840 Ricker, W. E. (1954). Stock and recruitment. *Journal of the Fisheries Board of Canada*,  
1841 11(5), 559–623. (Publisher: NRC Research Press Ottawa, Canada)
- 1842 Schnute, J. (1985, March). A General Theory for Analysis of Catch and Effort Data.  
1843 *Canadian Journal of Fisheries and Aquatic Sciences*, 42(3), 414–429. Retrieved 2020-  
1844 05-13, from <https://www.nrcresearchpress.com/doi/abs/10.1139/f85-057> doi:  
1845 10.1139/f85-057
- 1846 Schnute, J. (1987). A general fishery model for a size-structured fish population. *Canadian*

- Journal of Fisheries and Aquatic Sciences*, 44(5), 924–940. (Publisher: NRC Research Press Ottawa, Canada)
- Schnute, J. T., & Richards, L. J. (1998, February). Analytical models for fishery reference points. *Canadian Journal of Fisheries and Aquatic Sciences*, 55(2), 515–528. Retrieved 2020-01-14, from <https://www.nrcresearchpress.com/doi/abs/10.1139/f97-212> doi: 10.1139/f97-212
- Scrucca, L. (2013, April). GA: A Package for Genetic Algorithms in R. *Journal of Statistical Software*, 53, 1–37. Retrieved 2022-01-17, from <https://doi.org/10.18637/jss.v053.i04> doi: 10.18637/jss.v053.i04
- Scrucca, L. (2017). On Some Extensions to GA Package: Hybrid Optimisation, Parallelisation and Islands Evolution. On some extensions to GA package: hybrid optimisation, parallelisation and islands evolution. *The R Journal*, 9(1), 187–206. Retrieved 2022-01-17, from <https://journal.r-project.org/archive/2017/RJ-2017-008/index.html>
- Soetaert, K., Petzoldt, T., & Setzer, R. W. (2010, February). Solving Differential Equations in R: Package deSolve. *Journal of Statistical Software*, 33, 1–25. Retrieved 2023-05-29, from <https://doi.org/10.18637/jss.v033.i09> doi: 10.18637/jss.v033.i09
- Stein, M. (1987). Large sample properties of simulations using Latin hypercube sampling. *Technometrics*, 29(2), 143–151. (Publisher: Taylor & Francis)
- Von Bertalanffy, L. (1938). A quantitative theory of organic growth (inquiries on growth laws. II). *Human biology*, 10(2), 181–213. (Publisher: JSTOR)
- Walters, C. J. (2020). The continuous time Schnute-Deriso delay-difference model for age-structured population dynamics, with example application to the Peru anchoveta stock.
- Wanner, G., & Hairer, E. (1996). *Solving ordinary differential equations II* (Vol. 375). Springer Berlin Heidelberg.
- Yeakel, J. D., & Mangel, M. (2015, February). A generalized perturbation approach for exploring stock recruitment relationships. *Theoretical Ecology*, 8(1), 1–13. Retrieved 2023-06-03, from <https://doi.org/10.1007/s12080-014-0230-z> doi: 10.1007/s12080-014-0230-z